UNIVERSIDAD DE CHILE
FACULTAD DE CIENCIAS FÍSICAS Y MATEMÁTICAS
DEPARTAMENTO DE INGENIERÍA ELÉCTRICA

EFFECT OF TEMPERATURE-DEPENDENT DEGRADATION MODELS FOR LITHIUM-ION ENERGY STORAGE DEVICES ON OPTIMIZED MULTISERVICE PORTFOLIO STRATEGIES

TESIS PARA OPTAR AL GRADO DE DOCTOR EN INGENIERÍA ELÉCTRICA

ARAMIS PÉREZ MORA

PROFESOR GUÍA:

DR. MARCOS ORCHARD CONCHA

PROFESOR CO-GUÍA:

DR. RODRIGO MORENO VIEYRA

MIEMBROS DE LA COMISIÓN:

DR. MARCOS DÍAZ QUEZADA

DR. JORGE SILVA SÁNCHEZ

DR. JUAN YUZ EISSMANN

DR. BIN ZHANG

SANTIAGO, CHILE

2018

RESUMEN DE LA MEMORIA PARA OPTAR AL

TÍTULO DE: Doctor en Ingeniería Eléctrica

POR: Aramis Pérez Mora

FECHA: 30/01/2018

PROFESOR GUÍA: Dr. Marcos Orchard Concha

EFFECT OF TEMPERATURE-DEPENDENT DEGRADATION MODELS FOR LITHIUM-ION ENERGY STORAGE DEVICES ON OPTIMIZED MULTISERVICE PORTFOLIO STRATEGIES

Actualmente el uso de energías renovables está incrementando su popularidad. Como la disponibilidad de estos recursos puede ser limitada debido a factores ambientales, el uso de almacenadores de energía es algo que se debe considerar. En mercados eléctricos, el uso de sistemas de almacenamiento se vuelve interesante debido a que la posibilidad de obtener ganancias está latente. Esta investigación se enfoca en la integración de una estrategia de optimización de utilidades en conjunto con el modelo del proceso de degradación de una batería de ión-litio, para así cuantificar el beneficio económico que un usuario puede obtener dependiendo de cómo el almacenador sea operado. Dado que la operación del almacenador está sujeta a diferentes condiciones de mercado, es necesario analizar el proceso de degradación bajo estas condiciones. Esto significa que una batería no necesariamente trabajará completamente cargada o descargada en un ciclo de operación. En este sentido, definir apropiadamente un ciclo es importante puesto que el uso del almacenamiento de energía es altamente variable. El modelo de degradación fue creado utilizando información disponible en la literatura. Este modelo está basado dos sumandos, uno de los cuales tiene mayor impacto en el corto plazo de la vida útil, y el otro en el largo plazo. Además, una metodología que permite la estimación del proceso de degradación de las baterías cuando son utilizadas en condiciones de estado de carga variables también se incluye. En un primer enfoque, se utiliza información proporcionada por un fabricante, y con el apoyo de factores de escalamiento, es posible determinar el valor para la eficiencia de Coulomb para cada ciclo. Caracterizar el proceso de degradación según el estado de carga utilizado muestra hasta un 3.4% más de ciclos adicionales de uso. Posteriormente, se presenta otra metodología basada en algoritmos de similitud que incorpora la corriente de descarga, y los niveles del estado de carga como variables del modelo. Además, el efecto de la temperatura es incluido para ilustrar el efecto de la capacidad utilizable de la batería. Una vez que se establece el modelo, este se combina un algoritmo de programación lineal entera mixta que maximiza la utilidad obtenida de la venta de diferentes servicios. Distintas políticas de operación para el sistema almacenador fueron analizadas dando como resultados las horas de operación y el beneficio económico para cada caso. Es importante mencionar que no necesariamente operar el sistema de almacenamiento de forma libre asegurará el máximo beneficio económico para el dueño. Restringir el estado de carga puede significar hasta un 18% menos de utilidad bruta por año. Otros efectos externos tales como la intervención de un operador humano que modifique la estrategia, sensibilidad a cambios en la demanda o en los precios también son incluidos. El efecto de la temperatura también se incluye y la reducción en el beneficio económico es comparada con el caso donde las condiciones de temperatura están controladas. La temperatura puede afectar hasta en un 3% las utilidades esperadas para este caso.

SUMMARY OF THE THESIS TO OBTAIN THE

DEGREE OF: Doctor in Electrical Engineering

BY: Aramis Pérez Mora

DATE: 01/30/2018

ACADEMIC ADVISOR: Dr. Marcos Orchard Concha

EFFECT OF TEMPERATURE-DEPENDENT DEGRADATION MODELS FOR LITHIUM-ION ENERGY STORAGE DEVICES ON OPTIMIZED MULTISERVICE PORTFOLIO STRATEGIES

Nowadays the use of renewable energies are increasing their popularity. Since the availability of these resources might be limited due to environmental factors, the use of an energy storage device as part of the system is something to consider. On electricity markets, the use of storage systems becomes interesting since the possibility to obtain profit is latent. This research focuses on the integration of a revenue optimization strategy in conjunction with a degradation process model of a Li-ion battery, in order to quantify the economic benefit that the user can receive depending on how the storage device is operated. Since the operation of the storage device is subject to different market conditions, it becomes necessary to analyze the degradation process under these conditions. This means that the battery will not necessarily fully charge or discharge, in each cycle of operation. In this regard, defining a cycle becomes important since the usage of the storage device is highly variable. The degradation model was created using information available from the literature. This model is based on two summands, one of them having a major impact on the short term and the other one, on the long term of the lifespan. Furthermore, a methodology to estimate the degradation process of the batteries when operated under erratic state of charge conditions is included. In a first approach the information provided by a manufacturer is used, and with the support of escalating factors, and equivalent value for the Coulombic efficiency for each cycle is determined. Characterizing the degradation process according to the used state of charge show up to 3.4% additional cycles of operation. Afterwards, another similarity-based methodology to estimate the degradation process, by incorporating the discharge current and the state of charge levels is presented. Also, the effect of the temperature is included to illustrate the effect of usable capacity of a battery. Once the degradation model is established, it is combined with a mixed integer linear programming algorithm that maximizes the revenue obtained from selling different services. Several operation policies of the energy storage system were analyzed, giving as result different amount of operating hours and economic benefits for each case. It is important to mention that not necessarily operating the storage system freely will assure the maximum economic benefit to the owner. Constraining the state of charge and present nearly 18% of lower gross revenues per year. Moreover, within the case study, different external effects are also studied such as the intervention of a human operator that modifies the optimization strategy, sensitivity to changes in the demand or the energy prices. The effect of the temperature is also included and the reduction of the economic benefit is compared to the case where controlled temperature conditions are present. The effect of the temperature can affect up to 3% the gross revenues for this case due to the market conditions.

Dedication

To my kids: Antonio and Sara.

Acknowledgements

The work of Aramis Perez was supported by the University of Costa Rica (Grant for Doctoral Studies) and CONICYT-PCHA/Doctorado Nacional/2015-21150121.

This work has been partially supported by FONDECYT Chile Grant Nr. 1170044, and the Advanced Center for Electrical and Electronic Engineering, AC3E, Basal Project FB0008, CONICYT.

The author would like to thank all the Professors who were part of this Doctorate program. A special mention to Dr. Marcos Orchard and Dr. Rodrigo Moreno for all the lessons taught during these years. Also, to the rest of the commission for their valuable comments: Dr. Díaz, Dr. Silva, Dr. Yuz and Dr. Zhang.

To all the great friends and partners that I have met during this year, because they were an important part of this too: Francisco, Vanessa, Luis, Pablo, David, Oscar, Mauricio, and to all of my fellow doctorate program partners. Thanks for being part of this!

Also, special thanks to the administrative part of the universities, since sometimes their efforts are not seen on academic researches but definitely their collaboration is highly relevant. Thank you very much Milena. Also, special thanks to all the people that helped me in the OAICE at the University of Costa Rica.

Table of Contents

Table Index

Figure Index

1. Introduction

1.1 General Context and Motivation

It is a worldwide trend to reduce considerably the carbon footprint in all the applications. Since one of the major contamination sources is the coal or fossil fuels used for electric generation, the idea to use alternative energy sources in order to follow the Kyoto Protocol [1], the use of storage devices becomes more attractive. Even though these efforts are strongly supported by the governments all around the world, there are still some unresolved technical and economic issues of how to incorporate the storage to the grid.

The universe is full of energy resources and throughout the history, mankind has always been looking for ways to use it. Regardless of the energy source of choice, a common situation is that the energy is available at moments when it is not required. For these cases a device for storing the energy becomes very useful since it allows to use that energy on demand, when it is actually needed. In this thesis, a lithium-ion energy storage device (ESD) is going to be considered. Some of its characteristics are: high energy density, light weight, no memory effect, and high charge/discharge efficiency, and due to these advantages, this type of battery it is employed in a wide variety of applications such as consumer electronics, terrestrial and aerial vehicles and power electronics [2].

In order to comprehend topics regarding the incorporation of the storage units as part of the grid, the Smarter Network Storage project (SNS) was created by the UK Power Networks [3]. The project aims to provide a better comprehension of the technical and commercial challenges behind the energy storage when incorporated to the grid. The energy storage facility is located next to a UK Power Network 11 [kV] primary substation in Leighton Buzzard (a town 70 [km] northeast of London). This storage facility has a capacity of 6 [MW]/10 [MWh] and one of the main objectives is to explore revenue alternatives when integrated to a traditional network.

In this regard, an approach to understand market conditions was developed in [4]. The authors proposed an optimization strategy for multi-service portfolios in this energy storage facility. However, this effort did not consider a state of health (SOH) model for the ESD meaning that there is no aging or degradation of the battery considered. Even though this can give an idea of the possible gross revenue for an investor when operating the storage facility under a certain strategy (£311,353 per year for five different services), the real profit has to consider the useful life of the ESD in order to determine, in the long term, the sustainability of the strategy. Storage owners can benefit from three different products: network congestion management, energy price arbitrage and various reserve and frequency response services in order to maximize gross revenue in the short-term. However, in the long term, there are some consequent costs associated with battery degradation and replacement.

Two major concerns regarding the ESDs are the monitoring process of the state of charge (SOC) and the SOH. The SOC is associated to the amount of available energy at each instant when the battery is used, while the SOH is associated with the long term energy availability of the battery. For example a completely new battery when is fully charged will have a SOH and SOC of 100%, meaning that it can deliver its full nominal capacity. As the same battery is used, the capability to deliver the same amount of energy is diminished, meaning that even though the battery is fully charged (100% SOC), its SOH is less than the original 100%.

Figure 1 shows an example of this behavior. The image was adapted from [5]. The accumulation of residue and the wear of the electrodes and the rest of the battery makes it impossible to maintain a 100% SOH all the time.

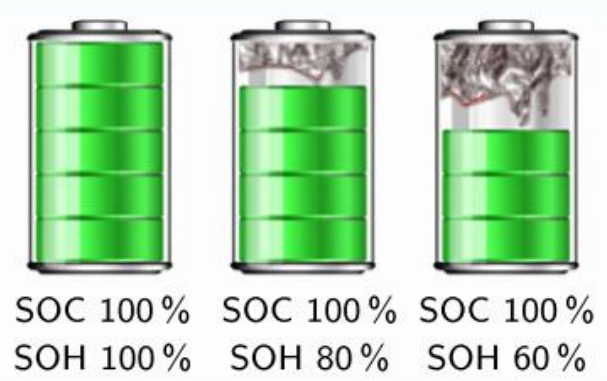

Figure 1. SOC and SOH evolution in time [5].

In this respect, being able to estimate the SOH in an accurate way is really important. This will allow to make decisions in the short and long term and determine a strategy of how the ESD will be used.

To manage this situation, a SOH estimation module is proposed to work in parallel with the operational policy optimization module. This way the storage owner can have real-time information regarding the remaining useful life (RUL) depending on how the ESD has been and how it will be used.

1.2 Problem definition

The incorporation of an ESD on electricity markets is a developing research area. Depending on the business model it is possible to obtain a profit with the storage through different services. Since the performance of ESD is related to several factors such as weather conditions, amount of energy withdrawn from the storage system, and capacity fade, combining a model that characterizes the degradation process of ESD with the a revenue optimization strategy will aid the decision making process to the user on how to operate the ESD.

1.3 Hypotheses

- If an optimized economical strategy for energy storage operation is used in conjunction with a SOH degradation model that includes information such as operating temperature, discharge current, SOC swing and swing range, the user can quantify the overall revenue depending on how the energy storage is operated in the long-term.

- It is possible to generate SOH degradation models using data provided by manufacturers of a specific battery type and extend these models to other types of batteries using similarity-based algorithms.

1.4 General Objective

This research aims at determining the effect of state-of-health degradation process on decision-making policies that define the criteria for battery usage on multiservice energy portfolios. Particularly, it is of interest to evaluate the impact of including temperature and C-rate (rate of discharge compared to the nominal capacity of the battery) dependent SOH degradation models into the optimization procedure, as well as incorporating the uncertainty inherent to the processes and temperature-dependent effects using a linear model of the dynamic Coulombic efficiency and an appropriate definition of cycles of operation.

1.5 Specific Objectives

1. Validate through simulations that depending on how the ESD is used there is direct effect on the amount of operative hours.
2. Evaluate the economic benefit of different optimized operational policies considering the degradation state of the ESD.
3. Define a cycle of operation properly, when undergoing partial charge and discharge conditions.
4. Assess the impact on the useful life of the ESD caused by two concepts related to the depth of discharge: SOC swing and swing range.
5. Propose a temperature and C-rate dependent SOH degradation model.
6. Include the effect of the temperature on the SOH degradation model and evaluate the impact of this variable in the battery cycle life.
7. Establish a similarity-based technique capable of modeling the degradation process for any type of Li-ion battery using information provided by the datasheet.

1.6 Contributions

- A novel model that incorporates the discharge current rates as a feature that affects the degradation process of Li-ion batteries is proposed. This empirical model can be easily and accurately adapted to different types of Li-ion batteries.
- Two extrapolation methods are proposed for the characterization of the degradation process when the Li-ion batteries are discharged regardless of range of the state of charge at which they are operated.
- A combined economic-degradation model that quantifies effects of various operational policies (which con- strain the State-of-Charge (SOC) to specified limits) on gross revenue, multiple services (namely energy arbitrage, balancing services and peak shaving or congestion management), degradation and lifespan of energy storage plants. The proposed economic model (a) presents a simplified (and convex) representation of reactive power that allows us to optimally coordinate active and reactive power for peak shaving purposes, and (b) ensures robustness and deliverability of the committed balancing services.
- An application on a real 6 MW/10 MWh Samsung SDI lithium-ion battery system installed in a UK Power Networks' primary substation in London (UK Power Networks owns and operates the distribution network and the storage plant), used to quantify the benefits of various practical operational policies that aim to reduce battery damage. It is demonstrated that although operational policies that focused on battery damage reduction will lead to a revenue loss in the short-term (since these policies fundamentally constrain storage operation), such loss can be more than compensated by long-term revenues due to a lengthier battery lifespan.
- Demonstration of the effects of ambient temperature fluctuations on storage plant revenue due to degraded capacity.

2. Theoretical Framework

2.1 Mixed Integer Linear Programming model for optimizing multi-service portfolios of distributed energy storage

Energy storage devices are able to provide different services through the electricity value chain: generation, transmission and distribution [6]. In order to integrate energy storage systems to the electricity market, factors such as the inclusion of renewable energy sources and the reduction of nuclear, coal or fossil fuel sources have to be considered. For instance, the intermittent generation of these type of energy sources when facing a peak demand period can induce to a degradation of the network assets increasing the costs. Energy storage systems have the potential to support this integration of different renewable technologies since they can support the load growth. For this reason, the electricity market industry is still trying to understand the procedure that assures energy storage investors to benefit for delivering the services. Also, since energy storage can be used for different services within an electricity market can generate a conflict among the provided services [7].

Several efforts have been made to understand the inclusion of energy storage as on electricity markets. In [7], the authors use the mixed integer linear programming (MILP) proposed on [4] to determine an efficient energy storage operation by maximizing the revenue to the storage owner. An interesting point of view is presented in [6], since the authors establish that most of the existing evaluation methods for energy storage usually conclude that energy storage does not pay off. For this reason the authors propose a business model demonstrating that it is possible to obtain revenue with energy storage, by planning ahead of time.

In this sense, there is no formal framework for understanding how to co-optimize and contract the different storage applications, in [4], a MILP model is developed to schedule the operation of distributed storage by coordinating provision of a range of system services which are rewarded at different market prices. The model maximizes distributed storage's net profit while providing support to three main services: network congestion management, energy price arbitrage and various reserve and frequency regulation services. For network congestion management, the storage system is intended to be used strategically to reduce peak loading conditions. With energy arbitrage the idea is to take advantage of energy prices by charging the battery at low price periods, and discharging the battery at higher price periods. The reserve service consists of a contract where the storage operator guarantees a certain level of energy at all times, and the frequency services is used to give support to the network when the defined frequency decreases or increases suddenly [8].

The main contributions of [4] are:

1. A MILP model that co-optimizes various storage applications to support distribution network operation and provide services in energy and balancing markets, ensuring:
    a. Profit maximization through the coordination of services.

b. Efficient control of reactive power in order to alleviate congestion and support energy arbitrage and frequency control.
c. Robustness of scheduled operation to guarantee deliverability of balancing services for real-time frequency control purposes.

2. Commercial strategy framework that establishes optimal multiservice portfolios in the long term.
3. Investment policy to upgrade distribution network capacity in order to efficiently balance network investment costs against the corresponding impacts on revenues of incumbent storage owners.

The model described is intended to determine the optimal storage operation by selecting those services that would maximize the profit to the distributed storage owner, given the prices associated to the services. The objective function maximizes net revenue associated with energy arbitrage, provision of frequency regulation and reserve services. Hence there will be a scheduled output of how the storage should be used ahead of time, allowing to analyze the possible degradation that the storage might suffer if used as supposed according to the optimization result. The constraints of the model include capacity limits and service deliverability. In this regard, capacity constraints must not be violated at any time instant.

Figure 2 shows the scheme of how the modules operate. First, all the operational policy constraints are going to be defined. These constraints include: time windows, energy prices, initial conditions of the storage system, and the SOC policy that will be used for all the simulation.

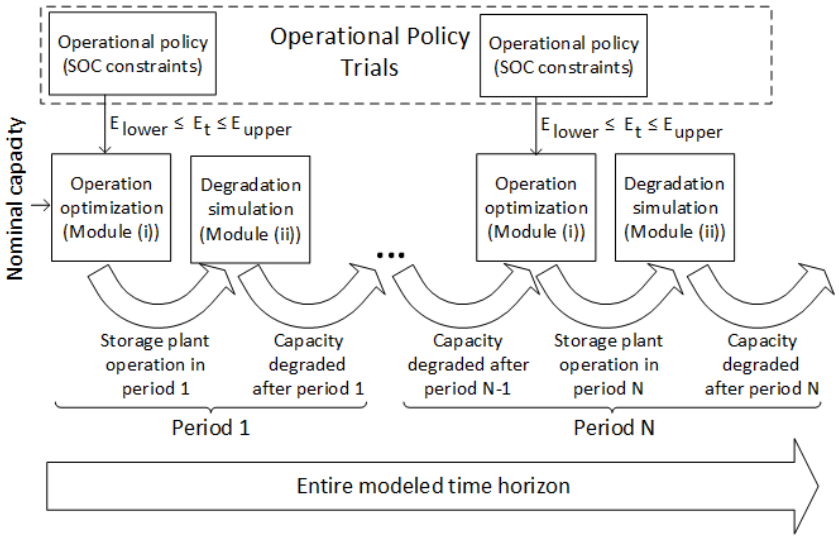

Figure 2. Proposed Operating Scheme of the Two Modules.

Once the constraints are defined the operation of the modules operate as follow: an economic-based, commercial strategy module that determines storage plant operation by optimizing multi-service portfolios of energy storage (network congestion management, energy price arbitrage and various reserve and frequency response services) to maximize gross revenue, and a degradation module that performs an analysis of how the storage is degraded by reducing its energy capacity.

In this regard, including a SOH degradation model will give the owner of the storage system an idea of how degraded the battery is in order to select an optimization strategy based on the remaining useful life or based on how much revenue can the ESD can produce. Although, for this research the operational policy will be defined at the beginning and it will remain the same during the simulation.

A more detailed explanation of this MILP model is included in Section 4.2.

2.2 Basic terminology

This section is intended to introduce the reader to common concepts used through within the context of any type of energy storage device. These concepts are related to the operation of the storage system mainly on the discharge part of the process.

2.2.1 State of Health and State of Charge

Before providing more details about the theoretical framework, there are some concepts that have been previously mentioned but need to be explained in more detail. The first concept to be explained is the State of Health (SOH). As long as the battery is used, its capacity to store energy degrades. This means that at certain point in time, the full capacity of the battery is a certain percentage less than when it was new. It is measured as a percentage, for instance a 100% SOH is used for a new, healthy battery, while a 0% is for a fully degraded battery. However, in practice, once the SOH reaches a point between 70%-80% of the SOH the battery is degraded [9], [10]. In this case, it can be said that the battery reached its End-of-Life (EoL). Depending on the application, different values for battery life is required. For instance, a calendar life of 15 years might be required for hybrid electrical vehicles, or 10 years for full electric vehicles, and a cycle life of up to 1000 cycles [11]. But these values can be completely different for small electronics or power grids.

The State of Charge (SOC) is associated to the available energy that the ESD is capable of delivering. It corresponds to a short term measurement, and it is indicated as a percentage. A 100% SOC indicates a fully charged battery, and a 0% SOC is used when the battery is fully

discharged. It is also said, when a battery reaches the 0% of the SOC, that it reached its End-of-Discharge (EoD).

2.2.2 Depth of Discharge

Another concept is the Depth of Discharge (DoD). The DoD is related to the SOC, since it represents the percentage of how much energy is used by the ESD. For instance it a fully charged battery is used to a point where the final SOC is 80%, it is said that the DoD is equal to 20%. However, if a battery starts fully charged, then delivers energy until it reaches a SOC of 70% and then charges up to a SOC of 80%, the DoD will be the difference between the highest and lowest values of SOC. In this case it would be a DoD of 30%, since the starting point to quantify the DoD is 100%. It is established that deeper discharges reduce the useful life of the ESDs. In this regard, since not always the starting point is a SOC of 100%, and the final value is not the lowest value of SOC, two concepts become useful. The first one is called the SOC swing, and is similar to the DoD. It measures the total difference between the starting SOC value and the lowest value in a cycle. Describing the DoD or the SOC swing is not always enough since this percentage can be calculated starting from any value of the SOC. For instance a SOC swing of 40% can be established, but it might result confusing to understand since not always the starting point would be the 100% SOC. This is why, the swing range (SR) becomes helpful. The SR indicates the range in which the SOC swing varies. It is important since the effect on the degradation is different depending on the initial state of the SOC, but with the same SR. In other words, if the SOC swing is defined as 50%, the degradation would be smaller if the SR goes from 50%-0% of the SOC than if it goes between [100%-50%] or [75%-25%].

2.2.3 C-rate

When talking about charging and discharging knowing how to interpret the C-rate is a must. The C-rate is a factor of the charge/discharge current in terms of the rated capacity expressed in Ampere-hours $C\ [Ah]$. This factor indicates the amount of current used to charge or discharge the battery. For example, if a battery has a rated capacity of $2\ [Ah]$, and it is discharged with a constant current of $1\ [A]$ then the C-rate can be determined with the equation $I = m \cdot C$. For this example the C-rate factor is equal to $C/2$. The C-rate is always expressed in term of the capacity C.

2.3 Understanding the Degradation Process as a Result of Different Operating Conditions

Numerous applications that involve some type of ESD have become very popular in recent years. For example, aerial and terrestrial vehicles whether they are unmanned on manned, smart grids, all kinds of electronic devices, and even wearables. Developing some kind of

on-line model for the SOC or the SOH is vital, in order to provide the user with real-time information. Several approaches have been made in order to determine a methodology to estimate these conditions.

Regardless of the type of model (whether is a SOC or SOH) that is being developed it is important to consider how it is going to be simulated or implemented. For instance, a model can be designed with many parameters, translating into an accurate model. However this model could be almost impossible to simulate due to its complexity, simulation time or computational cost, or furthermore the implementation of the model can become almost impossible due to the processing capability of the available hardware. On the literature is common to find many approaches for the estimation of the SOC, but the SOH is still at incipient point [12].

Battery models for the SOC can be divided into four major categories [13]: empirical, electrochemical, electric-circuit and abstract models. The electrochemistry-based models for SOH estimation vary depending on the chemical components of the battery but they all pretend to give the same result: a prediction of the battery's end of life (EoL).

The empirical models include a set of equations that describe the dynamics of the experimental data. Usually these models are easily determined but the accuracy is not very good. Electrical-circuit models are the ones based on the representation of the battery using voltage sources, resistors, capacitors and any other electrical part to build the essence of the battery. Usually these types of models are simplified using Thevenin equivalents. Finally, the abstract models include mathematical methods to explain the battery behavior. In this category the stochastic models based on Markov chains, analytical methods that use equations to explain part of the chemical behavior are included [13].

Different factors have a direct impact on the overall performance of the ESD, and some can be controlled by the user, while others cannot. The type of discharge-charge cycle, temperature, storage conditions, and pressure affect the aging of the ESD, and the atmospheric temperature are related to the performance [14]. The degradation caused in the ESD affects the capability of storing energy, in others words, as the ESD degrades the amount of energy that can be stored is less than when it is new. As mentioned before, one of the reasons that causes the aging effect is the type of discharge-charge cycle. For instance, on lithium-ion (Li-ion) batteries, the capacity fades due to the loss of active lithium ions due to a solvent reduction reaction [15]. For this reason, the authors proposed a model that control the required DoD by manipulating discharge time, and that the discharge voltage is estimated as a function of the cycle number. In this regard, a generalized charge-discharge model based on the loss of the active lithium ions due to electrochemical solvent reduction at

anode/electrolyte interface [16]. The way an ESD is charged and discharged has also an impact on the aging. For instance when discharging or charging, the higher C-rate, the less available cycles [17]. Figure 3 shows the different percentages of the capacity fade for different discharge rates. It can be noticed that as the higher value of C-rate, the more the degradation.

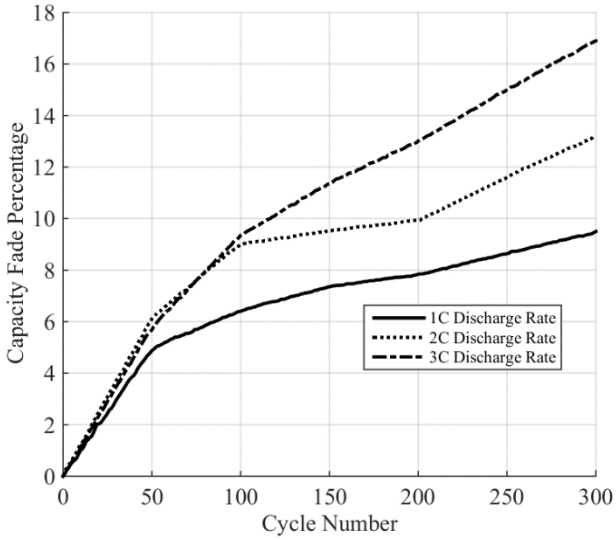

Figure 3. Capacity fade of Sony US 18650 batteries under different discharge rates [17].

Figure 4, Figure 5, and Figure 6 show results that demonstrate how a larger C-rate value have a direct impact on the electric values typically measured.

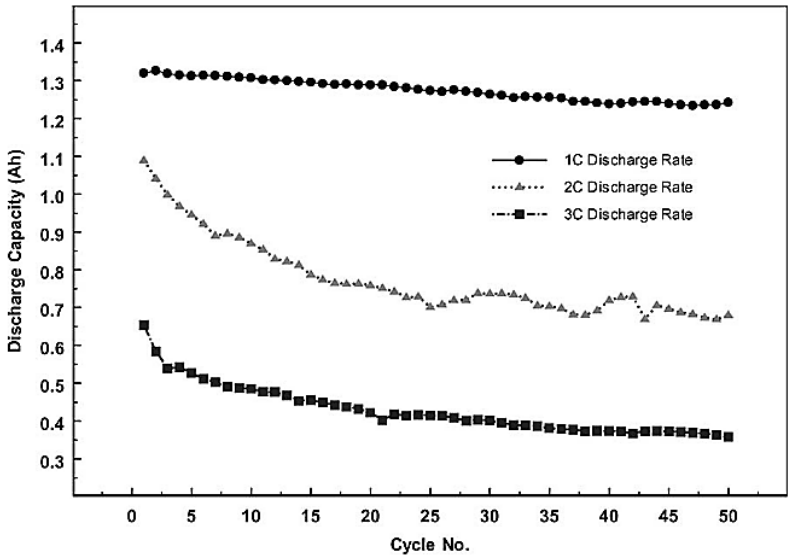

Figure 4. Discharge capacity of Sony US 18650 batteries as a cycle number function [17].

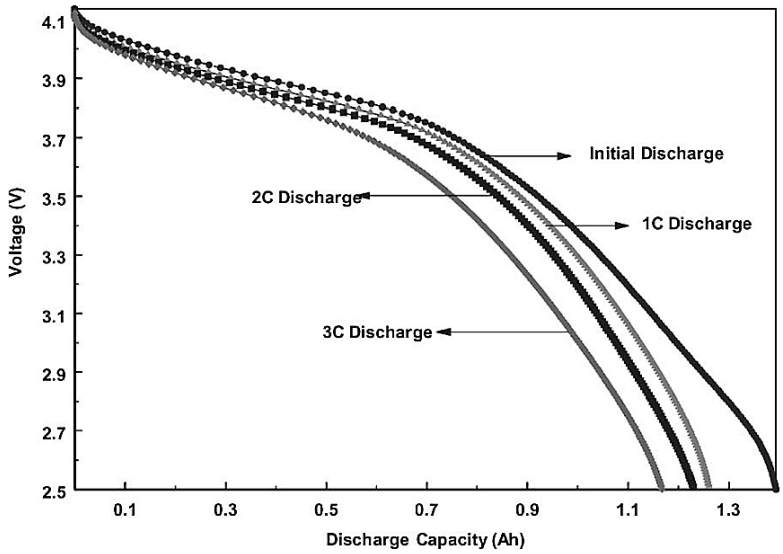

Figure 5. Discharge voltage profile of new and used batteries cycled up to 300 times under different discharge rates [17].

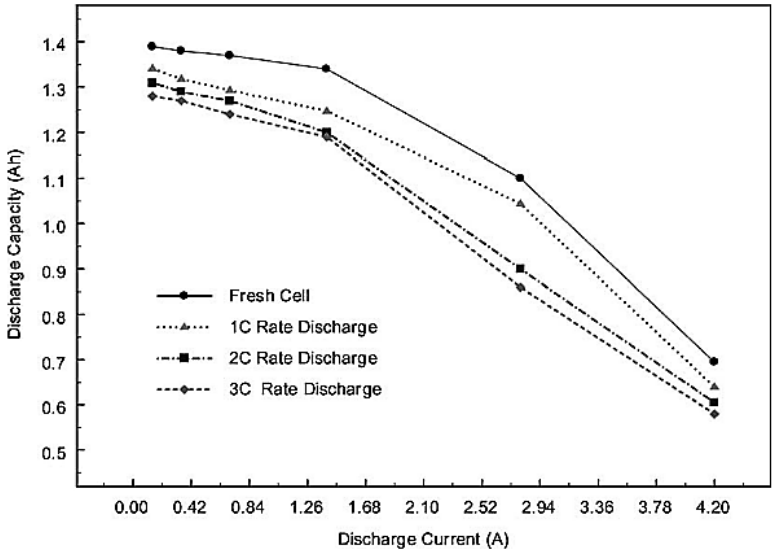

Figure 6. Rate capability of new and used batteries cycled up to 300 times under different discharge rates [17].

Semi-empirical approaches for the capacity fade modeling of Li-ion cells are also possible [18]. This way the testing can be done in a less expensive way than the electrochemical models.

Similar results were obtained in [12]. In this case, a new term must be explained: the internal impedance or resistance. The simplest battery model is the one described with a Thevenin

equivalent. Usually this resistance is used to explain all the losses due to heat, chemical reactions, wear and age. The following figures show how the internal impedance changes under different circumstances as the amount of cycles increases. Figure 7 shows how when the C-rate is increased the internal impedance also increases. This has an effect on the SOH, since the same value of impedance is achieved for a smaller number of cycles. Similar to this, Figure 8 shows that when the DoD is larger, the internal impedance increases for a less amount of cycles. Figure 9 explains the same effect as the previous two figures, but when the temperature is the variable under analysis.

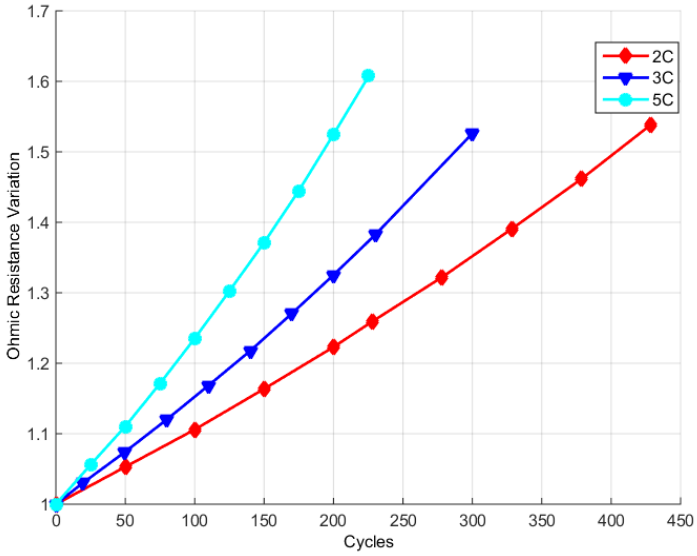

Figure 7. Resistance variation for different values of C-rate [12].

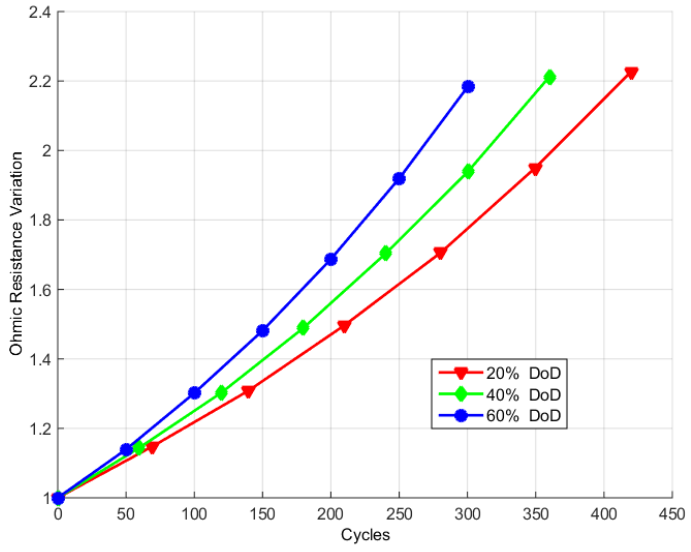

Figure 8. Resistance variation for different DOD cycles [12].

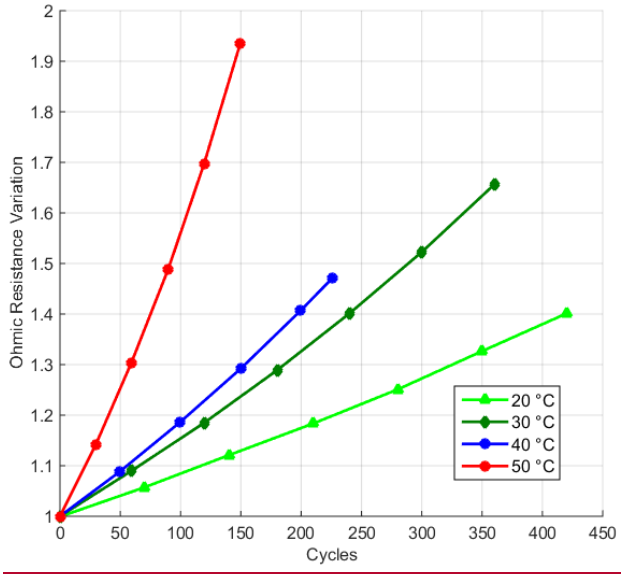

Figure 9. Resistance variation for different temperatures [12].

The battery life depends on the way it is operated, this also includes the SOC. On [19], the number of cycles is shown as a function of the SOC swing and the average SOC, since the same value of SOC swing can be reached with different starting and finishing values. Figure 10 shows their results. The horizontal axis can be interpreted as the battery's capacity, and the 0.2 value is equal to the point when the battery reached the point of 80% the original capacity. It becomes clear that for lower values of SOC swing the amount of cycles is higher. On [19], the authors propose that the SOH degradations is caused by larger values of SOC swing and larger values of the average SOC.

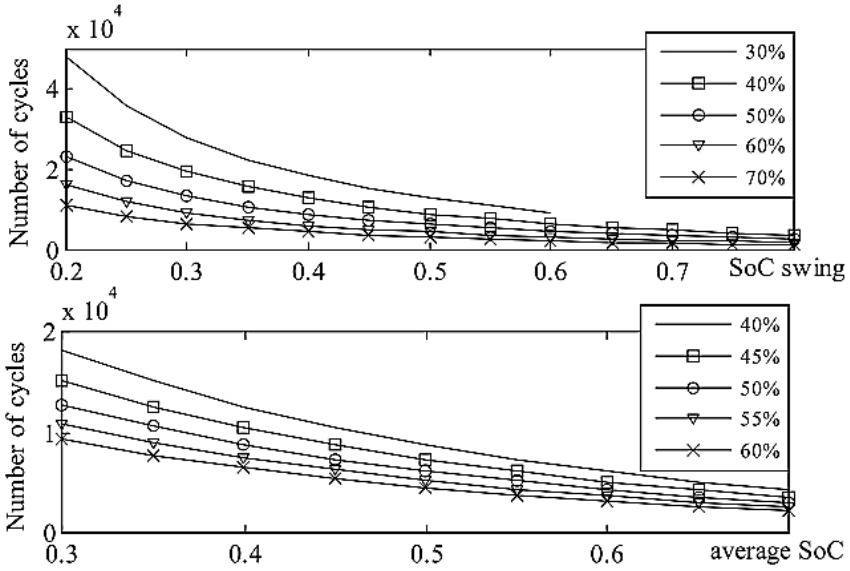

Figure 10. SOH degradation as a function of the SOC swing and Average SOC [19].

A similar result is provided by [20], but extended to different technologies of storage systems. Figure 11 shows that the number of cycles increases for lower values of SOC swings.

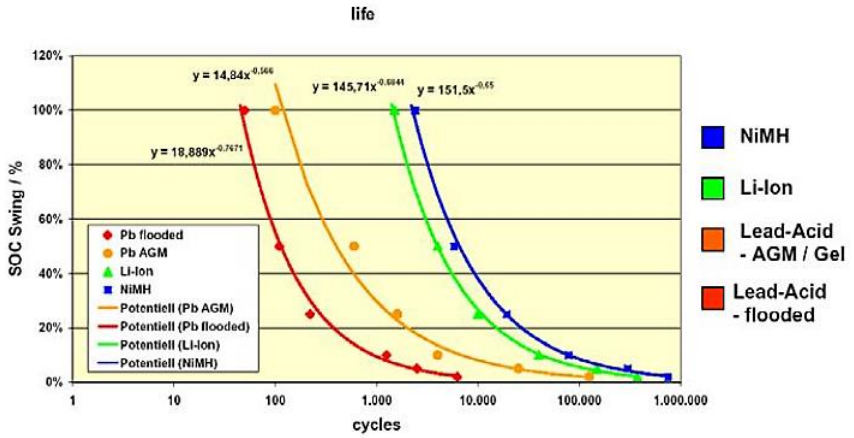

Figure 11. Battery Life as a Function of the SOC Swing [20].

2.4 Structure of State of Health Degradation Models

When working with ESDs, considering the information regarding the SOC or the SOH in an independent manner is not always enough. For this reason it is relevant to combine different techniques to estimate both characteristics and have a clear picture of the real situation. For instance, the owner of an electric vehicle would like to know the SOC on an everyday basis, but the SOH would become important when it is time to replace the car or just the battery pack. In the case of the current research proposal, since the ESD is going to be used for different services on a power network, the user would like to know the SOC in order to determine the short-term strategy, and the SOH is helpful in order to understand how the short-term strategies are degrading the battery and this way making long-term decisions in order to maximize the revenues.

Different methods and techniques have been developed and validated for the measurement of these characteristics (SOC and SOH) and some of these methods are intended for a specific type of ESD. On [21], a general structure for the estimation of the SOC and SOH was proposed. The results were demonstrated at a nickel manganese cobalt (NMC) pouch cell, but extended to any type of cell chemistry.

Another effort was done by [22] to estimate the SOC and SOH for Li-ion batteries. In this case, the SOC is determined through a first order resistor-capacitor (RC) model and the degradation of the battery is quantified with an Extended Kalman Filter (EKF). In this case the SOC is estimated online, and the SOH is updated offline.

Most of the efforts are oriented to determine a model for the SOC since it is a short term decision and in many applications determining the RUL is not important since the batteries are available everywhere and the prices are reasonable. However, there are several applications such as electric vehicles, unmanned vehicles (space or aerial or terrestrial), or grid storage where the replacement cost of the batteries or even the cost of the equipment itself is high and the need of a SOH degradation model becomes imperative [23].

The degradation of a battery can be modeled by the Coulombic efficiency, denoted with the greek letter η. This is defined as the fraction of the prior charge capacity that is available during the following discharge cycle [9]. Equivalently, it can be defined as the ratio of charges that enter the battery during charging compared to the number that can be extracted from the battery during discharge [24], and depending on the model there can be one efficiency for charging and another one different for discharging. This efficiency is affected by the depth of discharge and the temperature at which batteries are stored and operated. Figure 12 shows the degradation of battery capacity for different values of Coulombic efficiency.

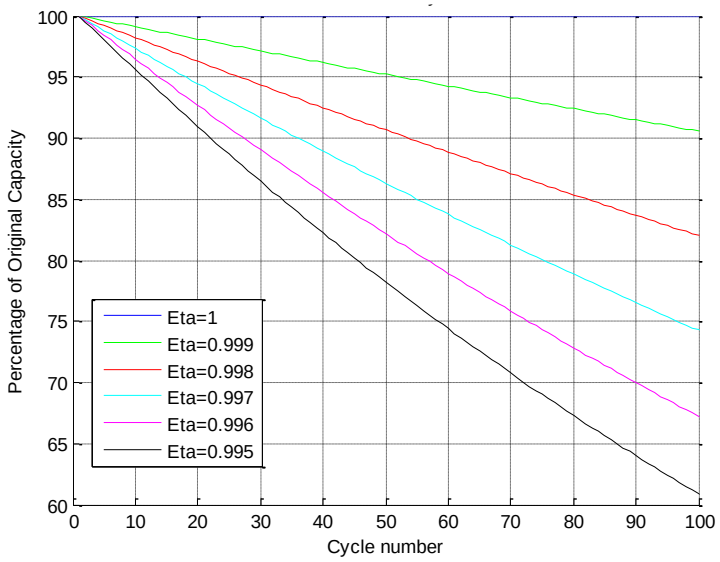

Figure 12. Coulomb efficiency effect during cycling [9].

Since the aim of this proposal is to include the effect of the temperature and a dynamic Coulombic efficiency, it is our interest to use a model based on the phenomenology of the degradation process of a battery or ESD. In this regard, a first model was proposed in [23] based on the work performed by [25]. The discrete space-state model is given by Equation (1).

$$\begin{cases} x_1(k+1) = \eta x_1(k) + x_1(k)x_2(k) + \omega_1(k) \\ x_2(k+1) = x_2(k) + \omega_2(k) \end{cases}$$
$$y(k) = x_1(k) + v(k) \qquad (1)$$

The state $x_1(k)$ indicates the SOH of the ESD, $x_2(k)$ corresponds to an unknown model parameter used to adjust minor differences with respect to the expected behavior (which are specific to the monitored ESD). In other words, $x_2(k)$ is a parameter used to explain the actual degradation trend with respect to the expected $x_1(k)$, under the concept of artificial evolution [2], and $y(k)$ is the measured SOH. The process noises and the observation noise are zero-mean Gaussian noise values.

A similar approach, but based on a particle filter framework was presented on [26]. In this work, the EoL of the batteries is estimated using this algorithm. In [26], the Coulombic efficiency is also incorporated on this model, and the EoL can be predicted using Equation (2) which corresponds to the measurement model equation:

$$C(k+1) = \eta C(k) + \beta_1 e^{\left(\frac{\beta_2}{\Delta t}\right)} \tag{2}$$

where $C(k)$ represents the charge capacity, Δt is the rest period between two consecutive time instants, β_1 and β_2 are model parameters to be determined. The model described by equation (2) is similar to the one proposed in [27]. A simulation result from this methodology are shown in Figure 13. The estimated values are obtained through a particle filter framework and then it is compared with the actual values and the ones obtained with equation (2).

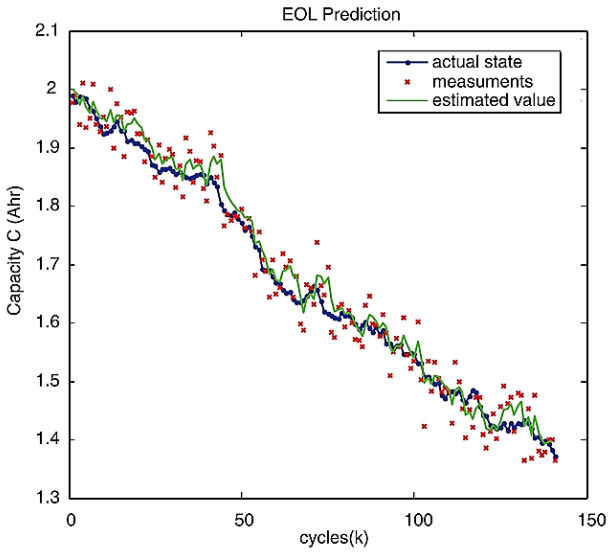

Figure 13. End of life prediction [26].

A completely different approach, was performed by [28]. In this case, the authors propose the concept of Sample Entropy (SampEp) used as an input feature to train two systems: one based in Support Vector Machines (SVM) and the other one is based on Relevance Vector Machines (RVM). The method proposed on [28] intends to predict the SOH of the battery using the nominal capacity at different periods of time. Since this method includes a learning algorithm, it requires to be validated before is implemented. Figure 14 shows the curves of the real and validated data after using the SVM technique.

When real data is available some algorithms incorporate the real measurements as a source of reliable information in order to estimate with a certain degree of accuracy the EoD or the EoL (depending on the application). Figure 15 shows the prognosis results with a 95% accuracy bound when the SVM and RVM schemes are used.

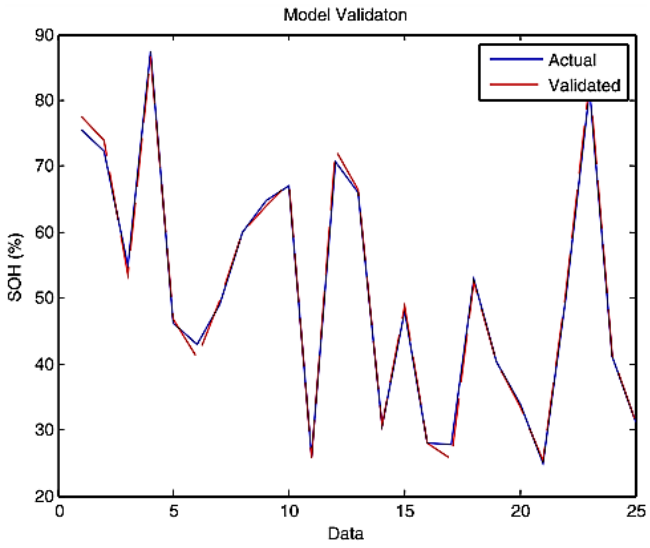

Figure 14. Validation process of SVM training for a dataset [28].

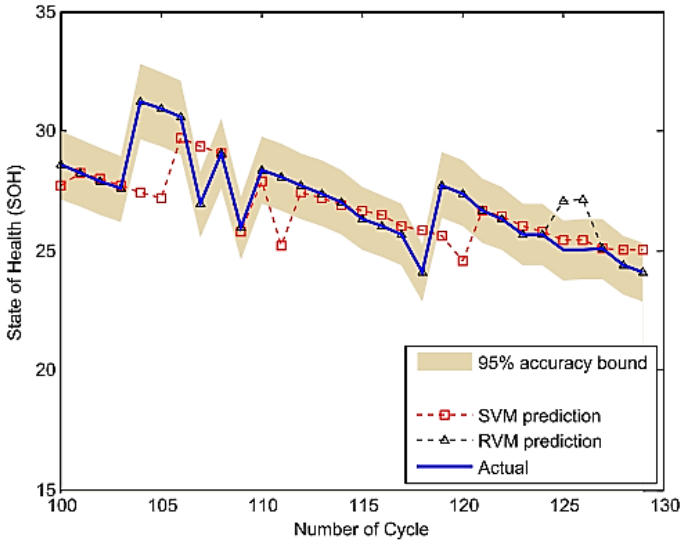

Figure 15. Battery health prognosis by SVM and RVM for a dataset [28].

In [29], a SOH degradation model is proposed considering data from the charging state. The features considered from the charging data were the length of constant current charge time (CCCT) and the constant voltage charge time (CVCT). Their model is able to predict that as the battery degrades the CVCT will increase and the CCCT will decrease. On their effort, an

experimental procedure was performed on 3 different prismatic batteries. The other two variables considered for the model are internal resistance and the capacity.

It has been mentioned that the internal resistance plays a key role in the SOC model and in the SOH degradation model, and different models have been developed in order to estimate its value. This task is not easy due to the nonlinearities present due to the internal chemical processes. In [30] a frequency-based method to determine the internal impedance. In this case, the authors prove that there is a direct linear relationship between the internal impedance with the SOH, in the frequency domain.

A different point of view is presented on [31]. The authors propose a SOH degradation model based on Ampere-hour throughput. This is defined as the current throughput and represents the energy delivered or stored in the battery. The Ampere-hour throughput can be described as a function of the open circuit voltage (OCV) of the battery (called Ah-V), and the intention is to use unique characteristics of the Ah-V in order to estimate the SOH as the battery ages. In this approach, the Ah-V function is generated using constant current charge and discharge profiles. Figure 16 shows an example of the curves obtained for one data set. The authors propose a quadratic fit in order to obtain the SOH value.

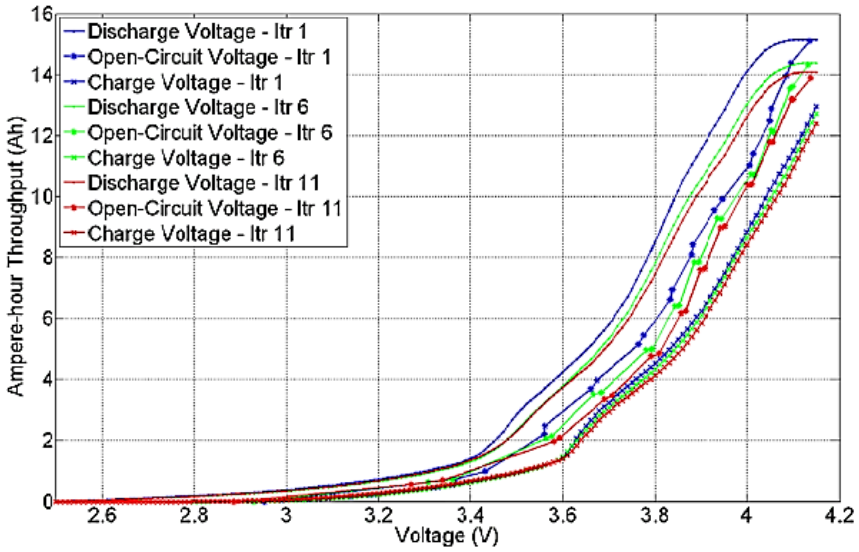

Figure 16. Ampere-hour Throughput as a function of the open circuit voltage for a dataset [31].

An analytical approach based on recursive least squares was proposed by [32]. The authors use this technique to determine certain parameters to estimate in real-time the SOC and SOH of a Li-ion battery used for an electric vehicle. The discharge profiles are designed to meet with different driving patterns. In this experiment the temperature was a controlled variable due to the battery cycler used in the process. The SOH degradation model is based on the online identification of the internal resistance.

2.5 Effect of the Temperature on Li-ion Batteries

Temperature conditions have two different effects on Li-ion batteries. On the short term, the amount of energy that the battery can deliver or store can be constrained if the temperature conditions are not adequate even if the battery is not degraded. Moreover, on the long term, if a battery is used under extreme temperature conditions the RUL of the battery will be reduced.

2.5.1 Effect of the Temperature on the Discharge Process of Li-ion batteries

When including the temperature to a SOC or SOH degradation model, one of the main concerns and drawback for any attempt to scale-up lithium-ion cells to a larger size desirable for high power applications is the non-uniformity that can be found [33]. Battery systems require a trade-off between overheating the large size cells and the cost of insulating or cooling this type of cell array.

Similar to the C-rate, the operating temperature of the ESDs also has an impact on the capacity. Experimental effects relate this effect to the loss of active material, degradation of the electrodes and decomposition of the electrodes [34]. The authors explain, using a chemical point of view, why the capacity fades at different temperatures. For instance, their attempt includes the estimation of how much of the lithium is faded at the anode and cathode of the battery.

Numerous efforts to include the effects of the temperature on the SOC can be found in the literature. In [35] and [36] two different SOC models, that include the effect of the temperature on the internal impedance are proposed. The models are different but their focus is mainly the same. Even though is not a SOH degradation model, it is important to keep this in mind since in the long term, the SOH of the ESD is affected by the SOC and how the battery is being used.

In [37] another electrochemical model was developed. In this case a simple model was proposed by measuring two variables: output voltage and temperature. The authors explain from a chemical point of view how the temperature affects the fading capacity of the batteries based on Arrhenius equation, described by:

$$\Phi = \Phi_{ref} e^{\left[\frac{E_a(\Phi)}{R}\left(\frac{1}{T_{ref}} - \frac{1}{T}\right)\right]} \tag{3}$$

In this case, Φ represents the battery chemical reaction rate, $E_a(\Phi)$ is the activation energy and its magnitude determines the sensitivity of Φ to temperature, R indicates the gas constant and the subscript ref is an indicator that the value should be used at the reference temperature. A similar effort was presented in [10] to explain the capacity fade on lithium-ion batteries.

Another model that includes the effect of the temperature is proposed in [38]. In this case, the model corresponds for the SOC, but it has been vastly explained that the SOC has an effect on the SOH. In this case, the authors propose a methodology to estimate two factors that are used to compensate on the model the effect. One of the factors compensate the discharge current and the other compensates the temperature. Figure 17 and Figure 18 are an example of how the compensating factors can be obtained.

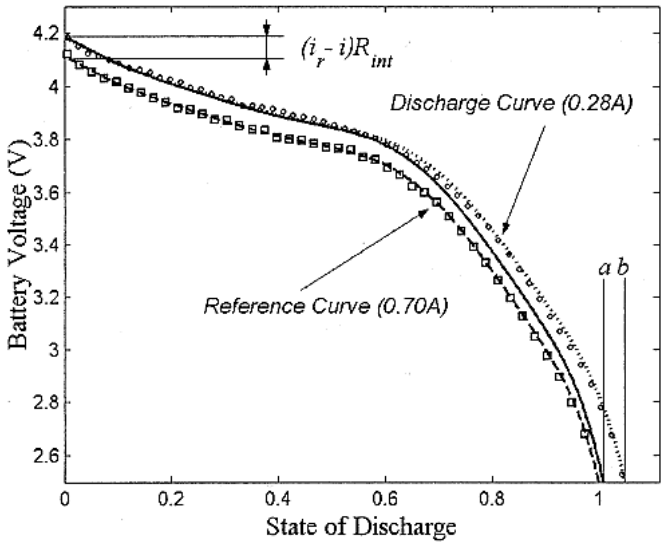

Figure 17. Rate factor for a discharge current with respect to the reference curve [38].

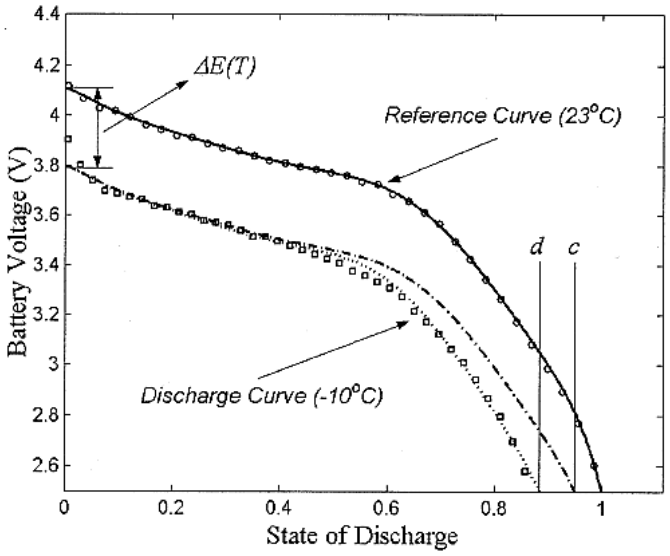

Figure 18. Temperature factor and the temperature-dependent potential-correction term [38].

The rate factor α can be calculated as a/b while the temperature factor β is obtained in a similar way c/d. It is important to keep in mind that these values are dependent on different conditions and they require to be recalculated if something changes, for example the discharge current or the temperature.

Continuing with this approach, Figure 19 shows the rate factor α when the discharge current is referenced at 0.7 A corresponding to a 0.5 C-rate. Figure 20 shows the temperature factor β when the reference temperature is 23°C.

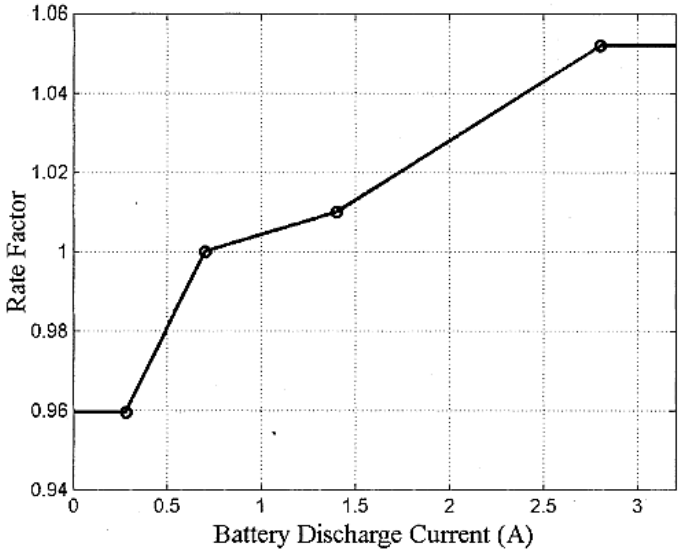

Figure 19. Rate factor α for the Sony US 18650 Li-ion battery at a 0.5 C-rate [38].

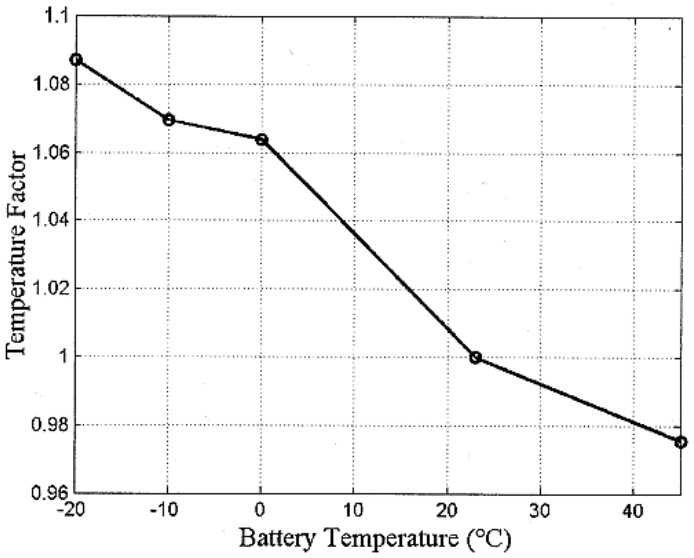

Figure 20. Temperature factor β for the Sony US 18650 Li-ion at reference temerature of 23 °C [38].

It is important to mention that if the operating conditions change, the curves have to be obtained again.

2.5.2 Effect of the Temperature on the Degradation Process of Li-ion Batteries

Another attempt to include the temperature effect, but in this case applied to a SOH degradation model, was presented on [39]. This effort is based on an electrochemical analysis, relates the discharge capacity, output voltage, average drawn current, battery temperature and the cycle count.

As mentioned before, temperature is one of the different variables that have a major effect on the degradation of ESDs. However, most applications do not consider this effect since there is a large portion of the temperature range, where the temperature is considered as an ideal range [40]. Figure 21 shows that the ideal range goes from about 10 °C to 60 °C. It can be easily determined that at a certain temperature range (the ideal range), the difference in cycle life is almost none, but outside this range, the differences change abruptly. In this regard, incorporating a temperature dependent factor for the SOH degradation model of the Li-ion battery becomes necessary.

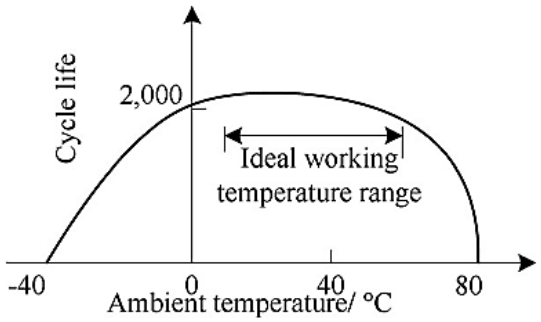

Figure 21. Effect of the operating temperature on the cycle life of the lithium-ion battery [40].

A SOH degradation model that includes the operation temperature was proposed in [2]. This model is based on the work performed by [23] where a SOH degradation model that includes a self-regeneration phenomena was proposed. This model incorporates the reaction rate of a battery described by the Arrhenius equation due to the temperature effect. Equation (18) describes the SOH degradation model.

$$\begin{cases} x_1(k+1) = e^{\alpha\left(\frac{1}{T-\beta}-\frac{1}{T_{ref}-\beta}\right)} x_1(k)\big(\eta + x_2(k)\big) + \omega_1(k) \\ x_2(k+1) = x_2(k) + \omega_2(k) \\ x_3(k+1) = \delta\big(U(k)\big)\omega_{31}(k) + \delta\big(1-U(k)\big)\big(x_3(k)\omega_{32}(k)\big) + \cdots \\ \qquad\qquad +\delta\big(2-U(k)\big)\big(x_3(k)\omega_{31}(k)\big) \end{cases} \tag{4}$$

$$y(k) = x_1(k) + \Big(\delta\big(1-U(k)\big) + \delta\big(2-U(k)\big)\Big) x_3(k) + v(k)$$

In the previous model, the temperature has to be used in Kelvins in order to obtain coherent results. The first two states are same as the ones defined in (1). The third state is linked to the increment of the available energy due to the regeneration phenomena. The noises ω_{31} and ω_{32} were characterized in [27], where ω_{31} is a log-normal noise that characterizes the amount of SOH added in the event of successive regeneration and ω_{32} corresponds to the typical damping ratio of self-recharge phenomena. The noise ω_{32} distributes as uniform over the range of $[0.75, 0.85]$. The operator $\delta(\cdot)$ is used to represent one of the following cases of consecutive regeneration is present: 0, 1, 2 or more. The other parameters have values of $\alpha = -5.1593$ and $\beta = 260.9565$ (Pola, 2014).

2.6 Degradation Process Models that Include the Discharge Current

One of the Li-ion battery degradation models that explicitly includes the C-rate was proposed in [41]. In this case, the authors study the performance of the vehicle-to-grid (V2G) interaction through a mathematical model of the battery, where the model parameters are adjusted through genetic algorithms. The model is based on an electric equivalent and a

decreasing capacity approach of the processed energy at different C-rates. Then the results are compared to the original datasheet, in order to obtain the capacity degradation. This degradation is reported to be proportional to the applied C-rate.

In [42], the authors propose an empirical model for the capacity reduction in electric vehicles under different operating conditions. The main idea is to optimize the lifespan of the battery by maintaining a low SOC, avoiding sudden temperature changes and, finally, by charging the battery to a certain SOC level that is just enough for the next trip. However, this constraint is difficult to meet since, in a more realistic scenario, it is not always possible to accurately plan or know the next trip. Also, this method does not inform about the degradation of the battery in terms of the number of cycles during the lifespan. Another model is proposed in [43], where the authors present a model that relates the increase in degradation with the increase in C-rate, analyzing different temperature conditions. The proposal corresponds to a mathematical pseudo-bidimensional model that integrates a solid electrolyte interface growth model.

All these efforts represent important steps towards the characterization of the battery SOH as a function of the manner in which the ESD is operated. However, their application on SOH prognostic approaches, where the main objective is to predict the moment in which the device has to be replaced, is still limited. Our proposal intends to provide the means to improve our prediction capabilities in terms of the evolution of the battery SOH as a function of future discharge current rates.

2.7 Cycle Definition of an Energy Storage Device when Operated

The most common definition for a cycle of a battery can be established as the process of discharging a fully charged battery and then charging it again. Clearly, the amount of cycles will depend on the manufacturer and the type of battery. When trying to convert the cycles into a time unit, the task becomes more complex since there are variables that influence the duration of the cycle, for example: temperature, depth of discharge, actual state of health of the battery, etc.

However, this definition can be slightly different depending on the manufacturer. On its website, Apple Inc. defines a cycle as the process in which a fully charged battery is used and 100% of the battery's capacity is discharged, regardless if there has been a partial charge in between [44]. Figure 22 was captured from the website and tries to explain this definition.

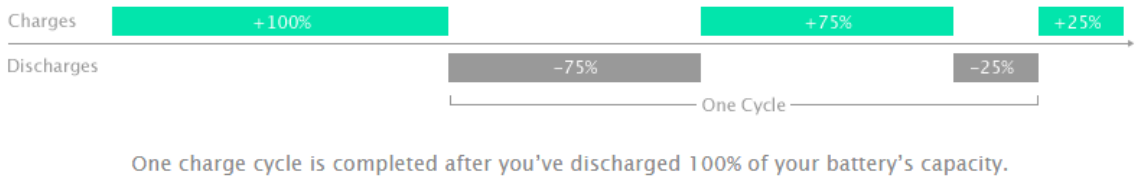

Figure 22. Charge cycle definition according to Apple, Inc [44].

Most datasheets provided by manufacturers include information of the life cycle under full discharge cycles and controlled temperature settings. Usually the amount of cycles is given to a full discharge or a fixed DoD. These cases are considered to be the worst case scenarios, but there are elements that are not accounted for. For instance, in the previous sections, some studies regarding the electrochemistry of the batteries were discussed and show to have a major impact in the capacity fading when the DoD was larger, or even when the starting point is different. In other words, if a datasheet establishes certain amount of cycles under a given DoD (different to 100%), the manufacturer is assuming that the initial capacity is 100%, but the amount of cycles would be different if the initial capacity is for example a 90% or 80%. This means, that the battery has the same SOC swing but different swing range, and therefore the degradation is different. This type of behavior is a little bit unrealistic. Most of the applications have different DoD and power requirements, making a difficult task to determine the real SOH of the batteries.

In [45], an effort was done to account for the behavior of the cycle life of lithium-metal-polymer batteries. In this case, the temperature was not a key factor since the battery is operated in a controlled environment. Their study considered the SOC under different DoD values. Figure 23 shows how the battery loses its capacity as the DoD is higher.

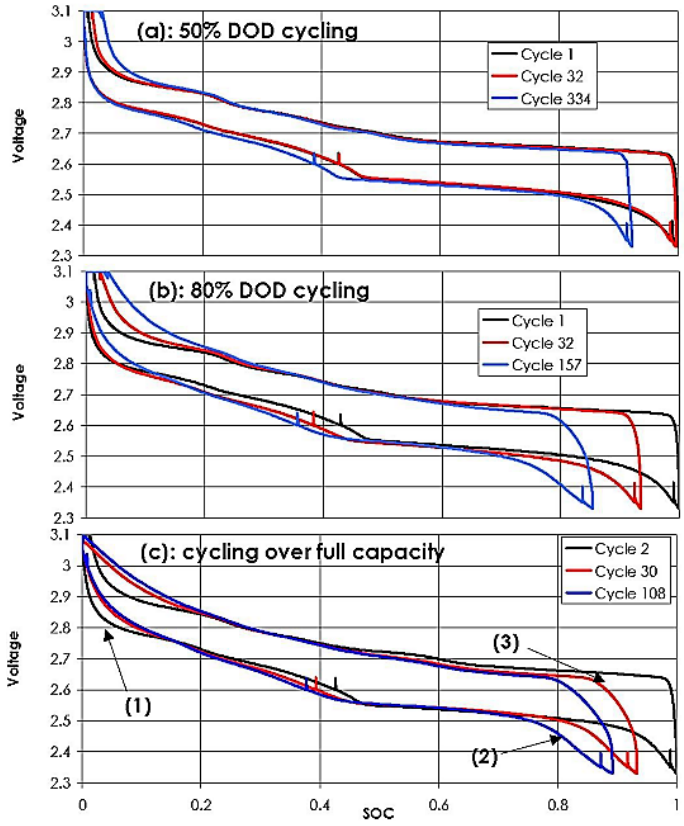

Figure 23. SOC evolution for different values of DoD. (a) 50% DoD. (b) 80% DoD. (c) 100% DoD [45].

Also, in Figure 24, the voltage at the end of a cycle is shown for different values of DoD. Similar to what has been previously discussed, as higher the DoD the lower the voltage, meaning a shorter SOC and more degradation per cycle.

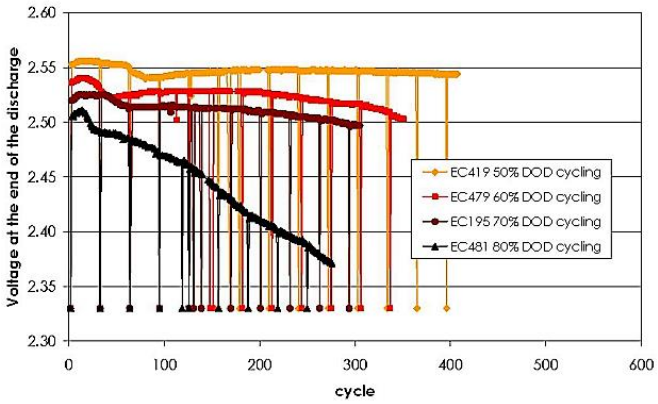

Figure 24. Evolution of the end voltage versus DoD cycling at a temperature of 60 °C [45].

On this effort, also a definition for cycle was proposed. The authors propose a term defined as the *Equivalent Full Cycles* as the relation between the cumulative capacities discharged divided by the rated capacity of the battery. This relation is another way to express the Coulombic charges involved in the charge-discharge process.

When dealing with partial discharges and charges, [46] proposes a SOH degradation model based on the studies performed by [47]. This model is based on two observations: the SOH degradation rate is a function of the SOC swing and the average SOC (the average SOC corresponds to the sum of the highest and lowest value of the SOC in one cycle, and divided by two). However, in this case the definition of cycle is also different from the traditional case. A cycle is defined as a charging process where the SOC moves from a lower value to a higher value and then is followed by a discharging process (moving from SOC value to a lower SOC value). Figure 25 is an example of the first observation. In this case, two SOC profiles with the same time duration are shown. The profile of the left has three cycles with a SOC swing of 20% and an average SOC of 50%. The profile of the right has only one cycle with a SOC swing of 60% and an average SOC of 50%. However, the figure on the right has a higher SOH degradation due to the SCO levels although it only has one charge/discharge cycle when compared to the figure of the left.

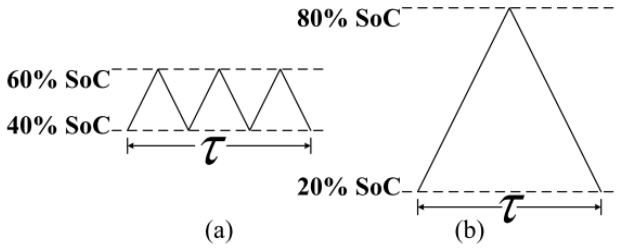

Figure 25. Illustrative example of Observation I. (a) Case with three cycles. (b) One cycle. [46].

The second observation is called the decoupling of the cycles. The main idea behind this observations consists on separating the cycles into equivalent cycles that are easier to interpret. Figure 26 explains the basic idea of how this observation is performed.

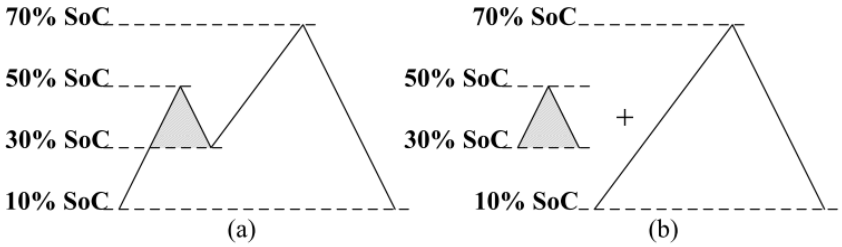

Figure 26. Illustrative example of Observation II. (a) Real usage profile. (b) Decoupled profile. [46]

After performing this decoupling the authors propose that the degradation of the period could be obtained by a recursive equation of this form:

$$SOH_{\ period} = SOH_{period} + SOH_{cycle}(SOC_{swing}, SOC_{avg}) \quad (5)$$

Unfortunately there is no more information regarding this method and how it can be implemented.

Since the SOC swing and SR have a direct impact on the SOH of the batteries, in [19] an efficient algorithm that aims to extend the overall cycle life. The model used in this approach is adapted from the one proposed in [47]. For this model, the SOH degradation depends on the average SOC and the SOC swing, and the cycles are computed with the effective throughput number. This number is a calculated with the integral of the charging/discharging current and the nominal capacity of the battery.

2.8 Energy Storage Devices as Part of Large Scale Distribution Systems

Even though the basic concepts behind the design of the Li-ion battery systems is the same independently from the battery capacity, when incorporating this technology to a large-scale systems, special attention is required. It is common to have storage systems as part of microgrids working in an isolated manner or as part of a larger network, and operating with renewable energy sources. This way the excess energy can be stored for future use. The cost for these storage systems is considerable so making the more out of the system is what every user would like. In this case, depending on the user requirements, different strategies can be proposed.

One of the major concerns when working with the large scale systems is the sizing of the storage. According to [48] a trade-off between the battery size and conditions due to the photovoltaic (PV) variation is present. On their effort, an autonomous microgrid working with PV and diesel is analyzed. In order to design the battery system, the authors considered the amount of carbon dioxide exhausted from the diesel engine and the frequency deviation when the capacities of the PV panels and the storage systems were changed. In this model, the minimum SOC is established at 30% and the maximum is al 90%. This means that the swing range is always 60%.

A similar procedure was proposed by [49]. In this proposal, the authors guarantee a highly reliable source of power, based on the optimal number of PV panels, wind turbines and storage units that ensure the total cost is minimized. The authors considered two efficiencies, one for charging and the other for the discharge process. The charging efficiency is a value between 0.65 and 0.85 depending on the available current, but the discharge efficiency is fixed at 1.Also, instead of considering the degradation of the battery, the authors included a total number of battery replacements for a 20 year period. The proposed model is applied to a location in Calabria, Italy.

Another effort for the determination of the optimal number of solar panel and batteries to be used in a PV-wind microgrid [50]. The weather and consumer data are from a certain area in Romania. Similar to the other cases, this approach gives an optimal result for the quantity of solar panel and batteries, but does not consider the long term degradation of the battery.

A case study in Great Britain is presented on [51]. In this case, the idea is to evaluate the contribution of a storage system when operating on the grid. The investment and storage capacity are optimized while the operation cost is minimized. As the other cases, there is no degradation model considered for the storage system.

A Self-adaptive Bee Swarm Optimization (SBSO) algorithm is applied to optimize the operation strategies and capacities of the storage system in a microgrid is proposed in [52]. The authors propose an extensive economical and weather analysis but unfortunately the battery model does not include the degradation effect.

In [53] a similar problem is approached. However, in this case, the way of looking at the problem is slightly different. In this case, the size of the storage system is given and the intention is to balance the cycle life of the batteries. The battery SOH is considered using the model proposed in [47]. The authors propose different techniques for balancing the cycle life and then, a comparison was performed. The results show that the cycle life can be extended up to 76% when applying a cooperative framework named Flexible Distribution of Energy and Storage Resources (FDERS).

Nevertheless, balancing the power supply and demand is a complex process [54], and according to the authors there needs to be some reengineering applied before the Li-ion are fully functional on grid applications. The authors present the advantages and disadvantages for several types of energy storage technologies.

An extensive approach that examines literature that involves analysis of life cycles, costs (capital, maintenance, operational and replacement) is presented on [55]. The authors study the main imperatives for the adoption of electrical energy storage systems:

- Meeting demand and reliability in grid's peak hours.
- Liberalized electricity markets.
- Intermittent renewable energy.
- Distributed generation and smart grid initiatives.

In [56], [57] the authors explain the benefits of incorporating energy storage systems when operating as part of a solar generator and a wind turbine into the energy grid. Some of the services they describe in the operation are: ramp rate control, frequency control, and reactive

support. The importance of the storage system in enhanced since the weather conditions can change abruptly and the customer can have interruptions on their service. As some of the previous references, the authors base their effort on explaining how the grid and battery should operate, but the storage system degradation is not considered.

3. Methodology

3.1 Overview

This chapter is intended to explain the different methods that were developed to characterize the degradation process of a Li-ion battery and later applied to a case study. The first section proposes a model for the degradation process when different discharge currents are used. The model is defined using the information available on the literature, and the validated with two sources of information: a custom designed experiment, and online public datasets available from NASA Ames repository. The next section explains a methodology that incorporates the use of K-nearest neighbors to explain the degradation process when the batteries are used at any combination of SOC values. The final section of this chapter, approaches the use of similarity based modeling (SBM) to characterize the degradation process for any combination of discharge current and SOC values. Also, the effect of the temperature is explained in terms of the usable capacity.

3.2 Characterization of the Degradation Process of Energy Storage Devices when Discharged at Different Current Rates

This research uses data provided in (15), where the authors cycled a Sony US18650 1.4 Ah Li-ion battery using different discharge rates (1-C, 2-C and 3-C), at a controlled ambient temperature. After 300 cycles, battery capacities were reduced by 9.5%, 13.2% and 16.9% when using 1-C, 2-C and 3-C, respectively. Figure 1 shows the capacity fade results measured every 50 cycles (please note that actual measurements are connected by straight lines in the figure).

The same information in Figure 3 can be used to build the associated capacity degradation curve (see Figure 27). Capacity fade curves are used by manufacturers to illustrate the battery degradation on datasheets. Typically, capacity fade curves are built by using data from batteries that are discharged under controlled conditions (depth of discharge, temperature, charging and discharging current rates). Although this information is helpful to compare the expected performance of batteries from different brands, it does not suffice to characterize the impact of higher currents.

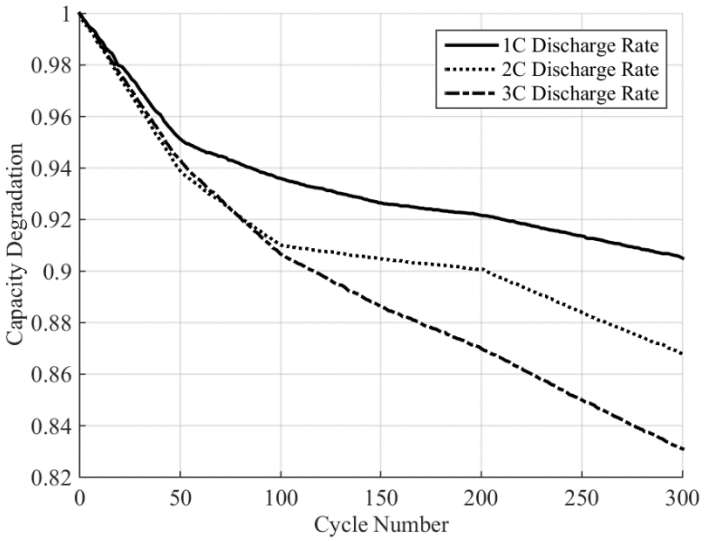

Figure 27. Capacity degradation process for different discharge currents.

As it was previously mentioned, degradation processes can be characterized through the concept of Coulombic efficiency. However, in this research, the intention is to include the C-rate as a variable of the degradation process. It is interesting to note, that all degradation curves shown in Figure 27 exhibit exponential decay regardless of the associated C-rate. We followed this intuition, and used the Curve Fitting Tool from Matlab to fit a two-summand exponential expression, $f(t) = ae^{bt} + ce^{dt}$, to actual degradation data. Figure 28 shows the measured data and the corresponding fitted curve.

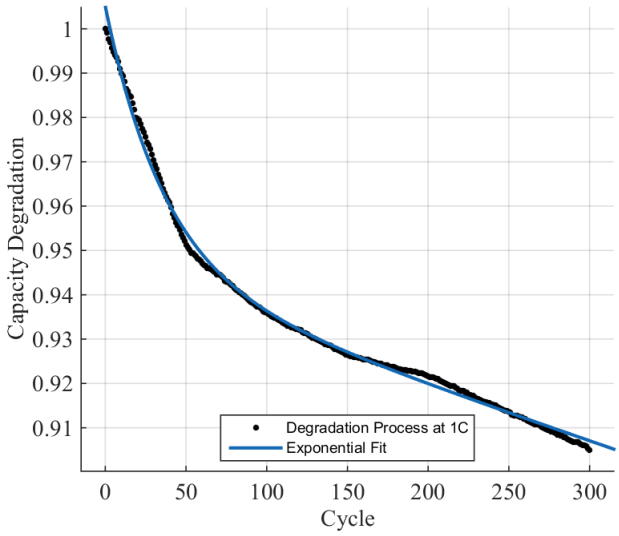

Figure 28. Capacity degradation process and fitted curve at 1C.

Figure 29 and Figure 30 show the individual contribution of each summand in $ae^{bt} + ce^{dt}$. It can be noted that each summand exhibit a different trend. On the one hand, the first summand represents a contribution that decreases exponentially in time, and where differences between diverse discharge rates are almost negligible after 200 cycles of

operation. In addition, the value of the first summand is insignificant in the long term, while it represents about 7% of the total battery capacity during the first operating cycles. On the other hand, the second summand represents an affine function of time, where the slope depends on the battery discharge current. This suggests that this component could be used for better characterization of the degradation trend. Also, it can be stated that while the first summand has a major impact in the short term the second summand has a major impact in the long term.

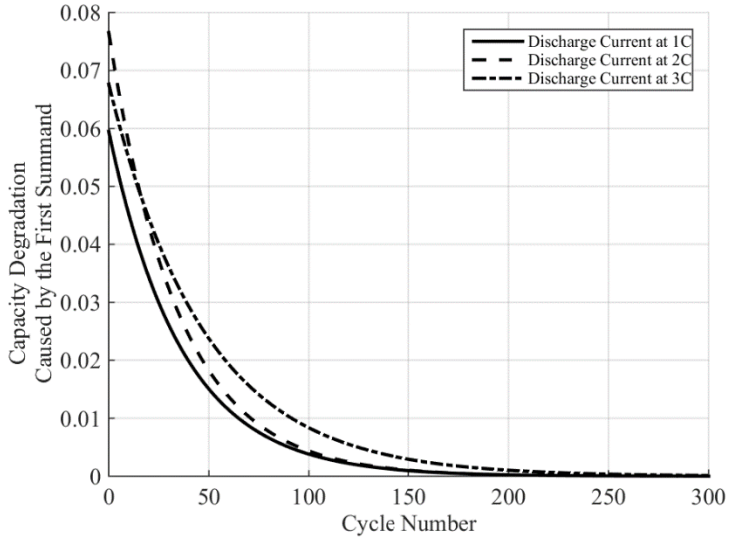

Figure 29. Capacity degradation process caused by the first summand.

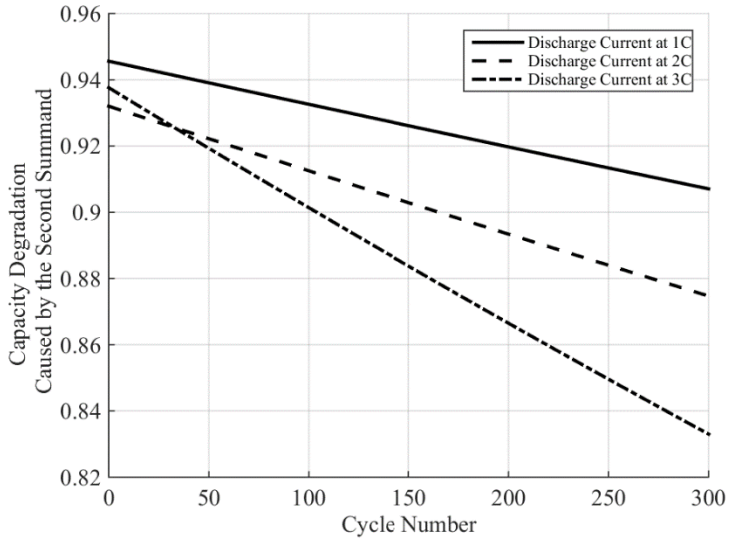

Figure 30. Capacity degradation process caused by the second summand.

3.2.1 Proposed SOH Degradation Model

Given that the degradation process can be modeled as the sum of exponential functions in time, a two-state space equation model is proposed:

$$\dot{\bar{x}}(t) = \begin{pmatrix} b & 0 \\ 0 & d \end{pmatrix} \bar{x}(t) \tag{6}$$

$$y(t) = (a \quad c)\bar{x}(t) \tag{7}$$

Equivalently, the continuous space-state model can be re-written in the following discrete-time form (sampling time equals to 1 cycle):

$$\begin{cases} x_1(k+1) = e^{bk} \\ x_2(k+1) = e^{dk} \end{cases} \tag{8}$$

$$y(k) = ax_1(k) + cx_2(k) \tag{9}$$

The values for the coefficients (mean value and the 95% confidence bounds) obtained through the Curve Fitting Tool of Matlab are shown in Table 1.

Figure 31 summarizes the contributions of each summand in $y(k)$, for three discharge cases, using the mean value of the coefficients. It is known that when a battery is new, its SOH will be 100% (or, equivalently, $y(0) = 1$). The procedure to determine initial conditions for the system states has to consider this fact. In this regard, we propose a step-by-step procedure to compute $x_1(0)$ and $x_2(0)$.

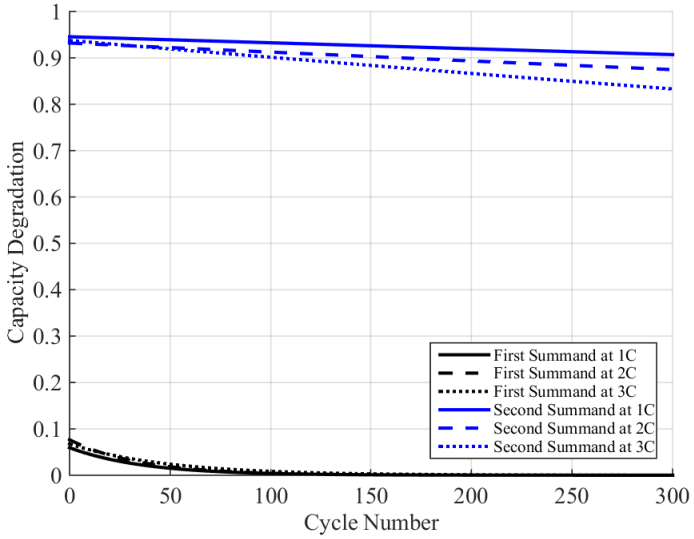

Figure 31.Capacity degradation components.

As mentioned previously, the second summand represents the major long-term contribution in the total value of $y(k)$. For this reason, the procedure prioritizes a reasonable initial condition for the state x_2 :

1. Determine the values of coefficients a, b, c, and d using a fitting tool.

2. Assign $x_2(0) = 1$.

3. Solve for $x_1(0)$, such that $y(0) = 1$.

In the example previously described, we have:

$$\begin{gathered} y(k) = ax_1(k) + cx_2(k) \\ y(0) = 0.06108x_1(0) + 0.946x_2(0) \end{gathered} \tag{10}$$

Fixing the value of $x_2(0)$ equal to 1, and knowing that $y(0)$ is equal to 1, then do as follows:

$$\begin{gathered} 1 = 0.06108x_1(0) + 0.946 \cdot 1 \\ x_1(0) = 0.8841 \end{gathered} \tag{11}$$

Now that the procedure for establishing the initial conditions has been explained, we verify the performance of the SOH model. Given that the curve fitting tool generates mean values and confidence bounds for each model parameter a, b, c, and d (see Table 1), we proceed to generate 10 sets of random coefficients, assign different initial conditions to each resulting model, and compare the evolution in time of the SOH model with actual measured data obtained from [17] (see Figure 32).

Table 1. Mean value and confidence bounds for the model coefficients.

		Discharge Current		
Coefficient	Parameter	1-C	2-C	3-C
a	Mean Value	0.06108	0.07653	0.06763
	Confidence bounds	(0.06084, 0.06132)	(0.07371, 0.07965)	(0.06588, 0.06937)
b	Mean Value	-0.02905	-0.02896	-0.02093
	Confidence bounds	(-0.02931, -0.02879)	(-0.03165, -0.02627)	(-0.02203, -0.01984)
c	Mean Value	0.946	0.932	0.9376
	Confidence bounds	(0.9457, 0.9462)	(0.9292, 0.9349)	(0.9357, 0.9395)
d	Mean Value	$-1.406 \cdot 10^{-4}$	$-2.115 \cdot 10^{-4}$	$-3.943 \cdot 10^{-4}$
	Confidence bounds	$(-1.416, -1.395) \cdot 10^{-4}$	$(-2.25, -1.98) \cdot 10^{-4}$	$(-4.026, -3.86) \cdot 10^{-4}$

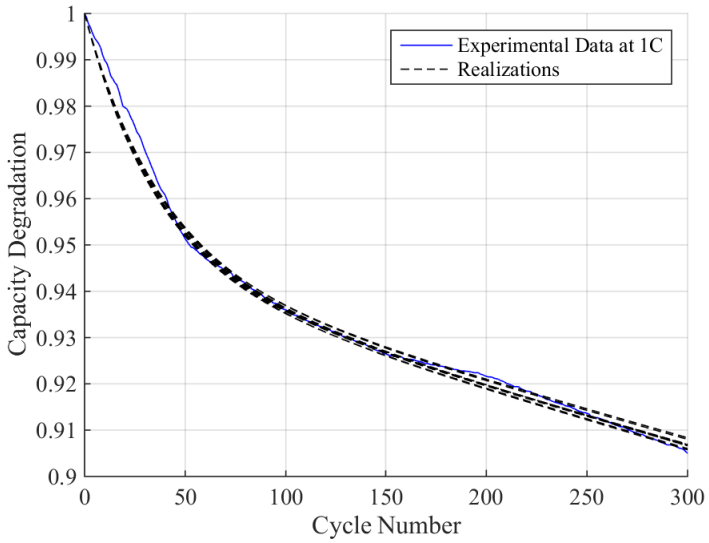

Figure 32. Proposed model generated with random coefficients.

Figure 33 compares the contribution of the first summand $ax_1(k)$ for each realization of random coefficients (and the corresponding set of initial conditions $x_1(0)$ and $x_2(0)$). Note that after nearly 50 cycles, all 10 realizations exhibit basically the same behavior.

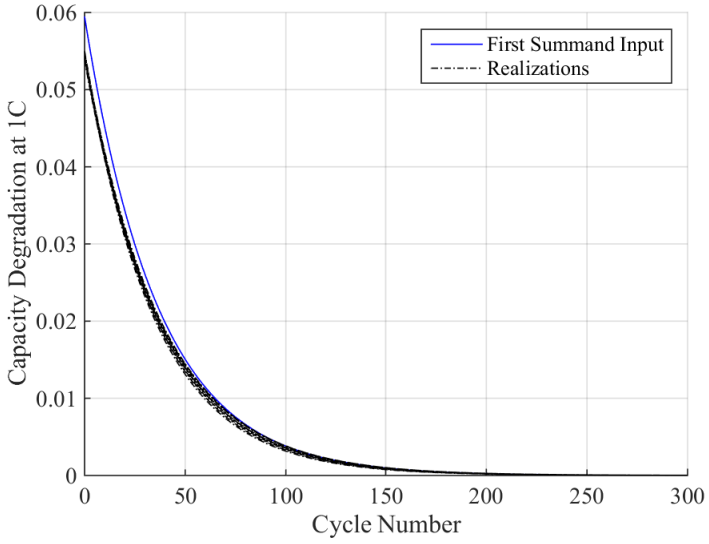

Figure 33. Comparison among first original summand and ten realizations.

In case of the second summand, $cx_2(k)$, and since the initial condition is always set to $x_2(0) = 1$, we observe a greater contribution to the overall characterization of the battery SOH in time (see Figure 34).

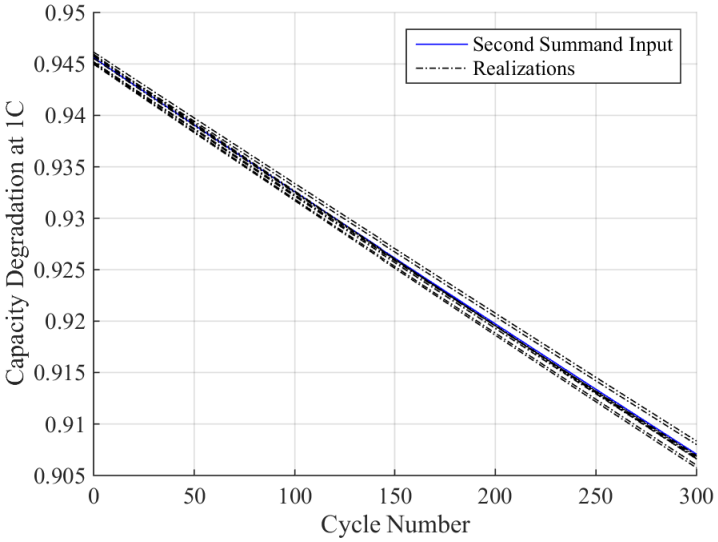

Figure 34. Comparison among second original summand and ten realizations.

3.2.2 Model Coefficient Analysis

As explained before, the model is composed of two-state space equation and the corresponding observation equation. A total of four coefficients are needed, all of them estimated via a curve fitting procedure. This section analyzes the model, in terms of the relationships between these parameters and operating conditions at each discharge cycle.

Coefficient a: There is no clear pattern that could relate the values of this parameter and battery discharge current. There is no overlap among confidence intervals. An interesting issue is that the mean value in the 2-C case is the highest of the three cases. In this regard, there is no evidence of a monotonic relationship between parameter values and discharge current rates.

Coefficient b: In this case, it is possible to note that, for both the 1-C and 2-C cases, the confidence bounds are reasonably similar. Furthermore, it can be noted that the mean value of the 2-C case, is within the confidence bounds of the 1-C case, and vice-versa. This situation suggests that these two cases can be merged into just one confidence interval. It is suggested to consider 3-C battery discharges as a separate case, given that that mean value of the parameter is about 30% less than in the other situations.

Coefficient c: This coefficient is closely related to the initial value of the second summand of the observation equation, $cx_2(0)$. When comparing mean values and confidence intervals for 2-C and 3-C discharges, differences are small. However, it is recommended to assume a

dependency between the parameter value and the battery discharge current in the implementation of estimation approach.

Coefficient d: This coefficient has a major effect on the characterization of the degradation process, since it is associated with the slope of the second summand in the observation equation, $cx_2(k)$. In this case, the mean values and confidence bounds are separated for each battery operating condition and, moreover, parameter values have a monotonic relationship with respect to the discharge current.

An interesting fact associated with the mean value of coefficient d is that the 1-C case is practically scaled to the nominal capacity of the battery (1.4 Ah). Table 2 summarizes the mean values of the three cases in terms of the nominal capacity. Another fact is that the mean values can be fitted through an exponential curve, as shown in Figure 35.

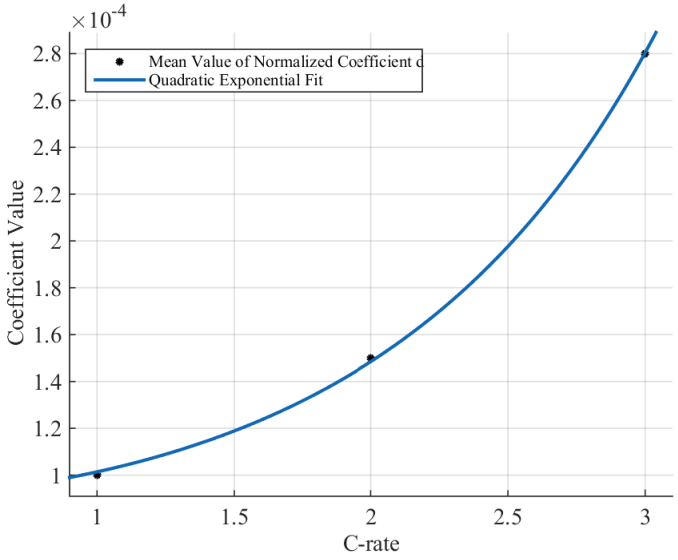

Figure 35. Quadratic exponential fit for the mean value of coefficient d.

Table 2. Mean value and confidence bounds for the d coefficient at various discharge currents

C-rate	Mean value	Confidence bounds
1C	$-1 \cdot 10^{-4} \cdot C_{nom}$	$(-1.01, -0.996) \cdot 10^{-4} \cdot C_{nom}$
2C	$-1.5 \cdot 10^{-4} \cdot C_{nom}$	$(-1.6, -1.4) \cdot 10^{-4} \cdot C_{nom}$
3C	$-2.8 \cdot 10^{-4} \cdot C_{nom}$	$(-2.88, -2.76) \cdot 10^{-4} \cdot C_{nom}$

Indeed, from collected evidence, we have found that it is possible to find an exponential relationship between values of the coefficient d (in the proposed SOH degradation model) and the battery discharge current rate. This relationship can be characterized by the

expression $y(\gamma) = \alpha e^{\beta \cdot \gamma^2}$, where γ is used to represent the C-rate and $y(\gamma)$ is a multiplier used to obtain the coefficient d of the model. Thus, we finally obtain a C-rate dependent model for SOH degradation over time, defined by state equations (1)-(2), and where:

$$d_1(C_{rate}) = \alpha e^{\beta \cdot (C_{rate})^2} \quad (12)$$

The mean value and the confidence bounds of α and β are shown in Table 3. In this case, the obtained value associated with the R-square parameter when fitting the data was 0.9997.

Table 3. Values for alpha and beta after adjusting the d coefficient through a quadratic exponential fit.

	Variable	
Parameter	α	β
Mean value	$8.93 \cdot 10^{-5}$	0.1271
Confidence bounds	$(6.947, 10.91) \cdot 10^{-5}$	(0.09863, 0.1556)

3.2.3 Experimental Results

In order to study the degradation process when cycling a Li-ion battery at high currents, a real experimental procedure was implemented. This procedure degraded a Panasonic CGR18650CH battery cell under controlled conditions for charge-discharge cycles and temperature (25 °C). The procedure starts with a brand new battery cell as received from the distributor and consists of the following steps:

Charging Procedure

- The constant current-constant voltage (CC-CV) charge procedure should be done at 0.5-C. This current must be applied until the voltage reaches 4.2 V. Then the voltage is fixed at this value and the current is reduced until it reaches 0.05-C.

Cycles 1-10: Initial cycles.

1. Perform discharge cycles at nominal current (1-C), (although the nominal current is defined at 2.25 A, for simplicity the experiments were done at 2.2 A).
2. Perform the CC-CV charging procedure.
3. Repeat steps 1-2 until completion of the ten cycles.

Cycles 11-12: Regular degradation cycles

1. Perform discharge cycles at 1-C.
2. Perform the CC-CV charging procedure.

Cycles 13-20: Accelerated degradation cycles

1. Perform discharge cycles at 2-C.
2. Perform the CC-CV charging procedure.

General considerations for all cycles

- A resting period of 30 minutes is established every time a battery is discharged, and every time the battery is charged.
- Cycles 10N + 11 and 10N + 12 (N = 1, 2, 3, ...) shall be regular discharge cycles.
- All other cycles shall be accelerated degradation cycles.
- Repeat this alternating sequence of discharge process (two regular degradation cycles, and eight accelerated degradation cycles).
- The charging procedure must be performed after every discharge cycle, to start the new cycle with the battery fully charged.

The experiment started in November 2016 and finished in July 2017. Nearly 600 cycles were completed. Figure 36 shows the degradation process for the normalized battery capacity. In this figure, it can be noted that two different trends co-exist. The uppermost set of points corresponds to discharges performed at 1-C, while the data points at the bottom correspond to cycles performed at 2-C.

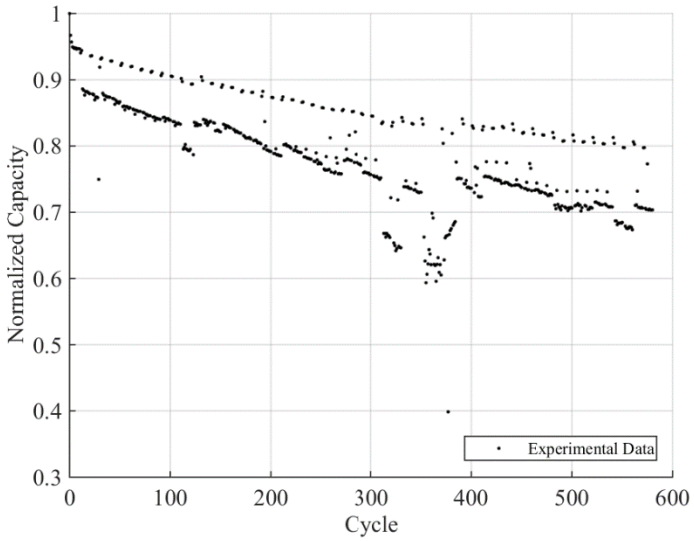

Figure 36. Experimental degradation process of the Panasonic CGR18650CH Li-ion battery.

An interesting situation happened between cycles 300 and 400. For unknown reasons the testing chamber stopped controlling the temperature, a fact that went unnoticed. Because of this fact, the amount of delivered energy decreased in those cycles. This effect has to be considered as a temperature-related phenomenon, and does not affect the degradation process in the long term. Indeed, once the issue with the testing chamber was fixed, degradation values came back to the expected trend. Using the proposed model (Equations 1 and 2), fifty random realizations were generated and compared with the experimental data at both discharge current levels. Results are shown in Figure 37. Note that all model realizations properly follow the trend of the experimental data. Without considering the experimental values that were affected by the temperature problem, the difference between model realizations and the experimental data is less than 2%.

In this regard, it is possible to mention that the proposed model is able to properly characterize the degradation process for a given discharge current. The next step is to evaluate the performance of the model using the data results at 2-C. In a similar way, Figure 38 shows fifty random realizations of the proposed model and the experimental data.

Figure 38 shows a bias between model realizations and measured data. However, an important fact to highlight is that the realizations follow the same trend as the experimental data, and that differences are between 5% and 7% in most cases. To verify this biased behavior, experimental data was fitted through the Curve Fitting Tool of Matlab. To avoid the errors induced by low capacities due to the temperature-related phenomenon, these data points were excluded from the fitting process. Figure 39 shows the result when data is fitted by using the proposed model, and the confidence bounds for all the coefficients. Similarly to our previous experiment, the resulting fitted curve follows the trend of the experimental data. The average offset is about 5%; and towards the end of the time series, the difference between

the fitted values and the experimental data is limited to 3%. It is important to notice that various measured data points match the fitted curve.

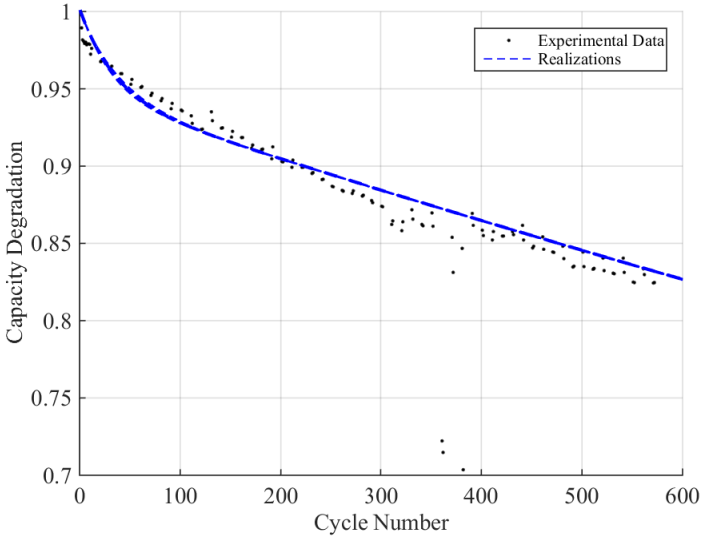

Figure 37. Comparison between experimental data at 1-C and fifty random realizations of the proposed model.

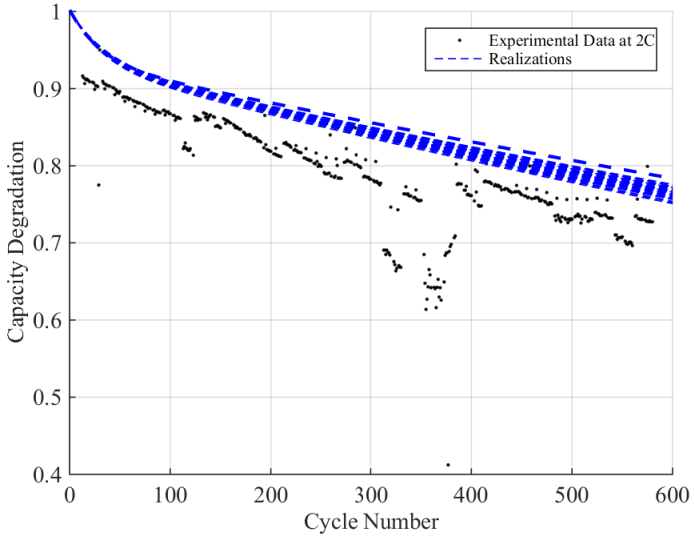

Figure 38. Comparison between experimental data at 2-C and fifty random realizations of the proposed model.

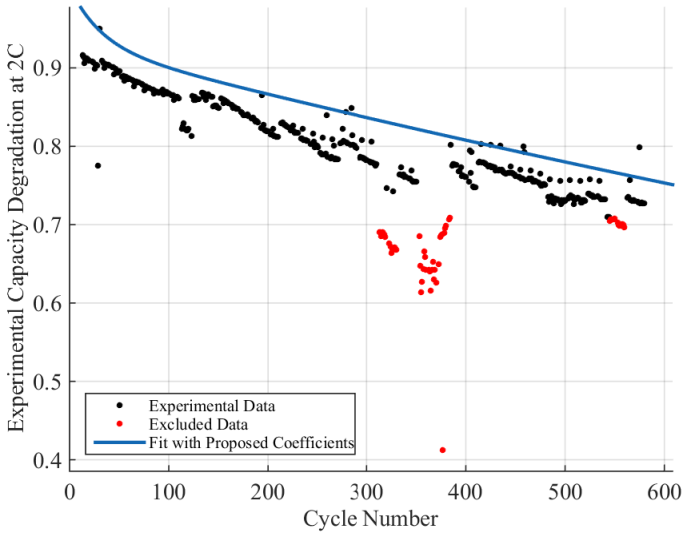

Figure 39. Fitted curve by using the proposed model and confidence bounds for all the coefficients.

To evaluate the model performance, we test the goodness of the fit (see Table 4). As expected, although the trend of the curve follows the experimental data, the results are not good enough. To overcome this situation, we have slightly modified the original parameter estimation procedure as follows.

Table 4. Goodness of the fit results for the experimental 2-C data.

Parameter	Value
SSE	0.7217
R-square	0.3982
Adjusted R-square	0.3997
RMSE	0.04237

As explained previously, the proposed model has two summands in observation Equation 2, which are parametrized by coefficients a and c. From those, coefficient c is the one that has the highest impact on the degradation characterization in the long term. In this regard, the coefficient c is left unbounded (or free) during the estimation process, while the feasible region for other coefficients is bounded within the confidence intervals shown in Table 1. Figure 40 shows the result of this special fit. Note how the bias is reduced just by setting the coefficient c free. For this new fit, the model is able to properly characterize the degradation process without the bias previously observed.

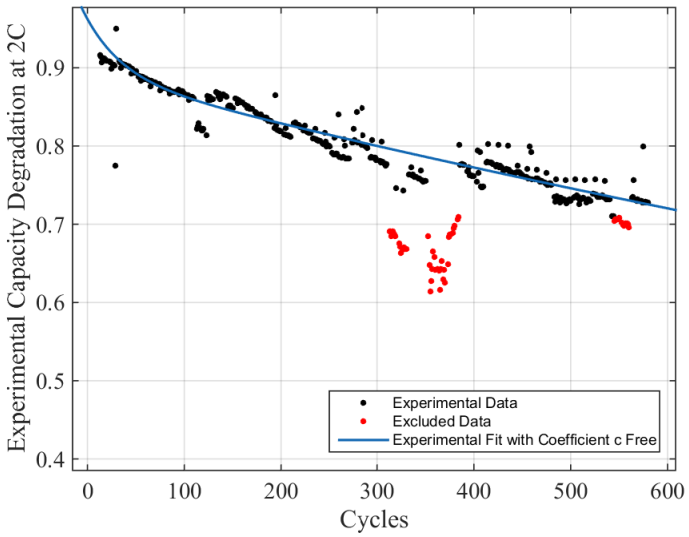

Figure 40. Fitted curve by using the proposed model setting coefficient c free.

For the sake of comparison, the fitting procedure is repeated. In this case, though, the four coefficients are set free to let the Curve Fitting Tool of Matlab adjust them; Figure 41 shows the results for this fit. As expected, the resulting fitted curve has a good performance when compared with the experimental data.

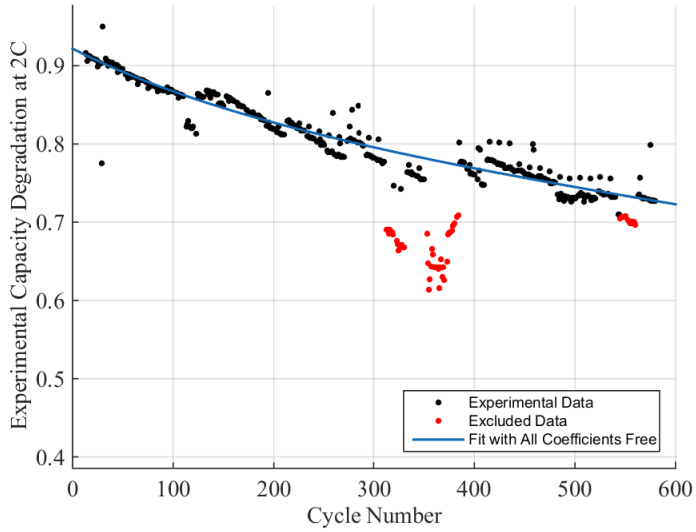

Figure 41. Fitted curve by using the proposed model with free coefficients.

A comparison between the goodness of both fits can be observed in Table 5. Expectedly, the results for the fit with free coefficients are better, although the results obtained where coefficient c is set free only are very similar.

Table 5. Comparison between the proposed model with coefficient c free only and all coefficients free.

Parameter	Coefficient c Free	All Coefficients Free
SSE	0.005995	0.0038
R-square	0.995	0.9968
Adjusted R-square	0.995	0.9968
RMSE	0.003866	0.00309

From these results, it is possible to state that the proposed model is able to properly fit the experimental data. Although using the obtained confidence bounds might induce a biased result, this does not mean that the model is not capable to properly represent the degradation process. In this case, the model and the confidence bounds were obtained for a specific type of battery, and later applied on a different type of battery. For instance, the biased result can be amended if one of the coefficients is set free. Although batteries are built under strict quality control conditions, due to the complex chemical processes involved, the results may vary from cell to cell, especially when batteries are not used under nominal conditions. As demonstrated, the proposed model is able to adjust the parameters in a simple and fast manner in order to characterize the observed process.

One final case study is performed using two datasets obtained from the public repository of the Prognostics Center of Excellence of the NASA Ames Research Center. In this case, the datasets used are those associated with Batteries #34 and #36. In these experiments the room temperature was controlled at 24 degrees Celsius. The batteries have a nominal capacity of 2 Ah. Battery #34 was discharged at a constant current of 4 A until the discharge voltage reached 2.2 V at each cycle, while battery #36 was discharged at nominal current conditions until the discharge cycle reached 2.7 V at each cycle. The experiment was performed until the nominal capacity was reduced by 20% (i.e. from 100% to 80%).

Similar to the previous case study, the idea is to compare the proposed model under two conditions. The first condition is to set the confidence bounds for coefficients $a, b,$ and d using the previously defined values. The second condition is to set coefficient c free and let the Curve Fitting Tool of Matlab to adjust it. The first results shown in Figure 42 correspond to Battery #36. Note how the results where coefficient c is set free are able to properly fit the real data.

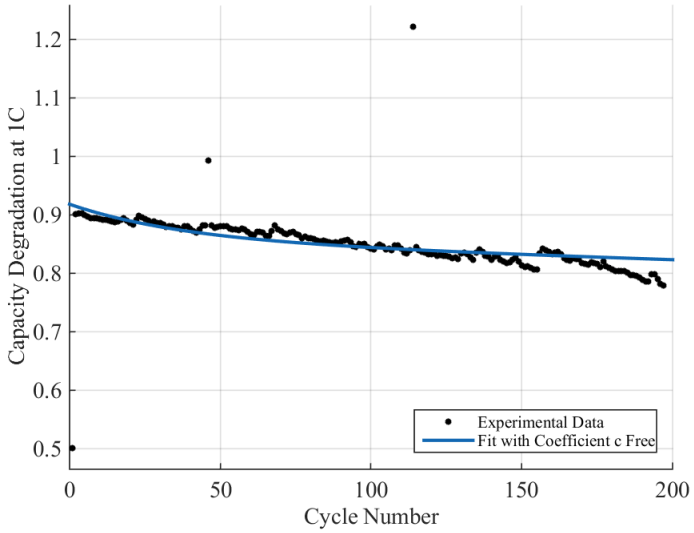

Figure 42. Fitted proposed model setting coefficient c free.

Figure 43 shows the results when all coefficients are set free. In this case the behavior of the fitted curve follows the trend of the data in a more precise manner, and there are no significant differences between the measured data and the fitted results.

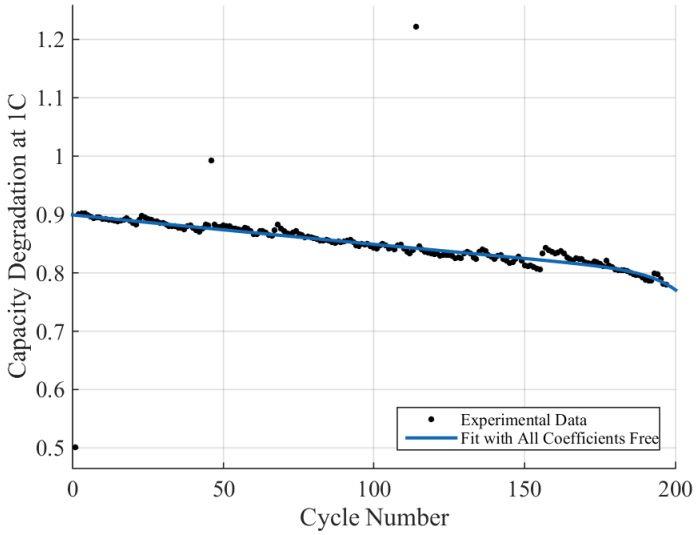

Figure 43. Fitted proposed model setting all coefficients free.

Similarly to the previous case study, the goodness of the fit is analyzed. Table 6 shows the obtained results. Note that the differences among the four parameters are very small, and therefore the proposed model is also able to characterize the degradation process of this battery when discharged at nominal current.

Table 6. Comparison between the proposed model with coefficient c free only and all coefficients free applied on Battery #36.

	Coefficient c Free	All Coefficients Free
SSE	0.0279	0.02377
R-square	0.9397	0.9486
Adjusted R-square	0.9397	0.9478
RMSE	0.0119	0.0111

The next step is to repeat the previous analysis on Battery #34. Figure 44 shows the result of the proposed model and confidence bounds except for those associated with coefficient c, which is set free, to be found by the software. Although the data looks irregular, the fitted result is capable to follow the trend.

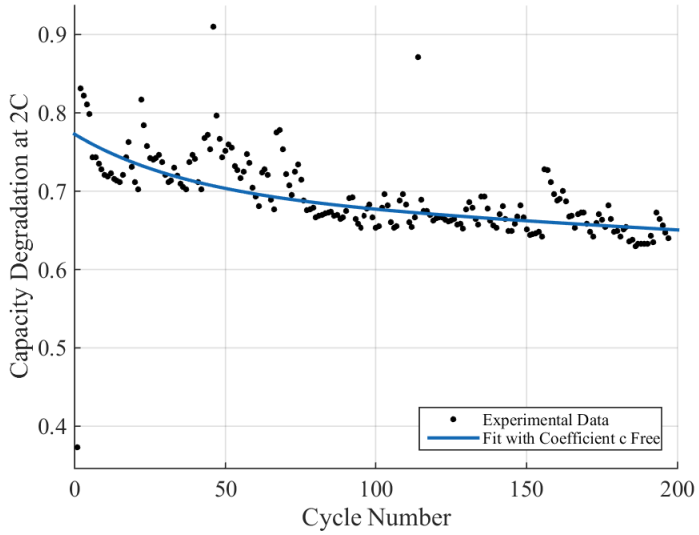

Figure 44. Fitted curve by using the proposed model setting coefficient c free.

Figure 45 shows the result where all coefficients are set free. In this case, it is more difficult to observe the differences between this and the previous result, since the measured data are more distributed.

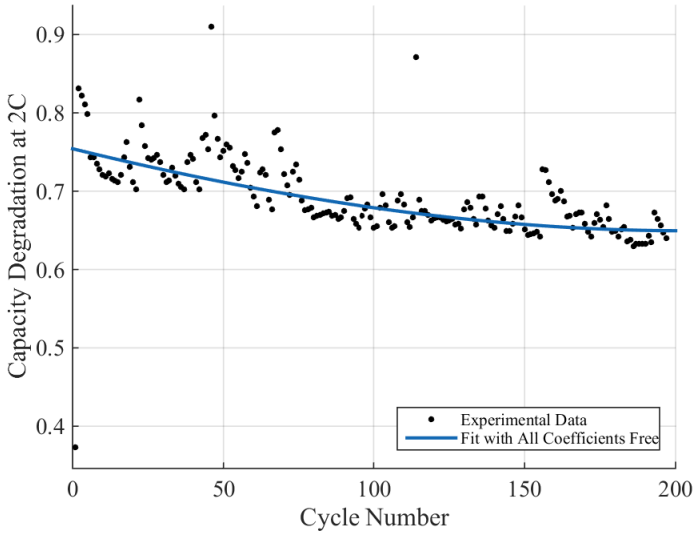

Figure 45. Fitted curve by using the proposed model setting all coefficients free.

Finally, both results are compared through the goodness of fit. Table 7 shows that the differences between both approaches are very small.

Table 7.Comparison between the proposed model with coefficient c free only and all coefficients free applied on Battery #34.

	Coefficient c Free	All Coefficients Free
SSE	0.02829	0.02584
R-square	0.946	0.9506
Adjusted R-square	0.946	0.9499
RMSE	0.01201	0.01157

3.3 Characterization of the Degradation Process of Energy Storage Devices when Operating at Erratic SOC Swing Ranges

This section is based on the procedure explained on Section Structure of State of Health Degradation Models. As mentioned, the degradation model is based on the concept of the Coulombic efficiency. Using the information given by the manufacturers it is possible to calculate the value of this efficiency.

Datasheets provide information regarding the trend of the capacity degradation after a certain amount of cycles, as shown in Figure 46, which is reconstructed from the datasheet of the Panasonic NCR18650B Li-ion battery. This is the degradation effect when batteries are

discharged at nominal current, with a SOC swing of 100% and charged by using the defined protocol defined by the datasheet.

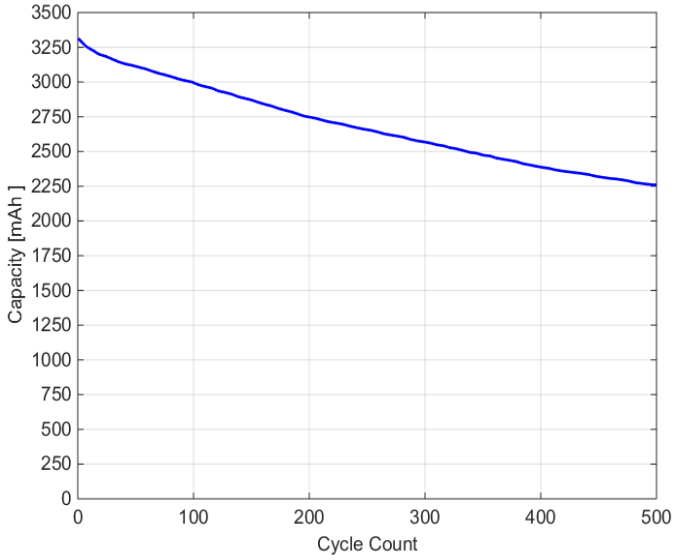

Figure 46. Panasonic NCR18650B lifespan characteristics.

Even though the degradation is caused by multiple effects, the Coulombic efficiency can be used to simplify and explain the entire degradation phenomenon by only one term. Basically, the higher the value of efficiency, the less degradation per cycle a battery will have. Since most Li-ion batteries have a lifespan of a several hundreds of cycles, it is imperative to work with several decimal points in order to obtain the most appropriate value of the Coulombic efficiency.

3.3.1 Proposed Method

This method was previously used in [23], although much more details are provided next. In the proposed method, the cycles are characterized by using its associated Coulombic efficiency $\bar{\bar{\eta}}$. In this sense, the storage capacity is degraded through each cycle k, by using equation (13).

$$\begin{cases} x_1(k+1) = \left(\bar{\bar{\eta}}(SOC\,)\right) x_1(k) \\ y(k) = x_1(k) \end{cases} \tag{13}$$

This proposal includes a methodology that uses information of the battery, regarding the amount of operating (regular) cycles and the values of SOC swing and SR. Using data provided by the manufacturer, it is possible to calculate the value of $\bar{\bar{\eta}}$. In this case, 11 SR (100-0%, 100-25%, 75-0%, 100-50%, 75-25%, 50-0%, 100-75%, 75-50%, 62.5-37.5%, 50-25% and 25-0%) and the total number of cycles for each of these SR is known. According to

Figure 12 and Figure 46 it is possible to calculate a value for the Coulombic efficiency if a constant decay rate is considered. By using the known amount of total cycles, and assuming that a cycle is complete after discharging the battery at nominal current between the defined values of SR, the following equation (14) simplifies the calculation of the Coulombic efficiency.

$$\bar{\bar{\eta}} = (\ Degradation\ Percentage)^{\frac{1}{Total\ Cycles}} \tag{14}$$

In this case, the degradation percentage should be defined as a value between 0 and 1, and it is equal to the percentage of the nominal capacity where the user or manufacturer defines the threshold to be considered as fully degraded. For instance, if a battery is rated to work for 5000 cycles, with a final nominal capacity of 80% (of its original value), the value of the Coulombic efficiency would be 0.99995537; but if this percentage is considered as 75% (of its original value), the value of $\bar{\bar{\eta}}$ would be 0.99994246. This procedure is performed for all the eleven cases mentioned before, so each one has associated a value of $\bar{\bar{\eta}}$. Even though we have a good amount of operating cases, this does not cover all the possible combinations of SR, however it is possible to interpolate and obtain an appropriate value of the Coulombic efficiency as follows. Using the known SOC swing and the average SR value, and distributing these values on a scatter plot as shown in Figure 47, where the asterisks represent the known operating conditions and the black circle represents a particular operational condition. The equivalent Coulombic efficiency will be determined as described next.

Since the scatter plot presents a triangular shape, using K-nearest neighbors (3 neighbors in this case due to the triangular shape), and by weighting the inverse of the distances to the known conditions (3 of them), it is possible to determine the value of an approximate Coulombic efficiency for all possible operating conditions.

Having all the SOC swing and SR information is not always possible. For this reason, a method for extrapolating the previous results in order to be used with other Li-ion batteries is defined, assuming that Li-ion batteries have similar behaviors.

Table 8 shows the corresponding escalating factors that can be used to characterize the efficiency when the batteries are operated at different SR. Also, it considers different degradation percentages since they can differ among manufacturers.

For example, let consider two types of commercial Li-ion batteries. The first case is the Samsung ICR18650-22P. Using the information provided by the manufacturer it is possible to calculate the Coulombic efficiency. In this case, the value of the Coulombic efficiency is 0.9992869 after 500 cycles since after at that point the capacity of the battery has degraded to 70% of the nominal capacity, meaning that there is a 30% loss of the original capacity.

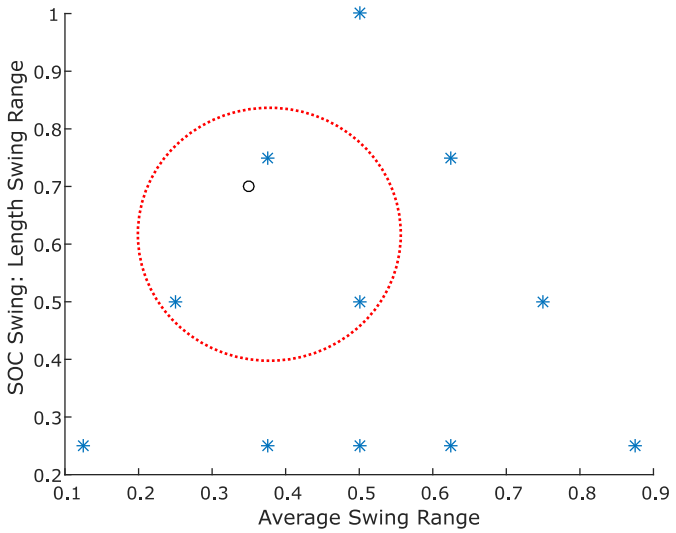

Figure 47. K-Nearest neighbor scatter plot. The asterisks indicate known operating conditions, and the black circle represent a random usage condition. The red circle encloses the three nearest neighbors to the random use.

Table 8. Escalating factors for three degradation cases.

	Degradation Percentage		
SR	**0.7**	**0.8**	**0.85**
100-0	1.000000	1.00000000	1.00000000
100-25	1.000003	1.00000266	1.00000193
75-0	1.000024	1.00001860	1.00001354
100-50	0.999989	0.99999203	0.99999420
75-25	1.000019	1.00001521	1.00001108
50-0	1.000037	1.00002874	1.00002093
100-75	1.000027	1.00002146	1.00001563
75-50	1.000011	1.00000881	1.00000642
62.5-37.5	1.000008	1.00000620	1.00000451
50-25	1.000043	1.00003347	1.00002438
25-0	1.000054	1.00004184	1.00003047

The second case corresponds to the Panasonic CGR18650, as seen in Figure 48. Calculating the same parameters as the first case, we obtain a Coulombic efficiency of 0.9995538, considering a degradation of 20%, since the available capacity at that point will be 80% of the original capacity, after 500 cycles of use.

Using the obtained value of η for each case, it is possible to calculate an approximate value of Coulombic efficiency when working at different SR. Table 2 shows the escalated values for the Coulombic efficiency for each of the SR.

With these results, the replicating the previously explained methodology in order to characterize in a better way the degradation effect when another type of Li-ion battery is operated under any SR conditions.

3.3.2 Simulation Example of the Degradation Process using K-NN

In this example the degradation process of the Samsung ICR18650-22P Li-ion battery using the results of Table 9 is modeled. A Monte Carlo simulation of 50000 realizations and operating the battery under any SR combination was performed. Also the degradation process in a deterministic way by using a fixed value of eta is used for comparison purposes. For the deterministic part, three values for eta were considered: a constant value of eta (obtained from the datasheet -and equal to the 100-0% SR-, and the maximum and minimum value of eta obtained from the Table 9. In this sense, the results are: constant value of eta is equal to 0.9992869, the maximum value is 0.9993409 and the minimum is 0.9992759. For the Monte Carlo simulations, the corresponding value of eta is calculated by the K-NN method explained in the previous section and using as a reference the values obtained in Table 9. This way, it is possible to simulate any random combination of SOC swing and SR and not only the 11 cases discussed earlier. However, the following considerations were taken into account for the simulation:

- The initial SOC level value at instant time k+1 must be higher than or equal to the final SOC level value at instant time k.
- There is always a discharge in every cycle.
- Each realization is finished after 800 cycles.

For the Monte Carlo simulations, the amount of total cycles after the normalized capacity reaches the threshold value of 70% were calculated, since at this point the battery is considered fully degraded. The bar diagram presented in Figure 49 shows the estimated total number of cycles until it reaches its EoL. In this case, it can be observed that the majority of the cases reach its EoL after 517 cycles (when used at different/irregular SOC swing values).

Figure 50 shows the obtained degradation curve for the following cases: the constant value of eta, the maximum and minimum value of eta, and one realization of the Monte Carlo. It is possible to see that the case of constant eta reaches the 70% threshold at 500 cycles, which is the value expected observed in the datasheet. In the case of the Monte Carlo simulation, the battery lifespan is 3.2 - 3.6% higher in terms of extra cycles (with respect to calculation with a constant eta). Furthermore, Figure 51 shows a zoom-in of the threshold area.

By looking at Figure 50, it can observed that the Monte Carlo results place the battery lifespan within the minimum and maximum degradation. Also, the EoL obtained through the Monte Carlo simulations can be considered the closest to the real one (or closer than that obtained through a constant eta).

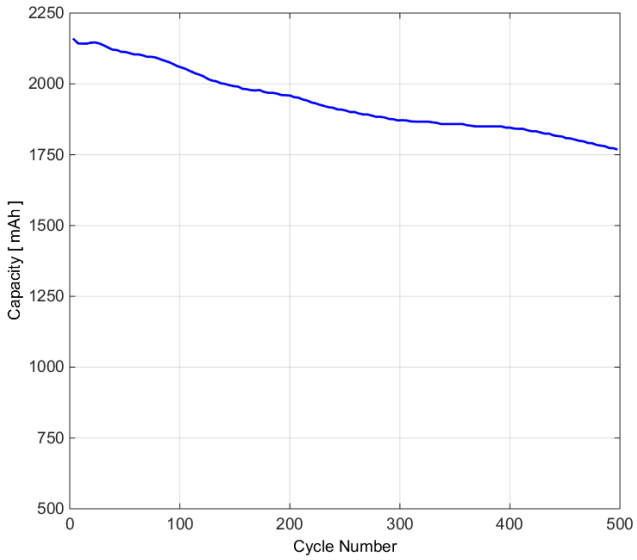

Figure 48. Panasonic CGR18650 lifespan characteristics.

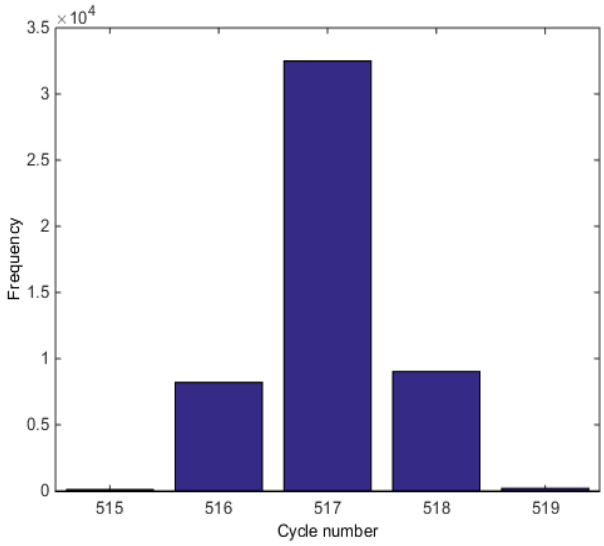

Figure 49. Bar diagram of the estimated total number of cycles.

Table 9. Escalating values for two commercial batteries.

SR	ICR18650-22P	CGR18650
100-0	0.9992869	0.9995538
100-25	0.9992899	0.9995565
75-0	0.9993109	0.9995724
100-50	0.9992759	0.9995458
75-25	0.9993059	0.9995690
50-0	0.9993239	0.9995825
100-75	0.9993139	0.9995753
75-50	0.9992979	0.9995626
62.5-37.5	0.9992949	0.9995600
50-25	0.9993299	0.9995873
25-0	0.9993409	0.9995956

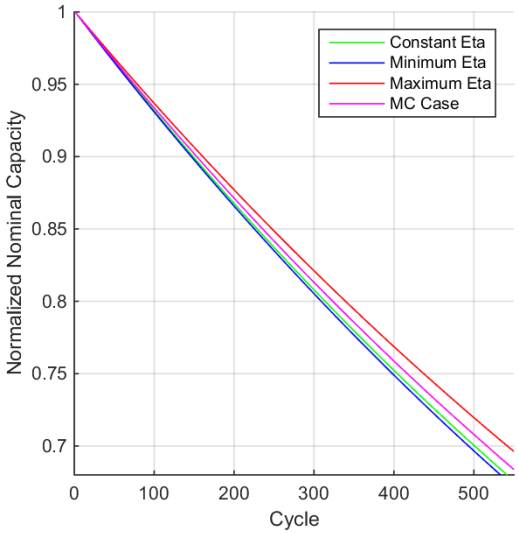

Figure 50. Simulated degradation process of the Samsung ICR18650-22 when operated under different conditions.

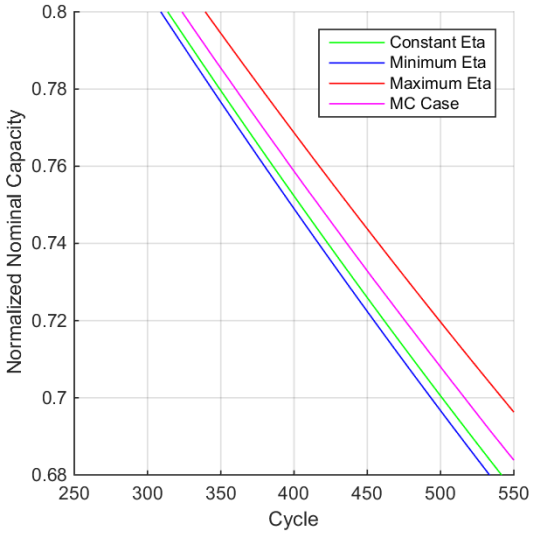

Figure 51. Zoom in over the 70% threshold area.

3.4 Characterization of the Degradation Process of Energy Storage Devices when Discharged at Different Current Rates using Similarity Based Modelling

This section is intended to explain the use of Similarity Based Modeling (SBM) to estimate the degradation process of a Li-ion battery. As explained previously, the degradation process shown in Figure 3 can be characterized through the sum of two exponential summands, regardless of the discharge current. Using the obtained characterization results, (as the ones shown in Figure 32) it is possible to calculate the equivalent efficiency per cycle. Figure 52 shows the evolution of the efficiency for the three discharge currents, and it can be noted that they have an exponential behavior. The value of the efficiency starts with a lower value than at the end, supporting what is stated by the literature that at early stages of the life cycle the degradation process is higher. In all three cases, after a certain number of cycles an inflexion point is reached and afterwards it appears to have reached a steady state value.

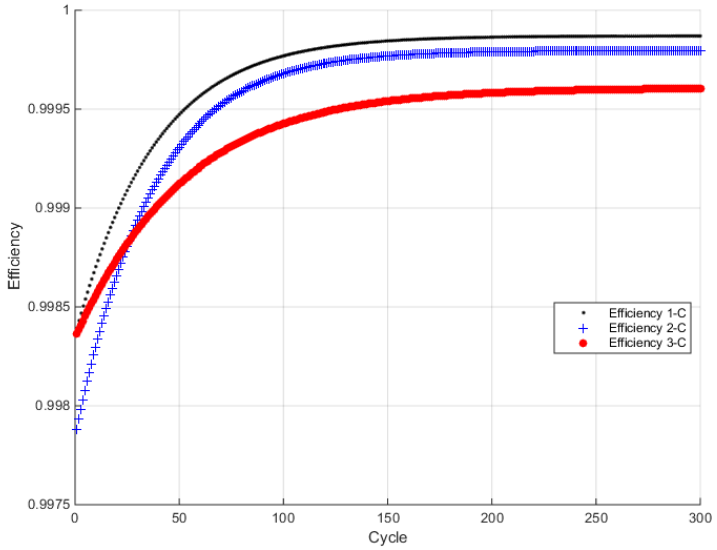

Figure 52. Evolution of the cycle to cycle efficiency for different discharge currents.

Due to the exponential behavior of the efficiency curves, an exponential curve with the structure $\mathrm{H}(k) = \mathrm{A} \cdot e^{\mathrm{B} \cdot k} + \Gamma \cdot e^{\Theta \cdot k}$ was fitted. This equation will allow to estimate the value of the efficiency at any cycle for the three discharge currents. Table 10 shows the values for each of the coefficients.

Table 10. Mean Value and Confidence Bounds for the Efficiency Structure.

Coefficient	1-C	2-C	3-C
A	0.9999 $(0.9999, 0.9999)$	0.9998 $(0.9998, 0.9998)$	0.9996 $(0.9996, 0.9996)$
B	$-1.711 \cdot 10^{-8}$ $(-1.79, -1.631) \cdot 10^{-8}$	$-2.415 \cdot 10^{-8}$ $(-2.541, -2.289) \cdot 10^{-8}$	$-3.75 \cdot 10^{-8}$ $(-3.852, -3.647) \cdot 10^{-8}$
Γ	$-1.533 \cdot 10^{-3}$ $(-1.533, -1.533) \cdot 10^{-3}$	$-1.996 \cdot 10^{-3}$ $(-1.996, -1.996) \cdot 10^{-3}$	$-1.288 \cdot 10^{-3}$ $(-1.288, -1.287) \cdot 10^{-3}$
Θ	-0.02684 $(-0.02685, -0.02683)$	-0.02801 $(-0.02802, -0.028)$	-0.01922 $(-0.01923, -0.01921)$

An important thing to mention is that the sum squared error for the fitted curve of the three cases, is less than $1 \cdot 10^{-11}$, while the R-square value is equal to 1.

Nevertheless, the previously degradation curves are the result of charging and discharging the battery from a 100% SOC to a 0% SOC. In order to include different values of SOC, the same methodology as the proposed on [58] is used. Since it is possible to estimate the equivalent efficiency at each cycle, this value will be used as the corresponding efficiency

reference prior to escalating the remaining cases. In other words, this efficiency reference is used when the SOC Swing is equal to 1 at each cycle, keeping in mind that depending on the discharge current the value is different. Table 14 on Appendix 1, Table 14shows the obtained efficiency values for the first three cycles of operation escalated when considering a degradation threshold of 15%, this means that the nominal capacity is reduced to an 85% of its original value.

As an example, this process is repeated for a total of 1000 cycles. Using this information, the input and output matrixes of the SBM are created. Each cycle, with the corresponding three discharge currents and eleven SOC swing combinations with the average SOC are used as input matrix, while the efficiency values are used as the output matrix of this SMB structure. This way, it is possible to estimate an equivalent efficiency regardless of the discharge current and SOC swing.

Figure 53 shows the obtained efficiency values when simulating 1000 cycles. As expected, the trend of the figures is similar to the observed in Figure 52, meaning that the results obtained with the SBM proposal are reasonable and within the reference values.

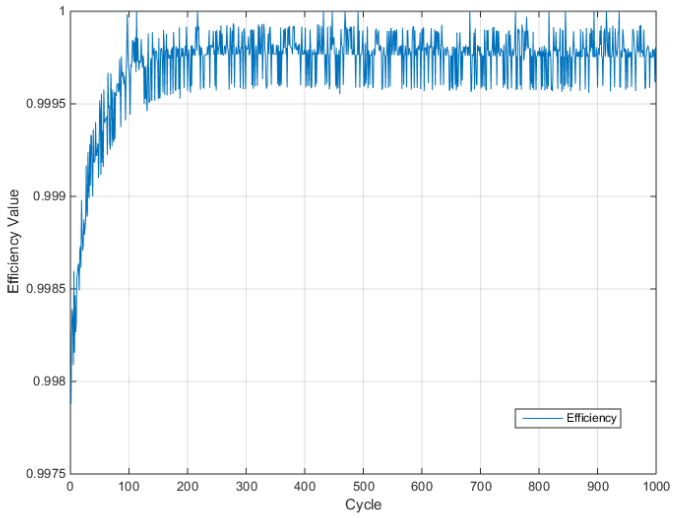

Figure 53. Evolution of the efficiency for random discharge currents through the simulation.

The distribution of the discharge currents for the 1000 cycles is verified with Figure 54, where the discharge current is constrained between 1 A and 3 A.

Since the distribution of the currents is done accordingly and the efficiency values follow the trend of the measured data, and the operational SOC policies are set to be free following the same restrictions as the previous case, it is possible to plot the resulting degradation curve for the simulation. Equation (15) represents the degradation model used for this simulation.

$$\begin{cases} x_1(k+1) = \left(\eta(Cycle, C_{rate}, SOC)\right) e^{\alpha\left(\frac{1}{T-\beta}-\frac{1}{T_{ref}-\beta}\right)} x_1(k) \\ y(k) = x_1(k) \end{cases} \quad (15)$$

Figure 55 shows the first 300 cycles of the degradation process when compared to the measured data. As seen, the structure of the degradation process curve follows the trend of the measured data, very similar to the 2-C case, since it is the average value between 1A and 3A.

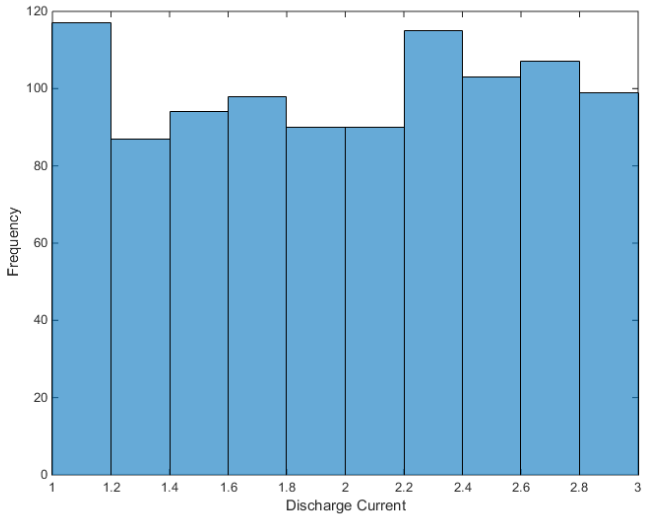

Figure 54. Distribution of the discharge currents for the performed simulation.

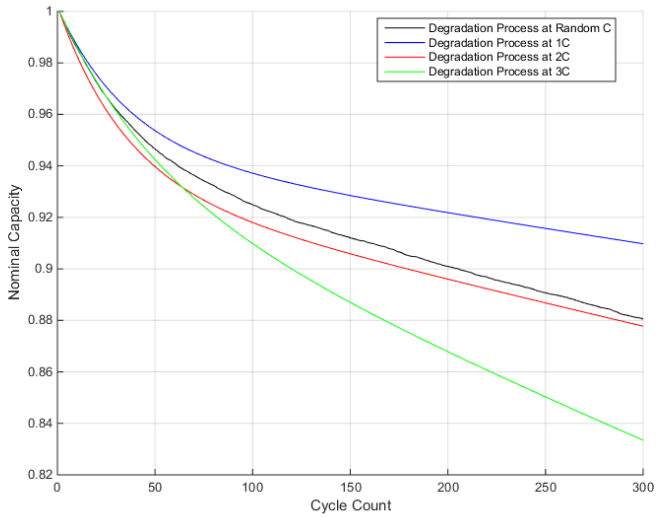

Figure 55. Degradation process for different discharge currents.

To illustrate what happens if a different range of discharge currents are fixed, Figure 56 shows the degradation process when it is set between 2 A and 3A. In this case, the degradation process of the simulation shifts to a trend between the 2C and 3C case.

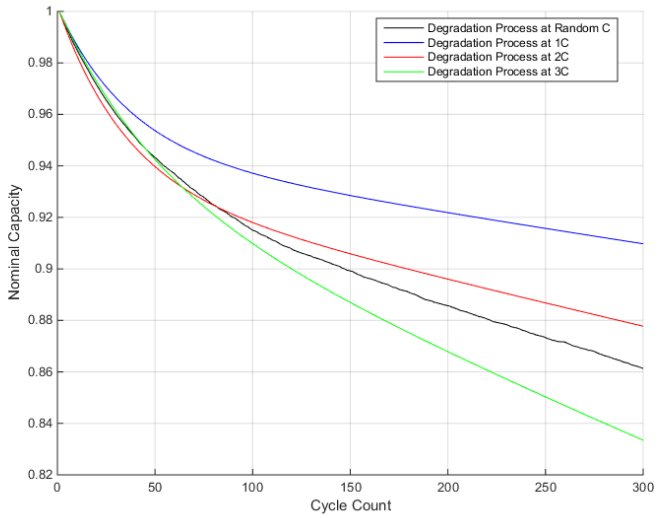

Figure 56. Example of the degradation process for different discharge currents. The random current is constrained between 2 and 3 Amperes.

These results show that the SBM method is capable of characterizing properly the degradation process, when operating at different discharge currents and erratic SOC ranges. As mentioned, the temperature can have an effect on the degradation process and also on the amount of energy that can be delivered. For this reason, the temperature effect is included on the previous result to demonstrate its effect.

The inclusion of the temperature was done as follows. Using historical data of the ambient temperature in London. The average temperature of each day is used, and also each day represents a cycle. In other words, the first 31 cycles represent the month of January (winter in the northern hemisphere), the next 28 cycles are used to represent February, and so on.

Figure 57 shows the plot for the degradation process when operating at both temperature conditions: controlled temperature and the average day temperature. It can be noted how the effect of the temperature on cold days, causes the battery to deliver less energy (usable capacity) although in terms of degradation the battery is able to deliver more energy. Also, since the controlled temperature is set to 25 °C on those days where the ambient temperature is close to this number, the usable capacity has almost the same value as the degraded capacity.

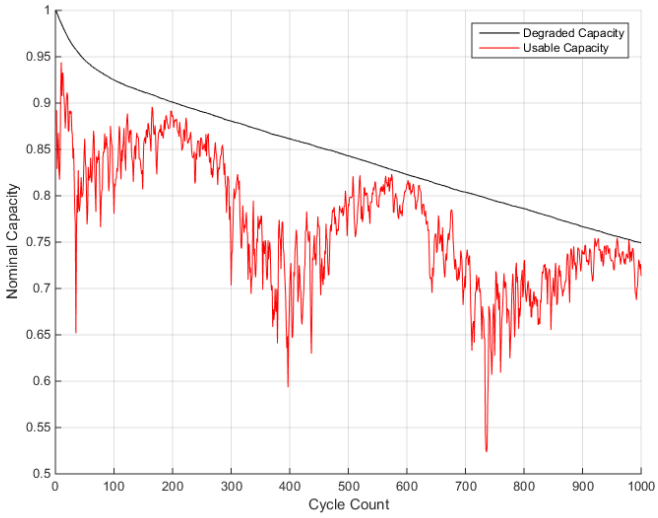

Figure 57. Degradation process of the nominal capacity and the usable capacity due to the temperature effect.

4. Case Study: Effect of the Degradation Process on Multi-Service Portfolios of Energy Storage

4.1 Context of the Provided Information Used on the Case Study

The first step is to define the information used for the simulations in the framework of this case study. Part of the information was provided by the UK Power Networks, and consists of historic information of the prices of the energy and energy demand for the years 2011 and 2012. Using this information, future scenarios are going to be built using the repetition of this historic datasets to complete a total of 20 years. In order to consider the frequency response and reserve services, the time windows and prices were also provided. This scenario is going to be considered as the base case.

Using the historic temperature data of the years 2011, 2012 and 2013 in London, time series were fabricated in order create different temperature scenarios. These time series were obtained using a combination of Fourier series and an ARMA model. Figure 58 shows two of the time series that were created.

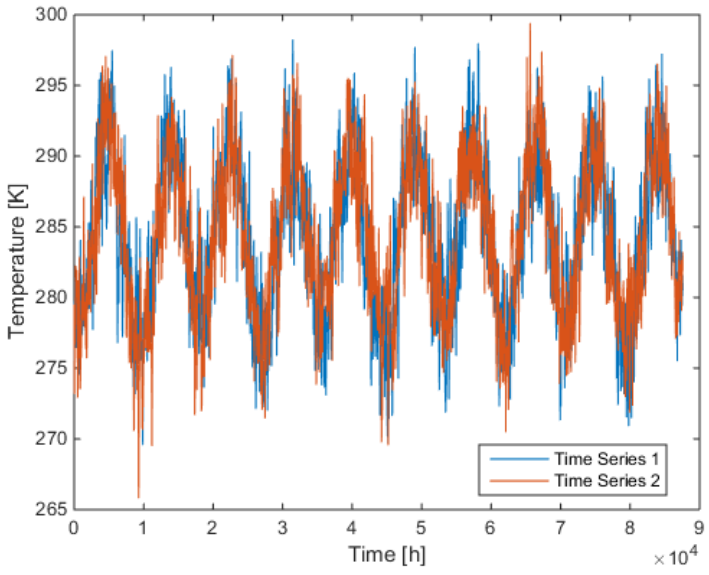

Figure 58. Time series for the temperature.

So as to analyze sensitivities for the Price and Demand variables, time series were also used. A 20 year dataset, of 10 different scenarios of prices was also provided for this simulation. For the Demand study, time series were created using the historic data provided.

In this case study, classifying the data into each of the four seasons and workdays or weekends, each of the 24 hours of the day that meet the same criteria was averaged. For

instance, all the 1:00 am demand data for summer weekdays were averaged separately from the winter, autumn and spring. With this procedure, an artificial dataset consisting of the averaged values of the two years was created. This was intended to be subtracted from the original values and with the residues an ARMA model was used. Finally the time series were created using the average values per hour, type of day and season and added with the results of the ARMA model. Figure 59 shows an example of the original dataset and two of the time series.

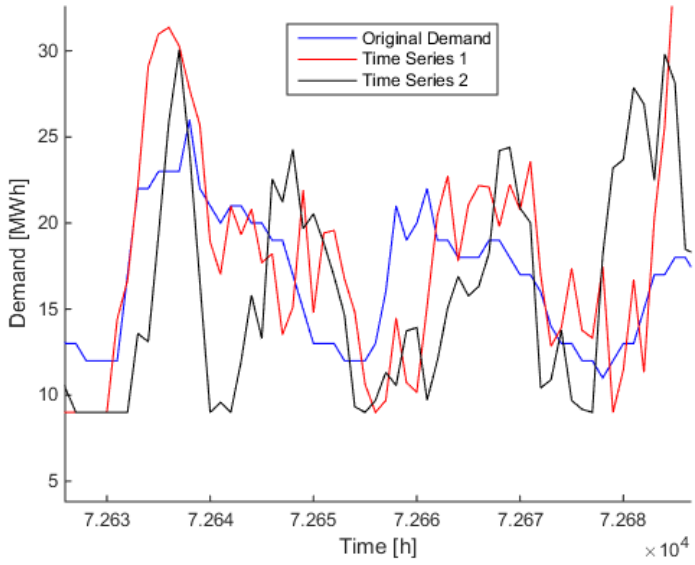

Figure 59. Original demand data and two time series.

4.2 Overview of the Methods and Models

Energy storage has the potential to provide multiple services to several sectors in electricity industry and hence support activities related to generation, network and system operation. In an electricity market environment, a service from storage presents both (i) a short-term revenue or remuneration associated with its provision to a market participant (who pays for it) and (ii) a consequent long-term cost associated with its effects on capacity degradation. Capacity degradation is related to the progressive reduction in the amount of energy that can be delivered by the energy storage plant or the growth of its internal impedance, which is a function of the time elapsed since the manufacture date, as well as the usage over consecutive charge and discharge actions. Therefore, storage owners need to take a decision between constraining operation of energy storage plant to prescribed charge/discharge volumes in order to maintain battery lifespan at higher levels, or maximize short-term revenues regardless of effects of degradation in the long-term (which may drive higher cost of investment since replacement of battery equipment may become more frequent). Clearly, this decision will have important effects on the portfolio of services provided by energy storage plant.

Figure 60 shows a general overview of our proposed approach with (i) an economic-based, commercial strategy module that determines storage plant operation (scheduled and real-time) by optimizing multi-service portfolios of energy storage (network congestion management, energy price arbitrage and various reserve and frequency response services) to maximize gross revenue, and (ii) a degradation module that progressively reduces energy capacity of storage plant as a function of its utilization profile determined in (i). While solution provided by module (i) is sensitive to utilization levels of network infrastructure (i.e. congestion), as well as various prices of energy and balancing services, module (ii)'s solution mainly depends on battery usage and type, besides ambient temperature. As shown in Figure 60, modules (i) and (ii) are applied on limited and sequential time periods (e.g. weeks) that covers a longer time horizon (e.g., several years) as follows:

1. Given storage plant capacity for period p (e.g., a week), module (i) determines optimal economic use of storage capacity within that period (when capacity is considered constant)
2. Given usage profile of storage capacity, module (ii) calculates capacity degradation by the end of period p (present week), which is then used as the storage capacity for next period p +1 (next week)

Hence, after applications of modules (i) and (ii) over various and consecutive time periods (that are part of a longer studied time horizon), storage plant operation and its capacity degradation was determined. This modeling framework is used to quantify effects of several operational policies (focused on constraining SOC) on gross revenue, portfolio of services, degradation and life of storage units. Sensitivity to market prices, network congestion levels and temperature were included.

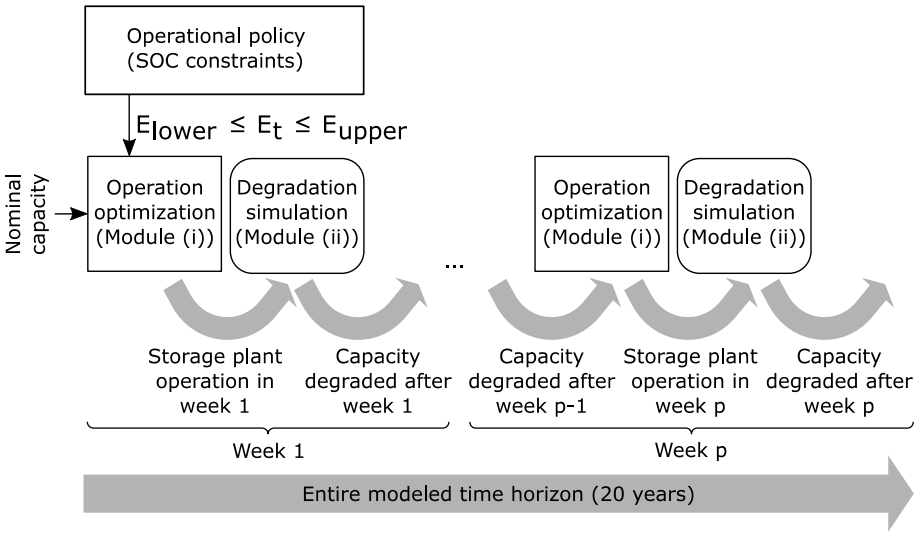

Figure 60. Overview of proposed economic-degradation model.

4.2.1 Economic Optimization Models

Storage operation is first scheduled ahead of real-time, albeit its utilization may change in actual, real-time operation. The term storage scheduled output refers to the planned output which is determined ahead of real-time and is sufficiently robust to cope with the delivery of contracted services, if exercised or called for in real-time. Scheduled output presents a plan of how storage should be operated under the most expected condition (i.e. no utilization of frequency or reserve services) to be able to deliver the contracted levels of services in case exercise is needed. This scheduled or planned output will be different from the real-time output since the latter will depend on the actual realizations of the delivery of services that storage is committed to provide. Submodules that determine scheduled and real-time storage operation are presented next.

Scheduled operation: this section presents a price-taker profit maximization model to determine uses of distributed storage capacity to provide multiple services to energy and balancing markets and Distribution Network Operators (DNO) as follows (see Figure 61):

a) Energy price arbitrage, associated with charging/buying at lower energy prices and discharging/selling at higher energy prices
b) System balancing services:
    i. The frequency response services, associated with the fast, automatic response when a system frequency deviation occurs. The upwards and downwards terms refer to the increment (upwards) or decrement (downwards) action to maintain the system's nominal frequency at the required value.
    ii. The reserve operating services, associated with the slower, centrally controlled demand–supply balance over a longer timescale. The upwards and downwards terms refer to the increment (upwards) or decrement (downwards) action to maintain the supply-demand balance of the whole system.
c) DNO peak demand shaving, associated with the congestion management at the primary substation level through active and reactive power control

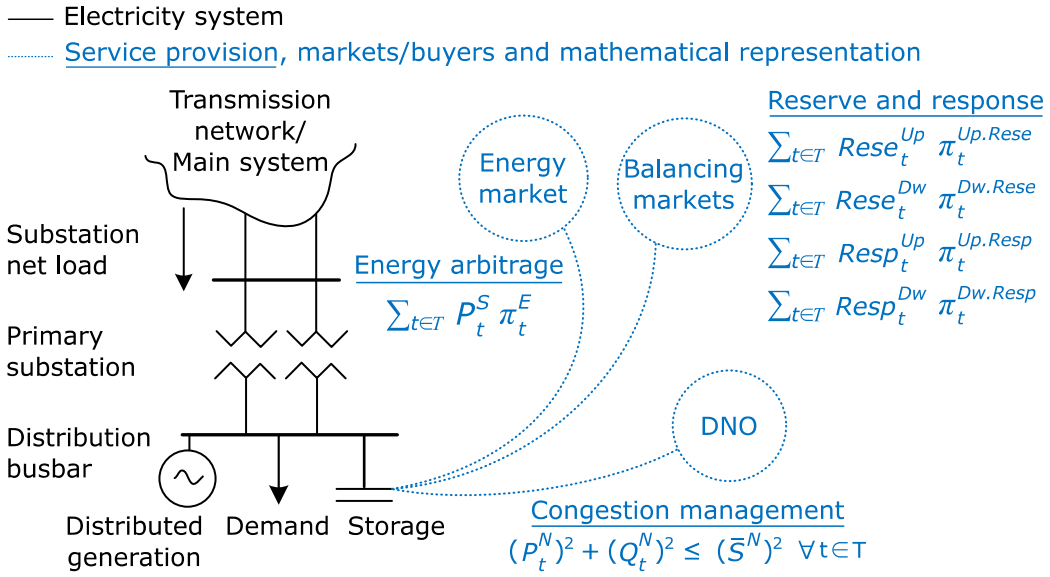

Figure 61. Diagram of modeled energy storage, demand, and primary substation along with service buyers.

The developed non-linear model maximizes, through Equation (16). The objective function maximizes the summation of several revenue streams as follows: energy arbitrage $\sum_{t\in T} P_t^S \pi_t^{\mathrm{E}}$, upwards reserve $\sum_{t\in T} Rese_t^{Up} \pi_t^{\mathrm{Up.Rese}}$, downwards reserve $\sum_{t\in T} Rese_t^{Dw} \pi_t^{\mathrm{Dw.Rese}}$, upwards response $\sum_{t\in T} Resp_t^{Up} \pi_t^{\mathrm{Up.Resp}}$, and downwards response $\sum_{t\in T} Resp_t^{Dw} \pi_t^{\mathrm{Dw.Resp}}$.

$$Max \left\{ \sum_{t\in T} P_t^S \cdot \pi_t^{\mathrm{E}} + Rese_t^{Up} \cdot \pi_t^{\mathrm{Up.Rese}} + Rese_t^{Dw} \cdot \pi_t^{\mathrm{Dw.Rese}} + Resp_t^{Up} \cdot \pi_t^{\mathrm{Up.Resp}} + Resp_t^{Dw} \cdot \pi_t^{\mathrm{Dw.Resp}} \right\} \quad (16)$$

Table 11 explains the meaning of the previous variables.

The overall revenue streams that energy storage could earn, given the set of prices associated with different services, by coordinating delivery of multiple applications while considering a number of constraints that represent inter-dependences among different services, the energy storage constraints and constraints of the local network infrastructure.

Hence, voltage support and network losses are not included in our model and this is considered a reasonable assumption to operate this installation since the focus is on

coordination of peak shaving services with grid-scale applications of storage such as energy arbitrage and frequency control and the associated degradation levels.

Table 11. Objective Function Parameters

P_t^S	Storage scheduled active power output at period t
$Rese_t^{Dw}$	Downwards reserve commitment at period t
$Rese_t^{Up}$	Upwards reserve commitment at period t
$Resp_t^{Dw}$	Downwards frequency response commitment at period t
$Resp_t^{Up}$	Upwards frequency response commitment at period t
π_t^{E}	Energy price at period t
$\pi_t^{\mathrm{Dw.Rese}}$	Availability price for downwards reserve at period t
$\pi_t^{\mathrm{Dw.Resp}}$	Availability price for downwards reserve at period t
$\pi_t^{\mathrm{Up.Rese}}$	Availability price for upwards reserve at period t
$\pi_t^{\mathrm{Up.Resp}}$	Availability price for upwards frequency response at period t

Real-time operation of storage plant: Once scheduled output is obtained, real-time storage plant operation will be determined by a simulation process that exercises the balancing services committed by the above scheduling submodule. The exercise of a balancing service occurs at given rate per period, e.g. 7 occurrences per week, and this is defined as a parameter for each balancing service. This exercise aims to analyze the impact of changing the real-time output on a daily basis due to a system operator's instruction, and how the lifespan of the storage system is affected. After a balancing service is exercised in real-time, storage plant will rapidly return to the scheduled energy stored levels by implementing a set of charge or discharge actions in real-time that will minimize the time exposure to imbalance fees (paid when a plant presents an imbalance between scheduled and real-time power output).

4.3 Capacity Degradation Algorithm

The concept of battery aging is typically related to the progressive reduction in the amount of energy that can be delivered by the energy storage plant or the growth of its internal impedance. Battery aging is a function of the time elapsed since the fabrication date, as well as the usage over consecutive charge and discharge actions. This work focuses on the latter aspect (which is closely entangled with the problem of economic multi-service operation of storage plants), characterizing usage cycles according to their swing ranges (defined by the minimum and maximum values reached, during a usage cycle, by the battery SOC). The proposed algorithm for computing overall capacity degradation over a given period (e.g. 1

week) is divided into 3 sections (or submodules) that are run sequentially as follows: (1) cycle length calculation, (2) cycle characterization and energy capacity degradation, and (3) temperature modulation (see Figure 62).

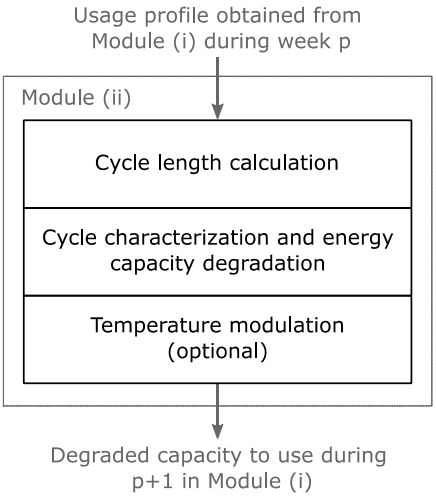

Figure 62. Submodules of the proposed algorithm.

4.3.1 Cycle Length Calculation

The purpose of this submodule is to determine the duration of each of the usage cycles that are present in a given operation profile. In this paper, a usage cycle is defined either by a charge action (or several successive charge actions) followed by a discharge action, or a discharge action (or several successive discharge actions) followed by a charge action. To find these patterns, the sign of the power to recognize when a cycle starts and finishes was used. Figure 63 illustrates the cycle recognition method.

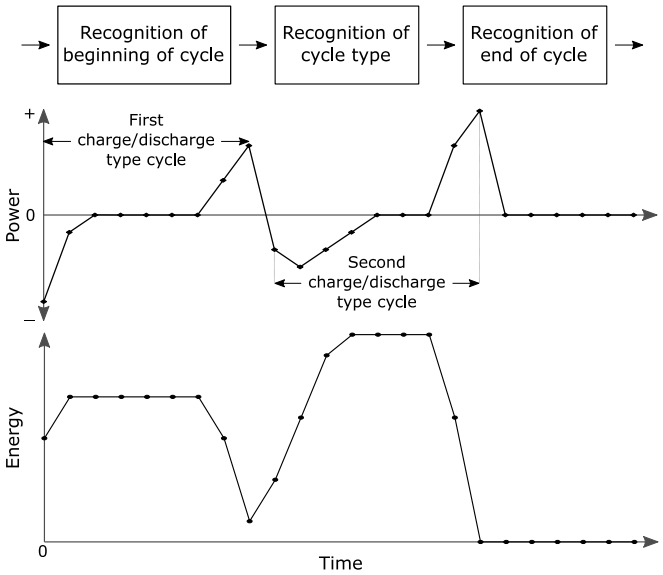

Figure 63. Cycle recognition.

4.3.2 Cycle Characterization and Degradation

Every cycle identified in the aforementioned submodule is characterized now in terms of the associated Coulombic efficiency ($\bar{\bar{\eta}}_k$). The value of this parameter corresponds to a measure of the expected capacity loss per cycle (as a percentage of the capacity offered by the battery during the previous discharge cycle). The Coulombic efficiency is used to degrade storage capacity after a cycle k through equation (17).

$$\bar{\bar{E}}_{k+1} = \bar{\bar{\eta}}_k \bar{\bar{E}}_k \tag{17}$$

To calculate $\bar{\bar{\eta}}_k$, data provided by manufacturer that characterizes the battery lifespan (i.e. number of cycles) when storage plant is sequentially charged and discharged at rated current, and following strict protocols that ensure specific swing ranges (11 swing ranges were provided: 0-25%, 0-50%, 0-75%, 0-100%, 25-100%, 50-100%, 75-100%, 25-50%, 25-75%, 50-75%, and 37.5-62.5%) was used. Also, it was assumed that battery may be used up to when degraded capacity reaches 75% of the initial, nominal capacity. This assumption is actually a standard practice, which is justified by the growth of the internal impedance of the battery (as battery cells degrade) and the subsequent increment in heat losses. The Coulombic efficiency was determined using the methodology explained in Section 3.3.

It is critical to emphasize here a few important facts related with battery degradation and the operating conditions informed by the manufacturer. On the one hand, capacity fade is typically accelerated by operating profiles that offer a combination of high average SOC levels, deep discharges, extremely high or low temperatures, and overcharging. On the other hand, operating a battery with low average SOC (e.g., SOC swing ranges between 0-25%) can be beneficial in terms of incrementing the lifespan. Nevertheless, the latter statement is only valid when avoiding cell over-discharge, or when the user does not store the battery discharged for an extended period of time (a procedure that leads towards permanent cell damage, because self-discharge phenomena can cause cell over-discharge). In this regard, when forcing operation at low SOC values it is important to differentiate between deep discharges (accelerated degradation) and small SOC swing ranges.

As to include the effect of the temperature, equation (18) shows the proposed structure for the SOH degradation model.

$$\begin{cases} x_1(k+1) = (\eta)\, e^{\alpha\left(\frac{1}{T-\beta}-\frac{1}{T_{ref}-\beta}\right)} x_1(k) + \omega_1(k) \\ y(k) = x_1(k) + \upsilon(k) \end{cases} \tag{18}$$

In this case, the state $x_1(k)$ is used to represent the SOH of the ESD. The temperature parameters have values of $\alpha = -5.1593$ and $\beta = 260.9565$ according to the structure proposed in (Pola, 2014). Since the effect of the SOC swing and swing range is going to be incorporated through the parameter η, and using the information provided by the manufacturer and this information is confidential only part of it will be shown. This information included the expected cycles when operating under certain SOC swing percentages and different swing ranges. The following table shows the provided information.

Table 12. Battery Usage and Efficiency Parameters

SOC swing %	Swing range	Cycles	*Eta*
Case A	A1	Confidential	*0.9999AX*
Case B	B1	Confidential	*0.9999BX*
	B2	Confidential	*0.9999BY*
Case C	C1	Confidential	*0.9999CX*
	C2	Confidential	*0.9999CY*
	C3	Confidential	*0.9999CZ*
Case D	D1	Confidential	*0.9999DX*
	D2	Confidential	*0.9999DY*
	D3	Confidential	*0.9999DZ*
	D4	Confidential	*0.9999DW*
	D5	Confidential	*0.9999DV*

The column labeled as *Eta* was not provided by the manufacturer and the results were obtained through the methodology explained in Section 3.3.

For the cases shown in Table 12, the values of η are almost the same and the difference is on the fifth and sixth decimal. However these small differences can have an impact of a 4:1 ratio on the total cycles. For confidentially reasons the last two decimals of η are not shown. The last two digits of the value of η are represented by capital letters but none of them is the same. For instance the digits CX and CY, do not imply that the C digit is the same for both cases,

it is just a representation method that is related to one of the SOC swing cases. Figure 64 shows the eleven previous cases of how the battery degrades (the legend is not included due to confidentially reasons). For the first 1000 cycles, the difference among all the cases is almost negligible, but after this point the differences of the end of life are considerable.

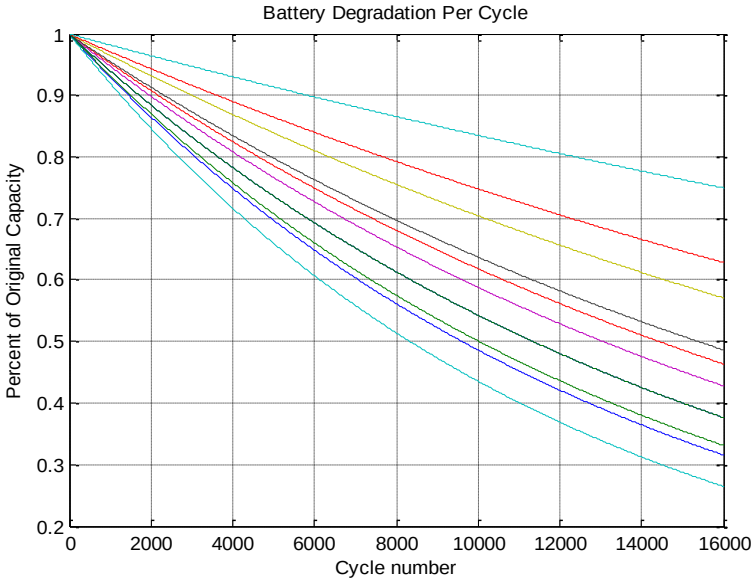

Figure 64. Degraded battery capacity depending on the Coulombic efficiency.

Until this point, it has been very common to use the word cycle to define the duration of the battery. The most common definition for a cycle corresponds to the amount of time that goes by, when a charged battery is used until is completely discharged. However in this case some considerations have to be taken into account. For instance, a strategy can be such that the battery starts fully charged, and then discharged until it reaches an 80% SOC, and from there it should be charged at a 90% SOC, and will maintain this swing range for ever. Since the battery will never be fully charged, does this mean that there is only one cycle? The reality is that this would be inaccurate, and to deal with this type of behavior, in this approach a usage cycle is defined either by a charge action (or several successive charge actions) followed by a discharge action, or a discharge action (or several successive discharge actions) followed by a charge action. To find these patterns, we use the sign of the P_t (power at time t) to recognize when a cycle starts and finishes by using the following algorithm:

- *For* all t
  - *If* a usage cycle has not been defined in t:
    - *If* $P_t = 0$, goto End-if(1)
    - *Elif* $P_t > 0$: define usage cycle as discharge/charge.
    - *Elif* $P_t < 0$: define usage cycle as charge/discharge.
    - *End-if*
  - *Else*
    - *If* usage cycle is discharge/charge type and $P_{t-1} < 0$ *and* $P_t > 0$
      - *Then* a usage cycle is set as finished in $t - 1$ and a new usage cycle is started in t and set as undefined.
    - *Elif* usage cycle is charge/discharge type and $P_{t-1} > 0$ *and* $P_t \leq 0$:
      - *Then* a usage cycle is set as finished in t-1 and a new usage cycle is started in t and set as undefined.
    - *End-if*
  - *End-if(1)*
- *End-for*

The above algorithm will determine complete and partial charge/discharge usage cycles, which will degrade storage capacity differently, in terms of their characterization.

The following step is to simulate the mentioned techniques. For the following results, the following assumptions were made:

- Temperature: constant at 25 °C.
- C-rate factor equal to 1.

The first simulation considers all the previous mentioned techniques and algorithms. The SOH degradation module is used to cooperate with the optimization module. Figure 65 shows the results for several different SOC policies. These results show that the working cycles obtained during the time of simulation are in the same order as the expected results using the provided information. The simulation was performed through a total of 20 years since this is the maximum lifespan guaranteed by the manufacturer.

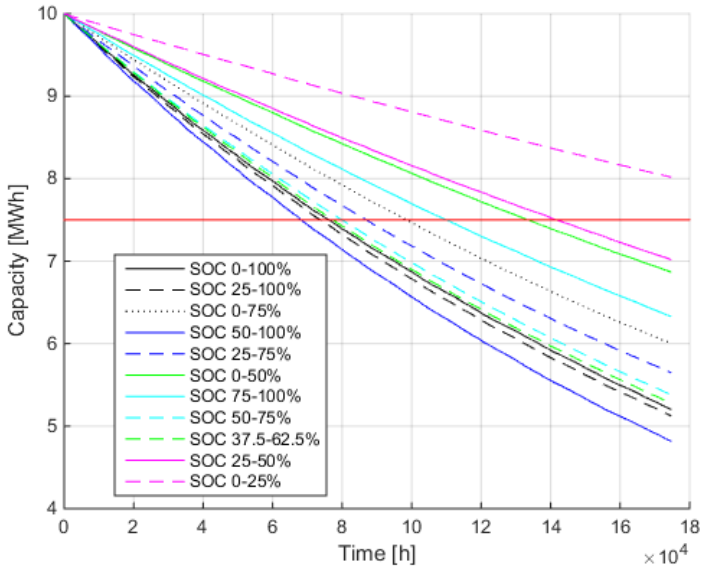

Figure 65. SOH degradation for different SOC policies.

4.4 Results

4.4.1 Effect of Operational Policies

Data provided by manufacturer suggest that battery lifespan can be significantly increased if plant is operated within a smaller swing range (e.g. 0-25%) rather than within its full energy capacity (e.g. 0-100%). Hence, we calculate revenues and degradation associated with 11 operational policies that aim at constraining the SOC. To do so, lower and upper limits were added in the scheduling submodule in order to constrain the SOC values to a given range.

In this context, Figure 66 shows that constraining the SOC when deciding optimal operation of storage plant presents clear benefits, since battery lifespan can be more than doubled. For example, battery lifespan lasts about 76,000 hours if the SOC is unconstrained, which can be increased up to more than 175,000 hours if the SOC is constrained between 0 and 25%. Another interesting feature, shown in Figure 66, is that it is more attractive to limit upper rather than lower bounds of the swing range. In fact, increasing lower bounds may decrease battery lifespan with respect to the unconstrained case (i.e. 0-100%) and this is consistent with manufacturer data.

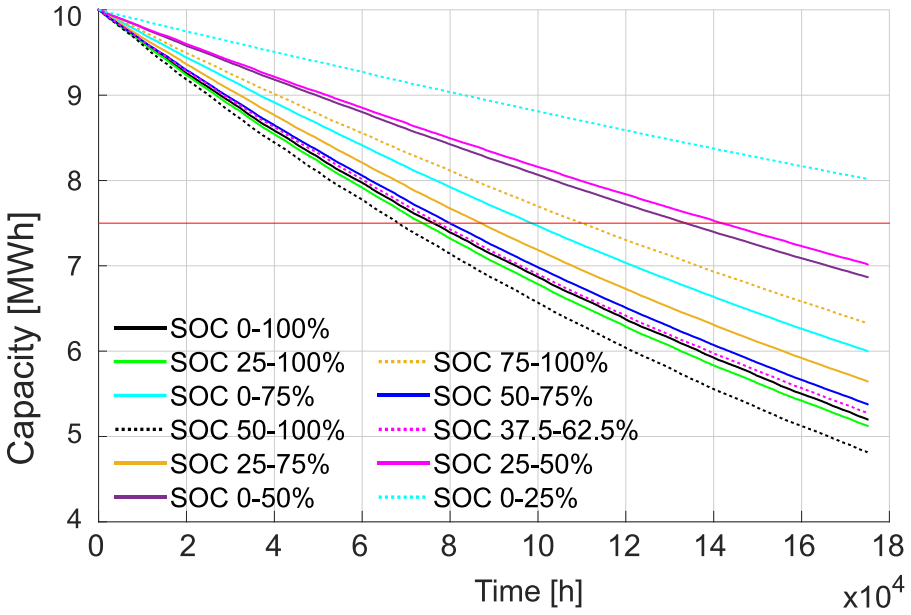

Figure 66. Energy capacity degradation for different operational policies. Horizontal red line indicates 75% of the nominal energy capacity.

The benefits shown on Figure 67 are in opposition to short-term opportunity costs of constraining SOC. In fact, constraining SOC between 0 and 25%, for instance, can present about 18% lower gross revenue levels per year as shown in Figure 67 (where results are sorted in decreasing order).

Despite this, lower average gross revenues (in £/annum) can be compensated by revenue streams in the longer term that are associated with a lengthier lifespan of storage plant and this is shown in Figure 68 (where results are sorted in decreasing order). Effectively in this case study, it is clearly more beneficial to constrain the SOC scheduled output since its benefits in terms of battery lifespan increase, more than compensate the revenue loss in the short-term incurred in energy and balancing markets. In fact, for the 0-25% policy, lifespan increase (i.e. >+100%) is clearly disproportionally higher than reduction in gross revenue (i.e. ~ –18 %).

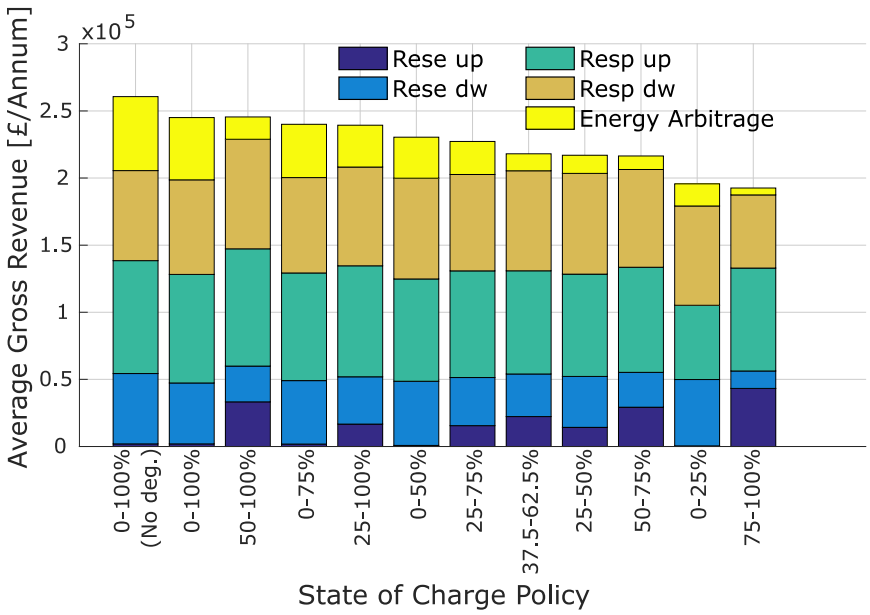

Figure 67. Average annual gross revenue during battery lifespan. "No deg." Refers to no degradation (where operation is optimized during 20 years without degradation and this case is used as a benchmark).

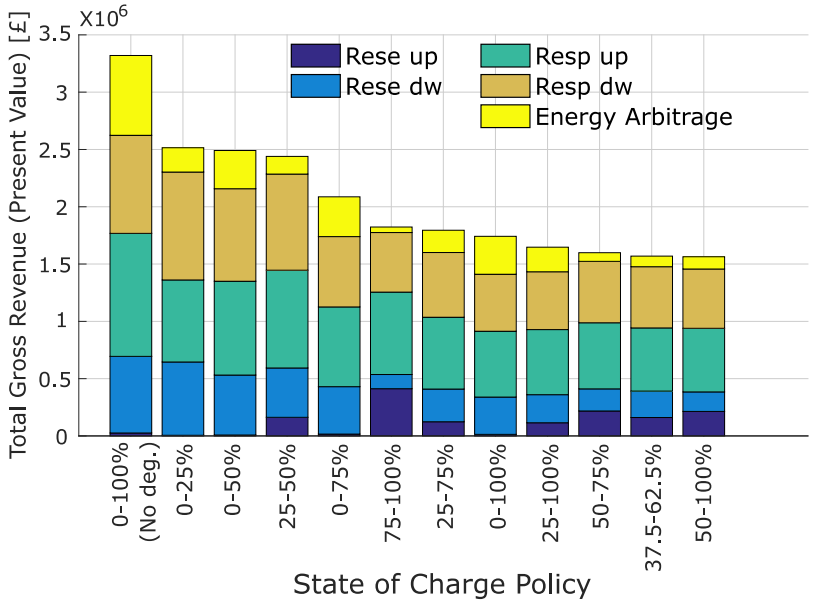

Figure 68. Total Gross Revenue during battery lifespan (5% discount rate).

4.4.2 Effect on Multi-Service Portfolios

Figure 69 (where results are sorted in decreasing order) suggests that all operational policies affect revenues in the short-term and that this is mainly driven by revenue changes in services that are more energy intensive such as energy and reserve, while revenue streams associated with frequency response services are more stable.

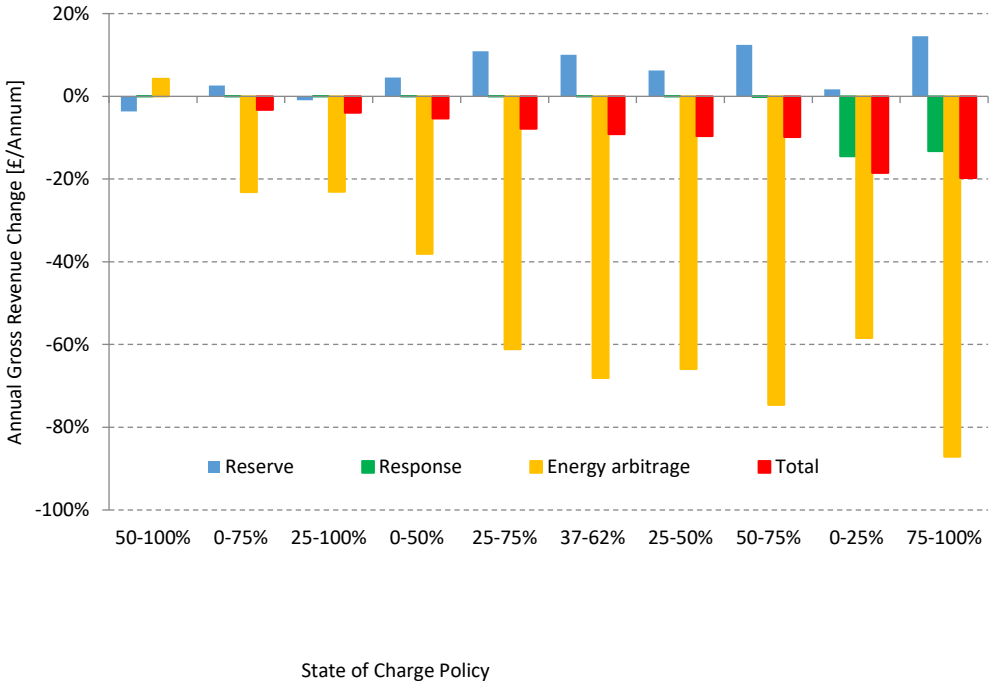

Figure 69. Average annual gross revenue change with respect to 0-100% policy.

Furthermore, Figure 69 also demonstrates that revenues associated with balancing services do not necessarily decrease when SOC is constrained to improve battery lifespan. In fact, as energy arbitrage is limited when SOC is constrained, there are capacity margins of storage plant that can be used for further services. Therefore, short-term revenue losses associated with operational policies that aim at increasing battery lifespan, will ultimately depend on energy and balancing markets conditions and can be limited if storage capacity is used for application in balancing rather than energy market.

4.4.3 Economics and Degradation in a Week

This section aims at illustrating and validating the used methods to optimize operation, and calculate gross revenue and degradation of a storage plant within a week. In this context, Figure 70 shows power outputs and energy stored levels for both scheduled and real-time operation of the storage plant.

Scheduled output shown in Figure 70 is optimized for the provision of multiple storage applications or services: energy arbitrage (162£/day by buying in the morning between 2:00h and 3:00h a total volume of 8MWh at an average price of 35£/MWh and selling in the evening between 22:00h and 23h a total volume of 6.8MWh at an average price of 65£/MWh with a 85% efficiency), frequency response (420£/day by holding 6MW of each upwards and downwards service in the morning between 4:00h and 8:00h at a price of 7£/MW), and reserve (180£/day by holding 3.4MW of upwards service and 1.6MW of downwards service in the afternoon between 16:00h and 21:00h at a price of 6£/MW –note that services are constrained by SOC at that time, which is equal to 6.8MWh–). This degrades capacity from 10MWh to 9.996781MWh due to occurrence of 7 partial cycles within a swing range between 0% and 68%, each with a Coulombic efficiency of 0.999954. If a balancing service is exercised every day during that week (which can potentially occur in real-time operation as shown in Figure 70), this would degrade capacity further from 10MWh to 9.993562MWh due to occurrence of 14 partial cycles within a swing range between 0% and 68%. Note that utilization of balancing services may not necessarily increase the number of cycles (as in the case above), but rather expand the swing range of charge/discharge actions.

This demonstrates that reserving capacity for balancing services may be detrimental in terms of degradation, depending on how frequent these services will be exercised by the system operator.

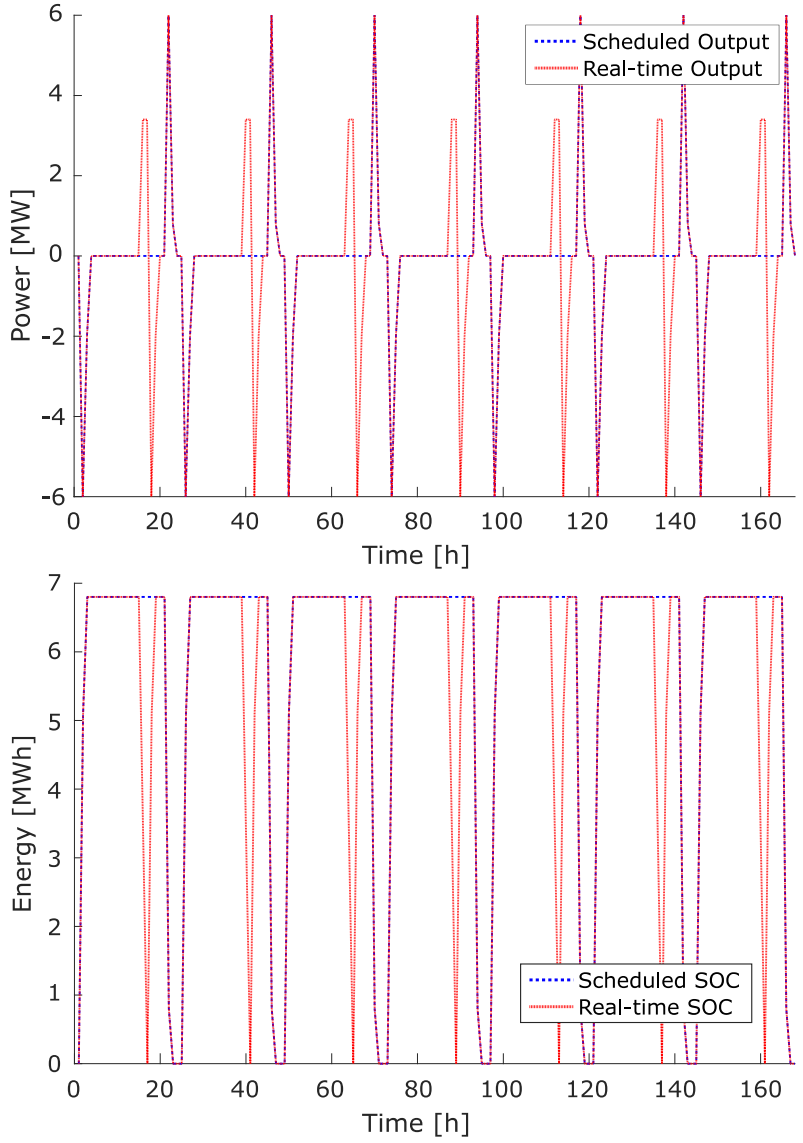

Figure 70. Scheduled and one potential real-time power output (top) and SOC (bottom).

4.4.4 Effect on Balancing Services Utilization in Real-Time on Battery Lifespan

Two cases are modeled: without and with utilization of balancing services for all operational policies when considering an exercise rate of one service per day. This demonstrates that battery lifespan can be reduced by 28% in the worst case. These results are shown in Table 13.

Table 13 also demonstrates that reserving capacity for balancing services may be detrimental, depending on how frequent these services will be exercised by the system operator and this

affects large majority of operational policies. Interestingly, 0-25% policy (which is the most profitable policy and that with the lengthiest lifespan) is not affected.

Table 13. Battery lifespan with and without balancing services utilization/exercise

SOC Policy	Balancing service utilization [h]	No balancing service utilization [h]	Reduction [h]	Reduction [%]
25-100%	52759	73738	-20979	-28%
37-62%	55517	77388	-21871	-28%
0-50%	96050	133479	-37429	-28%
0-100%	54987	76164	-21177	-28%
0-75%	71776	98531	-26755	-27%
25-75%	65067	87014	-21947	-25%
50-100%	52395	68200	-15805	-23%
25-50%	110717	141685	-30968	-22%
50-75%	64186	79887	-15701	-20%
75-100%	93638	109981	-16343	-15%
0-25%*	175200	175200	0	0%

*Modeled lifespan in both cases exceed figure provided by manufacturer

4.4.5 Effect of Temperature Control

Modeling the effect of energy capacity changes due to ambient temperature in the absence of controls that can maintain it constant at its nominal value (i.e. 25°C) was performed. Daily temperatures are based on historical data that is publicly available at the site of the storage plant to fit a time series model that can produce stochastic scenarios of temperatures up to 20 years. Figure 71, also shows energy capacity excursion of 3 operational policies compared with those obtained at nominal temperature, demonstrates that capacity can be significantly reduced during winter (below 75%), even during the firsts years of operation.

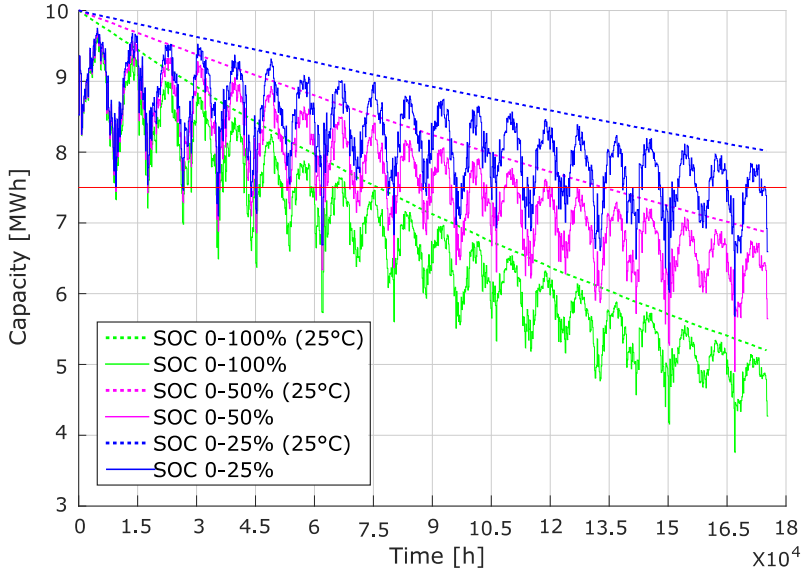

Figure 71. Energy capacity degradation for three operational policies with (dotted lines) and without (solid lines) temperature control.

Despite this and in line with results in previous sections, we found that effect of temperature on gross revenues is limited to about -3% due to market conditions in GB. In effect, capacity reduction due to temperature mainly affect revenues associated with the energy market (about -9%), which is less attractive than further balancing markets whose revenues are less dependent on fluctuations in capacity due to temperature and this is demonstrated in Figure 72.

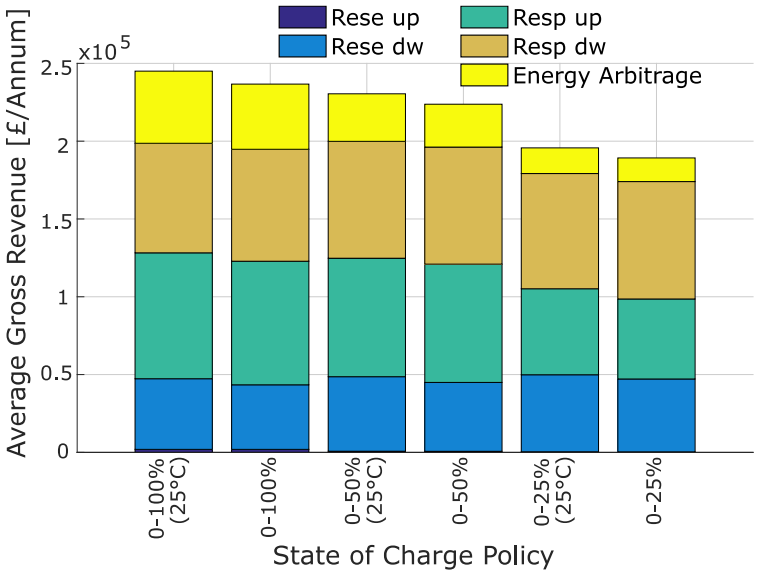

Figure 72. Comparison of average annual gross revenue during battery lifespan with and without temperature control.

Figure 73 shows the total gross revenue in present value (considering a 5% discount rate), with and without considering the effect of the temperature. Even though the differences on

the figure look small, depending on the operational SOC policy, they can go among the 60,000 £ up to 100,000 £. It important to recall that, these results were obtained through just one temperature time series, and it becomes important to analyze more of them in order to characterize the uncertainty in operation hours and gross revenue due to the temperature.

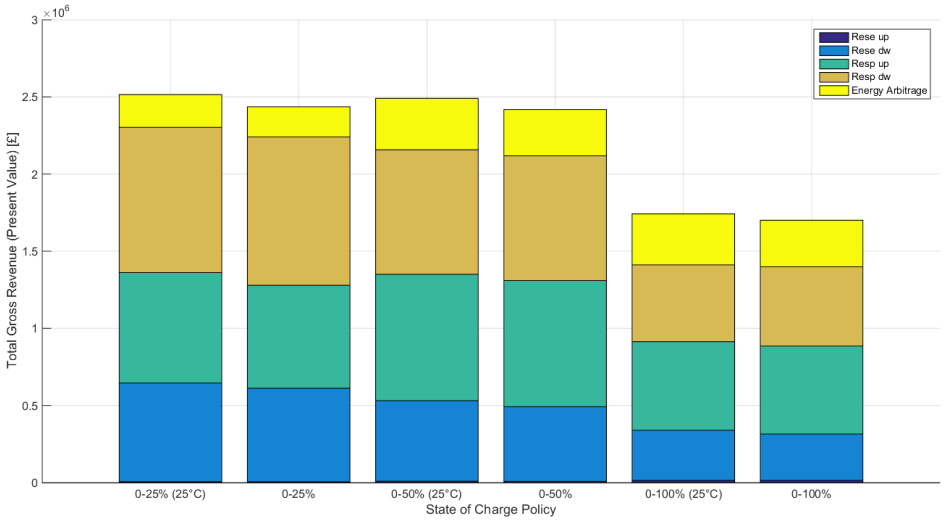

Figure 73. Total Gross Revenue for different SOC policies.

4.4.6 Sensitivities to Demand and Prices

In this research, a sensitivity analysis was used to study the robustness of the previous results with respect to future changes in demand and prices. To do so, 10 scenarios of demand and 10 scenarios of energy prices explained on Section 4.1. This analysis was performed only for the 0-100% SOC policy and at a temperature of 25°C. In this context, results proved robust and changes in battery lifespan were below 5% as shown on Figure 74.

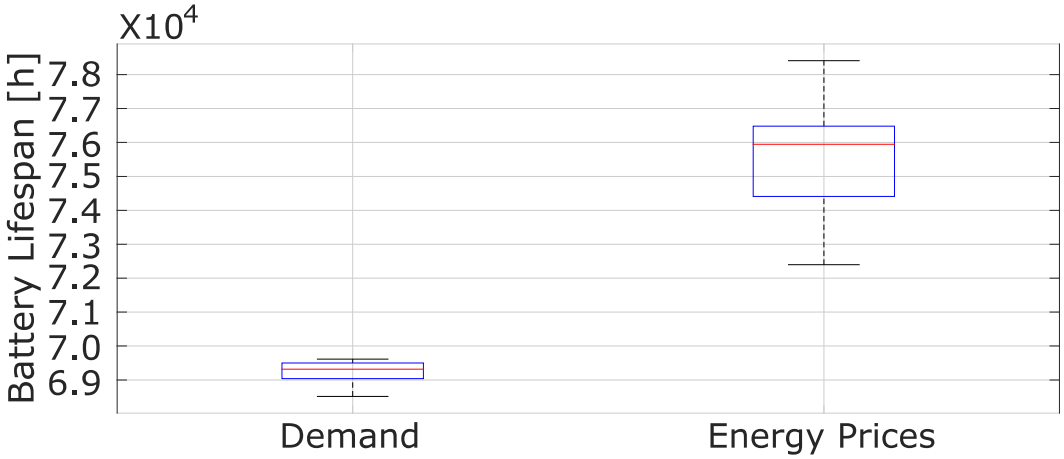

Figure 74. Sensitivity analysis for 10 scenarios of future demand and energy price time series (0-100% operational policy).

4.5 Limitations of the Presented Models and the Case Studies

The results showed on this work suggest that there even though there are still many areas to explore. It is important to keep in mind that the obtained results were generated with various restrictions and limitations.

One of them, is that the proposed capacity degradation model is able to fit a convex shape trend described by the studied batteries. Not all batteries degrade in the same manner, for this reason if the degradation process follows a concave shape, another approach must be implemented.

The extrapolation methods are based on information provided by a manufacturer. The provided technique is useful to characterize the degradation process when the batteries are discharged at different SOC swing ranges, although the results can differ when the discharge currents are different.

For the case study, the battery was considered to be degraded when the capacity of the battery was reduced to 75% of its nominal value. Although this threshold is supported by the literature, it is possible to have different results if the threshold changes, for example to 80%. During these simulations, the discharge current was assumed equal to 1-C. Furthermore, the complete battery pack was considered as just one battery for simplification purposes, since it is possible that one module, or just one cell degrades in a different way than the others.

Also, the obtained results belong to the particular market conditions used in the simulations. If the market conditions change, it would be expected that the results will be different. Also, in the simulations, two-year repetitions of different variables were considered. For example, there were no price changes or growth of the demand considered.

5. Conclusions

An empirical model that characterizes the degradation process of Li-ion batteries when discharged at various C-rates was proposed. The proposed model is based on a discrete space-state representation and uses two states and four coefficients, where one of the equations has a major impact on the short term degradation process, while the other affects the long term degradation. The proposed model can be adjusted to the discharge current used, demonstrating that one (out of four) coefficient presents a great impact on the degradation process in the long term.

The proposed model and coefficient values can be easily and accurately adapted to different types of Li-ion batteries. This was validated under different discharge currents and two sets of experimental data: our own experimental dataset and those from the Prognostics Center of Excellence of NASA Ames Research Center.

One of the main advantages of the proposed model is that the current SOH can be calculated by evaluating an algebraic expression. Although using all the confidence bounds for the all the coefficients might induce to a biased result, this can be amended by implementing a sequential learning method or other similar techniques to estimate coefficient c and we leave this for future research.

It is possible to used K-NN to model the degradation process of lithium-ion batteries when these are charged and discharged erratically. The proposed methodology uses information provided by the manufacturer and through the use of escalating factors, the values for the efficiency of each type of erratic cycle can be calculated. Using the concepts of (i) SOC swing, (ii) average swing range and (iii) Coulombic efficiency, it is possible to model degradation in a simple manner through interpolation techniques. By using both deterministic and Monte Carlo simulations, the capacity degradation as a function of the number of cycles was obtained.

Another alternative to the use of K-NN, is SBM. In this case a technique to model the degradation process of Li-ion batteries was presented. This method uses the cycle by cycle efficiency, and interpolates an equivalent value for the efficiency depending on the SOC limits and discharge current. Also, the effect of the temperature was used to compare the differences between e degraded capacity and the usable capacity.

A combined economic-degradation model to quantify effects of various operational policies (mainly focused on constraining SOC to prescribed levels) on gross revenue, multi-service portfolios, degradation and lifespan of energy storage plants was developed. Also, the model was used to demonstrate conflicts and synergies of different storage applications with battery

degradation. In particular, it was demonstrated that although operational policies focused on battery damage reduction will lead to a revenue loss in the short-term (since these policies fundamentally constrain storage operation), such loss can be more than compensated by long-term revenues due to a lengthier battery lifespan. In the presented study case, for instance, constraining SOC to a swing range between 0 and 25% has the potential to increase total gross revenues up to circa 44% (across the entire lifespan and considering a discount rate of 5%). Additionally, it was demonstrated that short-term revenue losses associated with the application of operational policies are mainly driven by revenue reduction in the energy rather than balancing market. Furthermore, this reduction in energy services can lead to both increase in balancing services (since there are more capacity margins available) and decrease in battery capacity degradation. Despite this, increased utilization rates of balancing services by system operators can be detrimental for storage plants and reduce battery lifespan (which can apply to any operational policy). Finally, it was demonstrated that variations of ambient temperature have the potential to decrease storage plants owners' profits (especially in winter), albeit it is not significant in the case of Great Britain (although this is dependent on market conditions and on how attractive the energy market is against balancing services markets).

This work can promote efficient integration of new distributed storage projects and provide insights associated with the development of efficient operational policies to ensure that storage plants are adequately operated by balancing both short and long-term costs and benefits, and thus that investors in storage plants are efficiently rewarded for the delivery of value to multiple electricity sectors.

5.1 Publications

This sections is intended to enumerate the participation on different publications during the doctoral program.

5.1.1 Journal Publications, H index, and SCImago Journal Ranking.

1. **Pérez, A.,** Quintero, V., Jaramillo, F., Rozas, H., Jimenez, D., Orchard, M., Moreno, R., "Characterization of the Degradation Process of Lithium-Ion Batteries when Discharged at Different Currents", Part I: Journal of Systems and Control Engineering. (Submitted September 2017). H index: 34, SJR: 0.436.
2. **Pérez, A**., Benavides, M., Rozas, H., Seria, S., Orchard, M., "A Practical Guide for the Characterization of Lithium-Ion Battery Internal Impedances in PHM Algorithms", *International Journal of Prognostics and Health Management: Special Issue PHMAP17 Highlights*. (Accepted). H index: 12, SJR: 0.426.
3. **Perez, A**.; Moreno, R.; Moreira, R.; Orchard, M.; and Strbac, G., "Effect of Battery Degradation on Multi-Service Portfolios of Energy Storage", *IEEE Transactions on Sustainable Energy*, vol. 7, Issue 4, pp. 1718-1729, 2016. H index: 61, SJR: 2.636.

4. Pola, D.; Navarrete, H.; Orchard, M.; Rabié, R.; Cerda, M.; Olivares, B.; Silva, J.; Espinoza, P.; and **Pérez, A.**, "Particle-filtering-based Discharge Time Prognosis for Lithium-Ion Batteries with a Statistical Characterization of Use Profiles", *IEEE Transactions on Reliability*, vol. 64, Issue 2, pp. 710-720, June 2015, H index: 77, SJR: 1.335.
5. Acuña, D.; Orchard, M.; Silva, F.; and **Perez A.**, "Multiple-imputation-particle-filtering for Uncertainty Characterization in Battery State-of-Charge Estimation Problems with Missing Measurement Data: Performance Analysis and Impact on Prognostic Algorithms", International Journal of Prognostics and Health Management, Vol. 6, (008), pp. 1-12, 2015, H index:12, SJR: 0.426.

5.1.2 Conference Publications

1. **Pérez, A.**, Quintero, V., Rozas, H., Jimenez, D., Jaramillo, F., Orchard, M., "Lithium-Ion Battery Pack Arrays for Lifespan Enhancement", IEEE ChileCon 2017, October 18th-20th, Pucón, Chile.
2. Espinoza, P., **Pérez, A**., Orchard, M., Navarrete, H., Pola, D., "A Simulation Engine for Ion-Lithium Battery Packs in Electric Vehicles Based on Autonomy and Remaining Life Criteria", Annual Conference of the Prognostics and Health Management Society 2017 - PHM17, October 2nd-5th, St. Petersburg, FL, USA.
3. Jaramillo, F., Quintero, V., **Pérez, A**., Orchard, M., "Spatio-temporal Probabilistic Modeling Based on Gaussian Mixture Models and Neural Gas Theory for Prediction of Criminal Activity", Annual Conference of the Prognostics and Health Management Society 2017 - PHM17, October 2nd-5th, St. Petersburg, FL, USA.
4. Seria, S. Quintero, V., Espinoza, P., **Pérez, A.**, Jaramillo, F. Benavides, M., Orchard, M., "Energy Management of Electric Bicycles Given a Traveling Elevation Profile", Annual Conference of the Prognostics and Health Management Society 2017 - PHM17, October 2nd-5th, St. Petersburg, FL, USA.
5. **Pérez, A**., Benavides, M., Rozas, H., Seria, S., Orchard, M., "A Practical Guide for the Characterization of Lithium-Ion Battery Internal Impedances in PHM Algorithms", First Asia Pacific Conference of Prognostics and Health Management Society, July 12th-15th, 2017, Jeju City, South Korea. **Nominated Best Academia Paper Award.**
6. **Pérez, A**.; Quintero, V.; Rozas, H.; Jaramillo, F.; Moreno, R.; and Orchard, M., "Modelling the Degradation Process of Lithium-Ion Batteries when Operating at Erratic State of Charge Swing Ranges", 4th International Conference on Control, Decision and Information Technologies - CoDIT'17, April 5th-7th, 2017, Barcelona, Spain.
7. Pola, D.; Guajardo, F.; Jofré, E.; Quintero, V.; **Perez, A**.; Acuña, D.; and Orchard, M., "Particle-Filtering-Based State-of-Health Estimation and End-of-Life Prognosis for Lithium-Ion Batteries at Operation Temperature", Annual Conference of the Prognostics and Health Management Society 2016 - PHM16, October 3rd-6th, 2016, Denver, CO, USA.
8. **Perez, A**.; Orchard, M.; Silva, J.; and Cornejo, F., "Dynamic Vector Model Applied to Wind Speed Prognosis for Eolic Generation", Third European Conference of the

Prognostics and Health Management Society 2016 - PHME16, July 5th-8th, 2016, Bilbao, Spain.

9. Flores, P.; Vergara, M.; Fuentes, P.; Jaramillo, F.; Acuña, D.; **Perez, A**.; and Orchard, M.; , "Modeling and Prediction of Criminal Activity Based on Spatio-Temporal Probabilistic Risk Functions", Annual Conference of the Prognostic and Health Management Society 2015, October 19th-24th, 2015, San Diego, CA, USA.
10. Tampier, C.; **Pérez, A**.; Jaramillo, F.; Quintero, V.; Orchard, M.; and Silva, J., "Lithium-Ion Battery End-of-Discharge Time Estimation and Prognosis based on Bayesian Algorithms and Outer Feedback Correction Loops: A Comparative Analysis", Annual Conference of the Prognostic and Health Management Society 2015, October 19th-24th, 2015, San Diego, CA, USA.
11. Acuña, D.; Orchard, M.; Silva, J.; and **Pérez, A**., "Multiple-imputation-particle-filtering scheme for Uncertainty Characterization in Battery State-of-Charge Estimation Problems with Missing Measurement Data", Annual Conference of the PHM Society 2014, September 29th - October 2nd, 2014, Fort Worth, TX, USA.

5.2 Future Work

The proposed degradation process model might induce to a biased result in case all the confidence bounds for all the coefficients are used. This can be amended by implementing a sequential learning method another similar technique to estimate the value of coefficient *c*.

More experimental analysis is required. In this regard, many other combinations must be taken into consideration. For instance, discharging the batteries at different C-rates that were not considered in this research will allow a better understanding of the process. Furthermore, combining different C-rates and SOC swing ranges will allow a more accurate characterization since this is a more realistic approach of how the batteries are used in different applications.

Characterizing the effect of the temperature is imperative. Its effect can be seen in two ways. The first one has to with the accelerated degradation if a battery is always used under extreme temperatures. The other effect has to do with the concept of the usable capacity which is associated with the modulation effect of using a battery at one temperature condition and then a different condition. The parameters that modulate this effect change in time, and thus need to be studied.

The results obtained in this research demonstrate the benefits of using a combined economic-degradation model to quantify the effects for different operational policies. However, if the economic strategy or the market conditions change, the results might be different. In this regard, modifying the market conditions to evaluate different scenarios can be helpful to understand the expected revenues for those conditions.

6. Bibliography

[1] U. Nations, “Kyoto Protocol to the United Nations framework convention on climate change,” 1998.

[2] D. Pola, “An Improved Prognosis Strategy wiht Temperature Dependent State-Space Model for the Analysis of the State-of-Health and State-of-Charge in Lithium-Ion Batteries,” University of Chile, 2014.

[3] U. K. P. Networks, “Smarter Network Storage- business model consultation.” 2013.

[4] R. Moreno, R. Moreira, and G. Strbac, “A MILP model for optimising multi-service portfolios of distributed energy storage,” *Appl. Energy*, vol. 137, pp. 554–566, 2015.

[5] I. Yvonex Energy, “Lithium-ion battery systems Retrieved October 1, 2015. http://www.ynovex.com/lithium/.” 2015.

[6] X. He, E. Delarue, W. D’haeseleer, and J.-M. Glachant, “A novel business model for aggregating the values of electricity storage,” *Energy Policy*, vol. 39, no. 3, pp. 1575–1585, 2011.

[7] R. Moreira, R. Moreno, and G. Strbac, “Synergies and conflicts among energy storage services,” in *Energy Conference (ENERGYCON), 2016 IEEE International*, 2016, pp. 1–6.

[8] G. Strbac *et al.*, “Opportunities for Energy Storage: Assessing Whole-System Economic Benefits of Energy Storage in Future Electricity Systems,” *IEEE Power Energy Mag.*, vol. 15, no. 5, pp. 32–41, 2017.

[9] B. Saha and K. Goebel, “Modeling Li-ion battery capacity depletion in a particle filtering framework,” in *Proceedings of the annual conference of the prognostics and health management society*, 2009, pp. 1–10.

[10] R. Spotnitz, “Simulation of capacity fade in lithium-ion batteries,” *J. Power Sources*, vol. 113, no. 1, pp. 72–80, 2003.

[11] J. Vetter *et al.*, “Ageing mechanisms in lithium-ion batteries,” *J. Power Sources*, vol. 147, no. 1–2, pp. 269–281, 2005.

[12] D. Haifeng, W. Xuezhe, and S. Zechang, “A new SOH prediction concept for the power lithium-ion battery used on HEVs,” in *Vehicle Power and Propulsion Conference, 2009. VPPC’09. IEEE*, 2009, pp. 1649–1653.

[13] K. M. Tsang, W. L. Chan, Y. K. Wong, and L. Sun, “Lithium-ion battery models for computer simulation.” 2010.

[14] M. Daigle and C. Kulkarni, “Electrochemistry-based Battery Modeling for Prognostics,” *Annu. Conf. Progn. Heal. Manag. Soc.*, pp. 1–13, 2013.

[15] G. Ning and B. N. Popov, “Cycle Life Modeling of Lithium-Ion Batteries,” *J. Electrochem. Soc.*, vol. 151, no. 10, p. A1584, 2004.

[16] G. Ning, R. E. White, and B. N. Popov, “A generalized cycle life model of rechargeable Li-ion batteries,” *Electrochim. Acta*, vol. 51, no. 10, pp. 2012–2022, 2006.

[17] G. Ning, B. Haran, and B. N. Popov, “Capacity fade study of lithium-ion batteries cycled at high discharge rates,” *J. Power Sources*, vol. 117, no. 1–2, pp. 160–169, 2003.

[18] P. Ramadass, B. Haran, R. White, and B. N. Popov, “Mathematical modeling of the capacity fade of Li-ion cells,” *J. Power Sources*, vol. 123, no. 2, pp. 230–240, 2003.

[19] Q. Xie, X. Lin, Y. Wang, and M. Pedram, “State of health aware charge management

in hybrid electrical energy storage systems," in *Design, Automation & Test in Europe Conference & Exhibition (DATE), 2012*, 2012, no. 2010, pp. 1060–1065.
[20] T. Markel, "Plug-in HEV vehicle design options and expectations," in *ZEV Technology Symposium, National Renewable Energy Laboratory*, 2006, vol. 9, no. 27, pp. 21–26.
[21] D. Andre, C. Appel, T. Soczka-Guth, and D. U. Sauer, "Advanced mathematical methods of SOC and SOH estimation for lithium-ion batteries," *J. Power Sources*, vol. 224, no. 0, pp. 20–27, 2013.
[22] Y. Zou, X. Hu, H. Ma, and S. E. Li, "Combined State of Charge and State of Health estimation over lithium-ion battery cell cycle lifespan for electric vehicles," *J. Power Sources*, vol. 273, no. 0, pp. 793–803, 2015.
[23] B. E. Olivares, M. A. Cerda Mu??oz, M. E. Orchard, and J. F. Silva, "Particle-filtering-based prognosis framework for energy storage devices with a statistical characterization of state-of-health regeneration phenomena," *IEEE Trans. Instrum. Meas.*, vol. 62, no. 2, pp. 364–376, 2013.
[24] K. S. Ng, C.-S. Moo, Y.-P. Chen, and Y.-C. Hsieh, "Enhanced coulomb counting method for estimating state-of-charge and state-of-health of lithium-ion batteries," *Appl. Energy*, vol. 86, no. 9, pp. 1506–1511, 2009.
[25] B. Saha, K. Goebel, S. Poll, and J. Christophersen, "Prognostics Methods for Battery Health Monitoring Using a Bayesian Framework," *IEEE Trans. Instrum. Meas.*, vol. 58, no. 2, pp. 291–296, 2009.
[26] M. Dalal, J. Ma, and D. He, "Lithium-ion battery life prognostic health management system using particle filtering framework," *Proc. Inst. Mech. Eng. Part O J. Risk Reliab.*, vol. 225, no. 1, pp. 81–90, 2011.
[27] Olivares, "Sistema de Pronostico para el Estado-de-Salud de Acumuladores de Energia Basado en Filtro de Particulas y Caracterizacion Estadistica de Fenomenos de Regeneracion," University of Chile, 2012.
[28] A. Widodo, M.-C. Shim, W. Caesarendra, and B.-S. Yang, "Intelligent prognostics for battery health monitoring based on sample entropy," *Expert Syst. Appl.*, vol. 38, no. 9, pp. 11763–11769, 2011.
[29] N. Williard, W. He, M. Osterman, and M. Pecht, "Comparative analysis of features for determining state of health in lithium-ion batteries," *Int. J. Progn. Heal. Manag*, vol. 4, pp. 1–7, 2013.
[30] W. Haiying, H. Long, S. Jianhua, L. Shuanquan, and W. Feng, "Study on correlation with SOH and EIS model of Li-ion battery," in *Strategic Technology (IFOST), 2011 6th International Forum on*, 2011, vol. 1, pp. 261–264.
[31] D. Le and X. Tang, "Lithium-ion Battery State of Health Estimation Using Ah-V Characterization," *Annu. Conf. Progn. Heal. Manag. Soc. 2011*, vol. 2, 2001.
[32] A. Eddahech, O. Briat, and J. Vinassa, "Real-time SOC and SOH estimation for EV Li-ion cell using online parameters identification," in *Energy Conversion Congress and Exposition (ECCE), 2012 IEEE*, 2012, pp. 4501–4505.
[33] S. Al Hallaj, H. Maleki, J. S. Hong, and J. R. Selman, "Thermal modeling and design considerations of lithium-ion batteries," *J. Power Sources*, vol. 83, no. 1–2, pp. 1–8, 1999.
[34] S. Santhanagopalan, Q. Zhang, K. Kumaresan, and R. E. White, "Parameter Estimation and Life Modeling of Lithium-Ion Cells," *J. Electrochem. Soc.*, vol. 155, no. 4, p. A345, 2008.

[35] T. Hirai, A. Ohnishi, N. Nagaoka, N. Mori, A. Ametani, and S. Umeda, “Automatic equivalent-circuit estimation system for lithium-ion battery,” in *Universities Power Engineering Conference, 2008. UPEC 2008. 43rd International*, 2008, pp. 1–5.
[36] S. X. Chen, K. J. Tseng, and S. S. Choi, “Modeling of lithium-ion battery for energy storage system simulation,” in *Power and Energy Engineering Conference, 2009. APPEEC 2009. Asia-Pacific*, 2009, pp. 1–4.
[37] P. Rong and M. Pedram, “An analytical model for predicting the remaining battery capacity of lithium-ion batteries,” *Very Large Scale Integr. Syst. IEEE Trans.*, vol. 14, no. 5, pp. 441–451, May 2006.
[38] L. Gao, S. Liu, and R. A. Dougal, “Dynamic lithium-ion battery model for system simulation,” *Components Packag. Technol. IEEE Trans.*, vol. 25, no. 3, pp. 495–505, 2002.
[39] P. Rong and M. Pedram, “An analytical model for predicting the remaining battery capacity of lithium-ion batteries,” *Proc. -Design, Autom. Test Eur. DATE*, vol. 14, no. 5, pp. 1148–1149, 2003.
[40] C. Zhou, K. Qian, M. Allan, and W. Zhou, “Modeling of the Cost of EV Battery Wear Due to V2G Application in Power Systems,” *Energy Conversion, IEEE Trans.*, vol. 26, no. 4, pp. 1041–1050, 2011.
[41] K. Thirugnanam, H. Saini, and P. Kumar, “Mathematical modeling of li-ion battery for charge/discharge rate and capacity fading characteristics using genetic algorithm approach,” in *Transportation Electrification Conference and Expo (ITEC), 2012 IEEE*, 2012, pp. 1–6.
[42] L. Lam and P. Bauer, “Practical capacity fading model for Li-ion battery cells in electric vehicles,” *IEEE Trans. power Electron.*, vol. 28, no. 12, pp. 5910–5918, 2013.
[43] Y. Xie, J. Li, and C. Yuan, “Multiphysics modeling of lithium ion battery capacity fading process with solid-electrolyte interphase growth by elementary reaction kinetics,” *J. Power Sources*, vol. 248, pp. 172–179, 2014.
[44] I. Apple, “Batteries - Why Lithium-ion? Retrieved November 10, 2015. http://www.apple.com/batteries/why-lithium-ion/.” 2015.
[45] T. Guena and P. Leblanc, “How Depth of Discharge Affects the Cycle Life of Lithium-Metal-Polymer Batteries,” in *Telecommunications Energy Conference, 2006. INTELEC ’06. 28th Annual International*, 2006, pp. 1–8.
[46] Y. Wang, X. Lin, Q. Xie, N. Chang, and M. Pedram, “Minimizing state-of-health degradation in hybrid electrical energy storage systems with arbitrary source and load profiles,” in *Design, Automation and Test in Europe Conference and Exhibition (DATE), 2014*, 2014, pp. 1–4.
[47] A. Millner, “Modeling Lithium Ion battery degradation in electric vehicles,” in *Innovative Technologies for an Efficient and Reliable Electricity Supply (CITRES), 2010 IEEE Conference on*, 2010, pp. 349–356.
[48] N. Saito, T. Niimura, K. Koyanagi, and R. Yokoyama, “Trade-off analysis of autonomous microgrid sizing with PV, diesel, and battery storage,” in *Power & Energy Society General Meeting, 2009. PES ’09. IEEE*, 2009, pp. 1–6.
[49] D. Menniti, A. Pinnarelli, and N. Sorrentino, “A method to improve microgrid reliability by optimal sizing PV/wind plants and storage systems,” in *Electricity Distribution - Part 2, 2009. CIRED 2009. The 20th International Conference and Exhibition on*, 2009, p. 1.

[50] P. Toma, P. Dorin, E. Radu, and M. Daniel, “Sizing photovoltaic-wind smart microgrid with battery storage and grid connection,” in *Automation, Quality and Testing, Robotics, 2014 IEEE International Conference on*, 2014, pp. 1–5.
[51] D. Pudjianto, M. Aunedi, P. Djapic, and G. Strbac, “Whole-Systems Assessment of the Value of Energy Storage in Low-Carbon Electricity Systems,” *Smart Grid, IEEE Trans.*, vol. 5, no. 2, pp. 1098–1109, 2014.
[52] B. Mozafari and S. Mohammadi, “Optimal sizing of energy storage system for microgrids,” *Sadhana*, vol. 39, no. 4, pp. 819–841, 2014.
[53] H. J. Khasawneh and M. S. Illindala, “Battery cycle life balancing in a microgrid through flexible distribution of energy and storage resources,” *J. Power Sources*, vol. 261, pp. 378–388, 2014.
[54] A. Poullikkas, “A comparative overview of large-scale battery systems for electricity storage,” *Renew. Sustain. Energy Rev.*, vol. 27, no. 0, pp. 778–788, 2013.
[55] B. Zakeri and S. Syri, “Electrical energy storage systems: A comparative life cycle cost analysis,” *Renew. Sustain. Energy Rev.*, vol. 42, pp. 569–596, 2015.
[56] C. A. Hill, M. C. Such, D. Chen, J. Gonzalez, and W. M. Grady, “Battery Energy Storage for Enabling Integration of Distributed Solar Power Generation,” *Smart Grid, IEEE Trans.*, vol. 3, no. 2, pp. 850–857, 2012.
[57] M. C. Such and C. Hill, “Battery energy storage and wind energy integrated into the Smart Grid,” in *Innovative Smart Grid Technologies (ISGT), 2012 IEEE PES*, 2012, pp. 1–4.
[58] A. Perez, V. Quintero, H. Rozas, F. Jaramillo, R. Moreno, and M. Orchard, “Modelling the Degradation Process of Lithium-Ion Batteries When Operating at Erratic State-of-Charge Swing Ranges,” in *4th International Conference on Control and Decision and Information Technologies*, 2017.

7. Appendix

Table 14. Example of the efficiency values for the first three cycles of operation.

Cycle	Current	SOC Swing	Average Swing Range	Efficiency: 0.85
1	1	1	0.5	0.998407581
1	1	0.75	0.625	0.998409508
1	1	0.75	0.375	0.9984211
1	1	0.5	0.75	0.998401791
1	1	0.5	0.5	0.998418644
1	1	0.5	0.25	0.998428478
1	1	0.25	0.875	0.998423187
1	1	0.25	0.625	0.998413991
1	1	0.25	0.5	0.998412084
1	1	0.25	0.375	0.998431923
1	1	0.25	0.125	0.998438003
1	2	1	0.5	0.997859108
1	2	0.75	0.625	0.997861034
1	2	0.75	0.375	0.997872619
1	2	0.5	0.75	0.997853321
1	2	0.5	0.5	0.997870165
1	2	0.5	0.25	0.997879993
1	2	0.25	0.875	0.997874705
1	2	0.25	0.625	0.997865514
1	2	0.25	0.5	0.997863609
1	2	0.25	0.375	0.997883436
1	2	0.25	0.125	0.997889513
1	3	1	0.5	0.998336481
1	3	0.75	0.625	0.998338408
1	3	0.75	0.375	0.998349999
1	3	0.5	0.75	0.998330691
1	3	0.5	0.5	0.998347543
1	3	0.5	0.25	0.998357377
1	3	0.25	0.875	0.998352085
1	3	0.25	0.625	0.998342891
1	3	0.25	0.5	0.998340984
1	3	0.25	0.375	0.998360821
1	3	0.25	0.125	0.998366901
2	1	1	0.5	0.998447088
2	1	0.75	0.625	0.998449015
2	1	0.75	0.375	0.998460607
2	1	0.5	0.75	0.998441297
2	1	0.5	0.5	0.998458151

2	1	0.5	0.25	0.998467985
2	1	0.25	0.875	0.998462693
2	1	0.25	0.625	0.998453498
2	1	0.25	0.5	0.998451591
2	1	0.25	0.375	0.99847143
2	1	0.25	0.125	0.99847751
2	2	1	0.5	0.997912694
2	2	0.75	0.625	0.99791462
2	2	0.75	0.375	0.997926205
2	2	0.5	0.75	0.997906906
2	2	0.5	0.5	0.997923751
2	2	0.5	0.25	0.99793358
2	2	0.25	0.875	0.997928291
2	2	0.25	0.625	0.9979191
2	2	0.25	0.5	0.997917194
2	2	0.25	0.375	0.997937023
2	2	0.25	0.125	0.9979431
2	3	1	0.5	0.998360496
2	3	0.75	0.625	0.998362423
2	3	0.75	0.375	0.998374014
2	3	0.5	0.75	0.998354706
2	3	0.5	0.5	0.998371558
2	3	0.5	0.25	0.998381392
2	3	0.25	0.875	0.9983761
2	3	0.25	0.625	0.998366906
2	3	0.25	0.5	0.998364999
2	3	0.25	0.375	0.998384836
2	3	0.25	0.125	0.998390916
3	1	1	0.5	0.998485547
3	1	0.75	0.625	0.998487474
3	1	0.75	0.375	0.998499067
3	1	0.5	0.75	0.998479756
3	1	0.5	0.5	0.998496611
3	1	0.5	0.25	0.998506446
3	1	0.25	0.875	0.998501154
3	1	0.25	0.625	0.998491958
3	1	0.25	0.5	0.99849005
3	1	0.25	0.375	0.99850989
3	1	0.25	0.125	0.998515971
3	2	1	0.5	0.997964798
3	2	0.75	0.625	0.997966724
3	2	0.75	0.375	0.997978311

3	2	0.5	0.75	0.99795901
3	2	0.5	0.5	0.997975856
3	2	0.5	0.25	0.997985686
3	2	0.25	0.875	0.997980396
3	2	0.25	0.625	0.997971205
3	2	0.25	0.5	0.997969299
3	2	0.25	0.375	0.997989129
3	2	0.25	0.125	0.997995206
3	3	1	0.5	0.998384053
3	3	0.75	0.625	0.99838598
3	3	0.75	0.375	0.998397571
3	3	0.5	0.75	0.998378262
3	3	0.5	0.5	0.998395115
3	3	0.5	0.25	0.998404949
3	3	0.25	0.875	0.998399658
3	3	0.25	0.625	0.998390463
3	3	0.25	0.5	0.998388556
3	3	0.25	0.375	0.998408394
3	3	0.25	0.125	0.998414474